NATIONAL AERONAUTICS AND SPACE ADMINISTRATION

*Technical Report 32-1570*

# *Gravitational Effects on Electrochemical Batteries*

*Robert E. Meredith*
*Oregon State University*

*Gordon L. Juvinall and A. A. Uchiyama*
*Jet Propulsion Laboratory*



JET PROPULSION LABORATORY
CALIFORNIA INSTITUTE OF TECHNOLOGY
PASADENA, CALIFORNIA

November 15, 1972

NATIONAL AERONAUTICS AND SPACE ADMINISTRATION

*Technical Report 32-1570*

# *Gravitational Effects on Electrochemical Batteries*

*Robert E. Meredith*
*Oregon State University*

*Gordon L. Juvinall and A. A. Uchiyama*
*Jet Propulsion Laboratory*

**JET PROPULSION LABORATORY**
**CALIFORNIA INSTITUTE OF TECHNOLOGY**
**PASADENA, CALIFORNIA**

November 15, 1972

# Preface

This report summarizes the results of published work on gravitational effects on batteries. Part of the experimental work was performed by the Guidance and Control Division of the Jet Propulsion Laboratory and the Department of Chemical Engineering of Oregon State University.

# Contents



## Tables

# Contents (contd)

## Tables (contd)



## Figures

# Contents (contd)

## Figures (contd)

# Contents (contd)

## Figures (contd)

# Contents (contd)

## Figures (contd)

## Abstract

The existing work on gravitational effects on electrochemical batteries is summarized, certain conclusions are drawn, and recommendations are made for future activities in this field. Theoretical evaluations of the problem have met with only limited success; theories based upon a treatment of natural convection have fallen short of the mark, partly because the mass transfer involved in the power-producing electrochemical reactions in a battery is not completely due to convection and partly because a battery is far removed from the idealized models necessarily employed in the development of the theory. The latter point is best illustrated by the fact that although theory generally predicts that the limiting current density will vary with the 1/4 power of the acceleration constant, the experimental data falls in the range of a 1/3 to 1/5 power dependence because of differences in the way the cell is constructed.

The effects of sustained high-*G* environments on cycled silver–zinc and nickel–cadmium cells have been evaluated over four complete cycles in the region of 10 to 75 *G*. Although no effects on high current discharge performances or on ampere-hour capacity were noted, severe zinc migration and sloughing of active material from the zinc electrode were observed. This latter effect constitutes real damage, and over a long period of time would result in loss of capacity.

The work of Arcand, based upon smooth zinc electrodes, predicted a limiting current density of 7 $mA/cm^2$. However, the Mariner 7 battery easily provided a current density of 10.5 $mA/cm^2$ in deep space. Fundamental battery studies performed at zero *G* are necessary to resolve the conflict. To this end, experiments have been planned and a breadboard model of an in-flight battery test unit has been designed and fabricated.

It is recommended that a zero-*G* battery experiment be implemented. Both an orbiting satellite and a sounding rocket approach are being considered.

# Gravitational Effects on Electrochemical Batteries

## I. Introduction

When current is drawn from an electrochemical cell or battery, certain of the chemical reactants in the system must move to and from the electrode surfaces at a rate corresponding to the passage of electrical current in the external circuit. Such chemical species may flow by three different modes of transfer: (1) migration—movement of charged particles or ions in an electrical field, (2) diffusion—bulk movement in a chemical gradient, or (3) bulk or mass transfer—bulk movement of material due to density gradients.

In conventional electrolyte-flooded batteries, where relatively high currents are demanded, the transport of the ionic reactants to support the external current is mainly brought about by bulk movement of liquid due to the density differences that exist near the surface of the electrodes in the cells. Without this method of chemical transfer, the maximum or limiting current that one could realize would be an order of magnitude smaller than the value obtained with this mode of convection or movement.

In batteries, density gradients exist because the mass of solution per unit volume differs from point to point as one moves from the electrolyte to the electrode surface. Such differences are due to the fact that the chemical products of the electrode reaction do not necessarily have the same density as the chemical reactants which created them. In many cases, such density differences or concentration gradients extend from the electrode surface into the liquid electrolyte for a very short distance; the thickness of this region of varying density, which is termed the boundary layer, may often be as small as 0.05 cm. A schematic of a typical boundary layer at a cathode electrode in which ions are plated or removed from solution is shown in Fig. 1.

Since the weight of matter approaches zero as the gravitational force approaches zero, density differences no longer provide a driving force for mass transfer in a zero-$G$ environment.[1] In zero- or low-$G$ situations,

[1]The symbol $G$ is used throughout this report to indicate relative acceleration. This is defined as the acceleration force $g$, divided by the standard value of the gravitational acceleration constant $g_0$ at the surface of the earth.

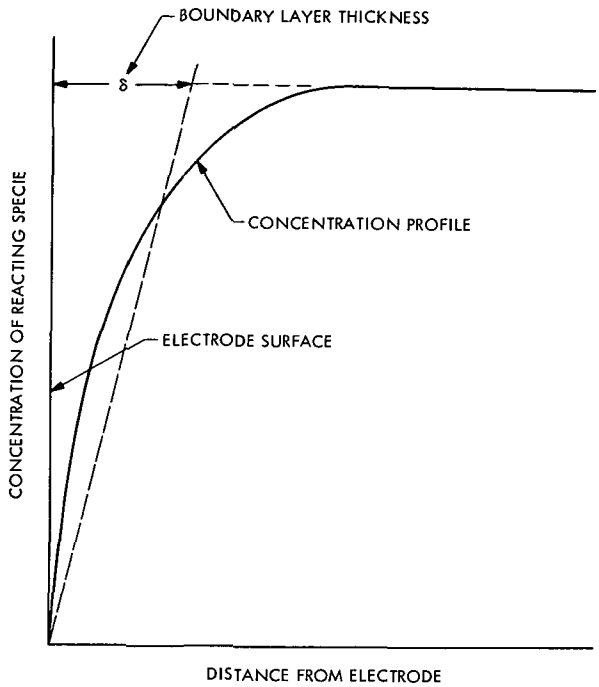


**Fig. 1. Boundary layer profile**

one of the main modes of chemical transfer is thus theoretically lost and one would predict that the maximum or limiting current that could be realized for a battery in such an environment would be less than could be obtained in the earth environment of 1 *G*.

This reasoning also would predict that if a battery were held in an acceleration field in which the effective gravitational force were larger than at the surface of the earth, a higher limiting current could be obtained than would normally be available from the battery in a 1-*G* environment.

It is relatively easy to simulate forces higher than 1 *G* by placing the unit or battery in a centrifugal machine of appropriate size; however, environments lower than 1 *G* cannot be satisfactorily simulated in the laboratory. Relative accelerations smaller than 1 *G* obtained by parabolic plane flights or by the use of drop towers are not maintained for a long enough period of time for steady-state current to be obtained. In the past, many workers have attempted to gain predictable battery behavior in low-*G* fields by noting the behavior in high-*G* environments.

The purpose of this publication is to bring together, under a single cover, a summary of the studies to date on the subject of gravitational effects on electrochemical batteries.

## II. Natural Convection

The phenomenon of moving or transferring heat or mass by virtue of density differences is collectively associated with the process of "natural convection." The analogy between heat and mass transfer makes it possible to predict somewhat the consequences of the transfer of chemical species at electrode surfaces by the use of equations or correlations developed for heat transfer at solid surfaces.

Even more appropriate, however, are the studies conducted by Levich (Ref. 1), Wagner (Ref. 2), and Keulegan (Ref. 3) on mass transfer in electrochemical systems. These authors have independently derived relations of the following type:

$$Nu' = C(ScGr)^{1/4} \tag{1}$$

Here, $Nu'$ is the dimensionless Nusselt number for mass transfer and is defined by Eq. (2):

$$Nu' = \frac{k_L L}{D} \tag{2}$$

The mass transfer coefficient $k_L$ is expressed in cm/s. The height of a vertical electrode $L$ is expressed in cm, and $D$ is the diffusion coefficient in cm²/s. The dimensionless Schmidt number $Sc$ is the ratio of the kinematic viscosity $\nu$ in cm²/s to the diffusion coefficient $D$. The constant $C$ varies with the work of each author but appears to have an average value of about 0.677. The symbol $Gr$ is the dimensionless Grashof number, which is defined as

$$Gr = g(\rho_i - \rho_0)\,\rho_{av} L^3/\mu^2 \tag{3}$$

where $g$ is the acceleration of gravity in cm/s²; $\rho_i$, $\rho_0$, and $\rho_{av}$ are the density of the solution at the electrode interface, the density of the bulk of the solution, and the average density, respectively, all in units of g/cm³. The symbol $\mu$ is the viscosity of the electrolyte in g/s-cm.

The significance of Eq. (1) in predicting the limiting currents from batteries in various types of gravitational fields can be seen when it is noted that $Nu'$ is related

to the mass transfer coefficient $k_L$, and that this coefficient is also related to the current drawn from a battery (when transfer due to migration is negligible) by the following relation:

$$k_L(C_i - C_0) = \frac{I(1 - t_i)}{n\mathbf{F}} \tag{4}$$

in which $C_i$ is the concentration of the potential-determining species at the electrode interface in moles/cm$^3$, $C_0$ is the bulk concentration of this same species, $I$ is the current density in A/cm$^2$, $t_i$ is the transference number (the fraction of the charge carried by the species in question), $n$ is the valence change of the reacting ion, and F is Faraday's constant in A-s/g-equivalent.

The combination of Eqs. (1–4) predicts that the limiting current in a 1-$G$ environment, $I_{L(G=1)}$, is related to the limiting current at some other value of $G$ (all other factors being equal) by the equation

$$I_L = I_{L(G=1)}G^{1/4} \tag{5}$$

The model assumed in the derivation of Eq. (1), and consequently in Eq. (5), is that the electrolytic concentrations are low (i.e., $\leq$ 0.1 M), that the flow along the surface of the electrodes is laminar, and that the current densities are low (i.e., $\leq$ 0.01 mA/cm$^2$). Because it appears possible, with the combination of high concentrations and high current densities, to generate a turbulent boundary layer near the electrode surface, one might predict that Eq. (5) would underestimate the limiting current density in high gravitational fields.

## III. Low-Gravity Simulation

In studying the effects of low-gravity phenomena on fluid motion in a confined system, it is possible in some experiments to obtain information by using the concept of dynamic similitude. Such an approach permits all experimentation to be conducted at unit-gravity. For example, if a correlation predicts that the Bond number or Weber number is an important parameter in estimating system behavior, one may scale the experiment in such a way that the reduction of one of the variables in the group is offset with an increase in another variable. Specifically, the Bond number is a dimensionless ratio expressing the balance between surface tension forces and acceleration-induced body forces and is written as $(\rho_1 - \rho_2)gL^2/\sigma$. Here $\rho_2$ is the density of the light or upper liquid, gas, or vapor, $\rho_1$ is the density of the heavier or lower liquid, $g$ is the local acceleration, $\sigma$ is the interfacial surface tension between phases, and $L$ is an appropriate container dimension. Thus, to simulate low-gravity conditions, it would appear possible to counter the reduction that occurs in $\rho$ and $g$ by increasing the value of $L$.

Similarly, the Weber number is a dimensionless ratio expressing the relative value of the liquid inertia forces to the surface tension forces. It is written as $\rho v^2 L/\sigma$, where $v$ is a characteristic fluid velocity. An examination of this group shows that a reduction in $\rho$ may be compensated by increasing $L$ or $v$ or both, whichever the system permits.

In practice it is not generally possible, with common test liquids, to meet the requirements of Bond and Weber number simulation and also to fulfill the requirements of Reynolds number simulation. Thus, while the approach of dynamic similitude may be interesting from a theoretical aspect, it may not be very practical in certain fluid motion studies.

In many studies the term "zero-gravity" is generally employed to suggest an apparent absence of weight due to the fact that the system is moving without constraint in a gravitational field. Thus, while zero gravity and "free fall" are not exactly synonomous, the terms are often used interchangeably. Even the "zero-gravity experiments" conducted in orbiting satellites are really free fall studies. Here the satellite accelerates towards the earth with an acceleration determined by the local acceleration due to gravity. Because the orbiting system has a high tangential velocity with respect to the earth, it does not fall to the surface of the earth, but it falls instead into a continuous orbit about the earth.

In a system which depends upon the behavior of a liquid, the physical phenomena of the environment change rapidly as one approaches zero gravity, mostly because the density or inertial forces are reduced to nearly zero, and surface tension forces control the behavior of liquids and gases. Equilibrium configurations are thus governed by the criterion of minimum interfacial energy rather than minimum potential energy.

The experimental techniques for providing or simulating a low-gravity environment fall into two broad categories: (1) bench tests at standard or accelerated

gravity conditions with the results extrapolated into the low-gravity region and (2) relatively short tests in reduced gravity conditions if earth orbital flights are not available.

The approach of trying to predict low-gravity results by extrapolating from "high-gravity" experiments is generally a poor procedure since surface tension forces do not begin to control the phenomena until the gravitational effect is significantly less than unity. For information down to relative gravitational values of 0.7 or 0.5, this technique may be of some utility since inertial forces are still significant in this range.

Short periods of free fall are available for experiments by the use of aircraft or rockets flying in a Keplerian or ballistic trajectory, and by the use of "drop towers." In terms of economy and availability, the drop tower is by far the most useful tool. It does, however, have the major disadvantage of giving only a short period for the time of the test.

The time of free fall in a drop experiment is close to

$$T = 0.449h^{1/2} \tag{6}$$

where $T$ is the time available in seconds, and $h$ is the drop height in meters. A fall of approximately 30 m gives only 2.5 s, and not much additional time is gained by increasing the height of the tower by a moderate amount.

To avoid the effect of atmospheric drag, the experimental package is usually placed in a drag shield before it is dropped. If the shield is made of heavy material it will be virtually unaffected by the surrounding flow of air. Supporting connections between the experimental package and the drag shield are such that the experiment is held at the top of the shield. Once the assembly is dropped, the experiment is free to move with respect to the shield. In a drop lasting only a few seconds, the relative motion between the experiment and the shield is so small that the extra space provided in the bottom of the drag shield ensures adequate slip motion.

Intermediate values of acceleration between 1 and 0 may be realized in a drop tower experiment by using a near-frictionless pulley and counter weights. Kotake (Ref. 4), for example, used this method to study nucleate boiling in a reduced gravity field.

Somewhat longer periods of free fall may be obtained in an airplane that is made to fly in a ballistic trajectory. The zero-gravity state is brought about by allowing the experiment to float freely within the body of the aircraft without allowing it to come into contact with the walls or any other part of the structure. The trajectory can be approximated to a parabolic arc with a vertical axis, and the flight parameters that affect the shape of the trajectory are a function of the airplane's aerodynamic characteristics such as maximum entry speed, Mach number, and minimum control speed. A free fall time of 20 s is not difficult to achieve with high-speed aircraft, but the time before the experimental package collides with a portion of the plane is generally much less and is strictly a function of the skill of the pilot. It is usually important to reduce longitudinal and lateral accelerations to zero before reducing the normal acceleration which causes the package to free float. Control by the pilot is achieved with instruments and mirrors to keep the experiment in the center of a free float area. Figure 2 shows some of the details involved in the Keplerian trajectory for a KC-135 airplane.

In some studies, rockets have been used to carry experiments on ballistic flights. Certain rockets, which have been designated as sounding rockets, have been developed into a group of rather widely applicable research tools since the first rocket-based observations of the solar ultraviolet spectrum were made in 1946. These rockets are relatively small but would be capable of carrying a battery experiment and instrumentation through a variety of positive and negative acceleration values, including a prolonged period of free fall, while traveling along a near-vertical trajectory.

## IV. Pseudo-Zero-G Investigations of Cells

The difficulty of performing zero-$G$ studies of electrode performance in batteries has led to alternative methods of demonstrating the importance of certain physical phenomena in what may be termed pseudo-zero-$G$ environments. In effect, natural convection at the surface of an electrode may be enhanced or suppressed by orienting the cell in different arrangements with respect to the earth's gravitational field. In one such arrangement, it is possible to virtually eliminate mass transfer by natural convection and one might expect that the results obtained in such a situation might be closely similar to those realized in a true zero-$G$ environment.

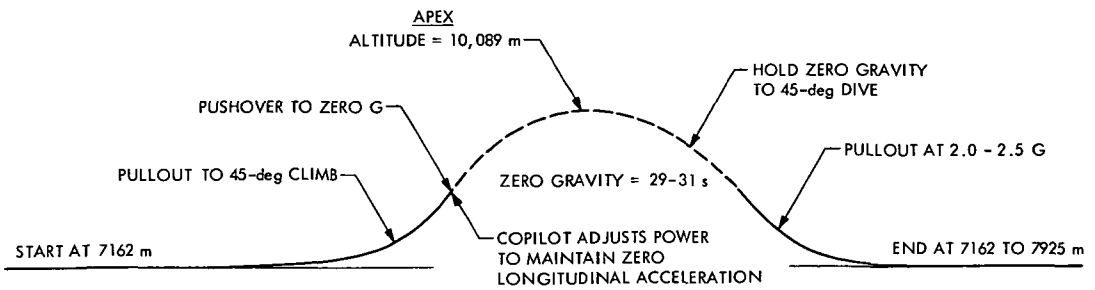


**Fig. 2. Keplerian trajectory for KC-135 airplane**

A study of this type has been performed by Eisenberg, Bauman, and Brettner (Ref. 5), who investigated the orientation effect on a smooth zinc electrode in a potassium hydroxide electrolyte. These authors demonstrated the importance of free or natural convection versus diffusion by means of measuring the time required to reach anode passivation at constant current, while the cell was oriented in one of three positions. The three orientations examined were as follows: (1) the cell electrodes were parallel to the earth's gravitational acceleration vector, (2) the cell electrodes were perpendicular to the vector, with the anode at the bottom of the cell, and (3) the cell electrodes were perpendicular to the vector, with the anode at the top of the cell.

The cell used in this study had a silver oxide cathode, a smooth zinc anode, and an electrolyte containing about 30% by weight of KOH. Two types of geometry were used. In one, the active anode area was 34.2 $cm^2$, and, in the other, the area was 28.5 $cm^2$. To avoid problems with gas bubbles from the cathode, a screen of nylon cloth was placed between the anode and cathode compartments. The zinc anode potential was determined with a standard Hg–HgO reference electrode. The authors measured the passivation time, which was defined as the time from closing of the switch until the time when passivation occurred. The flow of current was kept constant, and passivation was noted as happening when the anode polarization became very large.

Some of the results of this study are summarized in Fig. 3. Here we see that the time of anode passivation is a function of cell orientation. Maximum convection effects occur when the cell is oriented so that the anode is at the top of the cell and is perpendicular to the earth's gravitational field, because the products of the anode reaction make up a solution layer with a greater density than that of the bulk electrolyte solution. When the cell is turned over, there is no tendency for convective mixing to occur, and the system would act as if there were almost a total absence of free convection. In this latter case, the situation would be comparable to a zero-*G* environment.

When the anode is on the bottom of the cell, for low current densities, the time to reach anode passivation is shorter than for the other two cell orientations. Viewed another way, this would mean that in the absence of natural convection the limiting current would be much smaller and would be solely controlled by diffusion.

As the time to reach passivation is made very short (i.e., high current densities) all three curves in Fig. 3 approach a common curve or line. By a least-squares fit of data, the authors give

$$I = 0.0636 + 0.846\, t^{-1/2} \qquad (7)$$

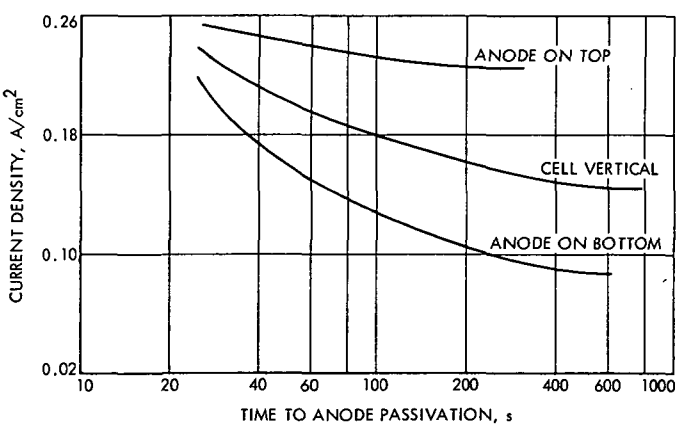


**Fig. 3. Effect of Zn anode orientation on limiting current density**

as a correlation which appears valid when the passivation time $t$ is less than 20 s. For passivation times in excess of 20 s, each of the three orientations results in a curve with a different slope. By extrapolating the curves or lines to $t \rightarrow \infty$, a limiting current value is obtained for each case, which is interpreted to be the maximum current density for which no passivation would occur regardless of time. It is suggested that this is perhaps the only way in which to visualize the concept of limiting current for a situation in which the electrode undergoes passivation. For the cases in which the anode is horizontal on top, is vertical, and is horizontal on the bottom, these three extrapolated values are respectively 0.228, 0.143 and 0.067 A/cm$^2$.

Another study involving mass transfer from horizontal electrodes has been performed by Fenech (Ref. 6). In this investigation, a free convection study was made using copper sulfate–sulfuric acid electrolyte and copper electrodes aligned perpendicular to the earth's gravitational field. Fenech found the following correlation:

$$Nu' = 0.129\,(Sc^{1.1}Gr)^{1/3} \tag{8}$$

in which, as previously stated, $Nu'$ is the dimensionless Nusselt number for mass transfer, $Sc$ in the dimensionless Schmidt number, and $Gr$ the dimensionless Grashof number. This relation would predict a limiting current relation of the form

$$I_L = I_{L(G=1)}\, G^{1/3} \tag{9}$$

which places a 1/3 rather than 1/4 power dependence on $G$. The difference in these two functions is seen in Fig. 4. The 1/3 power function, as compared with the 1/4 power form, predicts higher limiting currents for values of $G$ greater than 1 and smaller values for cases in which $G$ is less than 1.

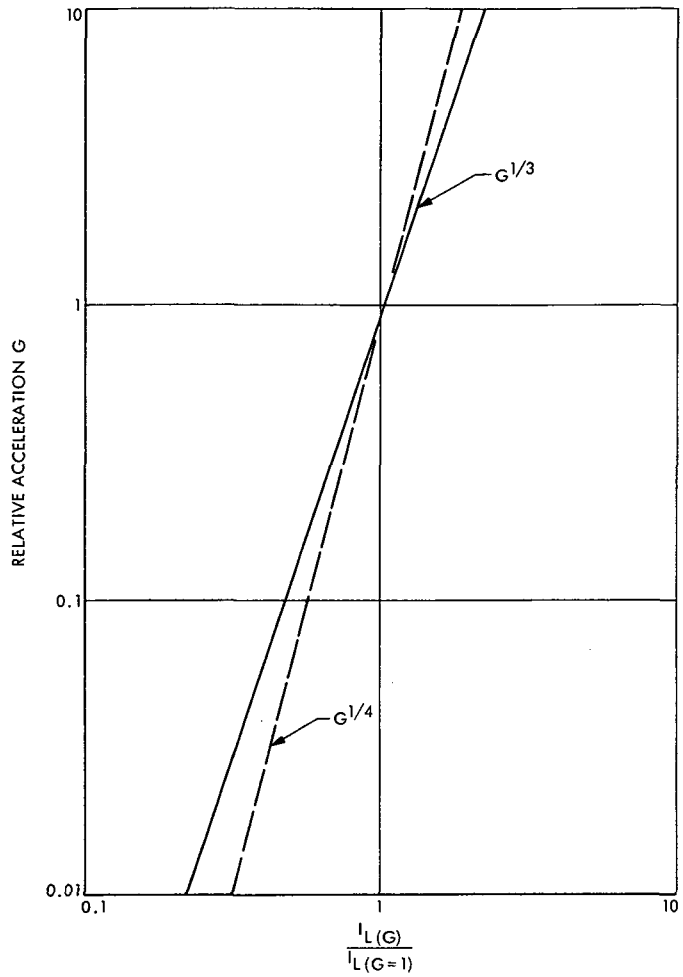


**Fig. 4. Dependence of limiting current density on relative acceleration**

## V. Limiting Current Densities Between Electrodes Without Separators

In order to understand the effect of the electrolyte on the limiting current density between two electrodes, Divine (Ref. 7) studied the behavior of the system $CuSO_4$–$H_2SO_4$–$H_2O$ between copper electrodes. The electrolyte was completely free to move between the electrodes, which were of various length, width, and separation. In order to vary $G$, the relative acceleration, the cells were mounted in a centrifuge with appropriate slip-ring attachments. The copper sulfate system was chosen since all of the physical properties of this system had previously been determined.

A theoretical analysis of the system by Divine resulted in the following relation:

$$I_L = \frac{16F\,D_1C_1}{3}\left\{\frac{g_0G\,C_1\left[\dfrac{\partial \ln \rho}{\partial C_{CuSO_4}} - \left(\dfrac{e^2}{3}\right)\left(\dfrac{\partial \ln \rho}{\partial C_{H_2SO_4}}\right)\right]}{(1-t_1)120\,H\,D_1\left[\upsilon + 12.5(1-t_1)D_1e^2\left(\dfrac{4}{3} - e + \dfrac{e^2}{5}\right)\right]}\right\}^{1/4} \tag{10}$$

where $I_L$ is the limiting current density, F is Faraday's constant, $D$ is the diffusivity, $C$ is the concentration, $g_0$ is the gravitational acceleration constant, $G$ is the relative acceleration, $\rho$ is the density of the electrolyte, $H$ is the electrode length, $\upsilon$ is the kinematic viscosity, $t$ is the transference number, and the subscripts 1 and 2 refer to $Cu^{++}$ and $H^+$ respectively. The symbol $e$ is defined by

$$\frac{2t_2}{5(1-t_1)} = e\left(\frac{e}{3} - \frac{1}{3} + \frac{1}{6e} - \frac{1}{30e^2}\right) \qquad (11)$$

To obtain these results, Divine assumed appropriate velocity and concentration profiles and applied Pohlhausen's method to von Karman's integral equations, which allowed him to integrate the mass and momentum equations.

The relation obtained differs from one previously derived by Wagner (Ref. 2) by the factor

$$\left\{\frac{\upsilon}{(1-t_1)\left[\upsilon + 12.5(1-t_1)D_1e^2\left(\frac{4}{3} - e + \frac{e^2}{5}\right)\right]}\right\}^{1/4}$$

which is approximately equal to unity.

The major assumptions made in this derivation are:

(1) Infinite electrode spacing (that is, the electrodes do not influence one another).

(2) No end or edge effects.

(3) Constant physical properties of the electrolyte except in the buoyancy term.

(4) Attainment of limiting current without detrimental effects from hydrogen evolution.

(5) The electrolyte is an ideal solution.

Experimentally, Divine obtained the limiting current density for each case by plotting the current density $I$ versus the cathode polarization $\eta$ and choosing the limiting current density to be that value which gave $dI/d\eta = 0$.

Data were collected for various electrolyte concentrations, various electrode lengths, and variable electrode separations. Plots of the limiting current density versus relative acceleration are given in Figs. 5–13 and the results are compared with Eq. (10). Although, in some of the figures, the data appear to be slightly unpredictable, the agreement of the experiments with Eq. (10) is quite good. The variation of the limiting current density with the relative acceleration is seen to follow the 1/4 power dependence within experimental error.

The effect of electrode separation is best seen for the longer electrode lengths. Figure 14 shows a plot of limiting current density versus electrode length for an electrolyte containing 0.0505 M $CuSO_4$. The parameters shown are relative acceleration and electrode separation. From this figure, one can see that deviations from the 1/4 power dependence seem to occur for the longer electrodes and the small electrode spacings. Based on this plot, one might expect that batteries with tightly fitted electrodes might show a different power dependence on the relative acceleration. Such variation must occur due to changing flow patterns which result as the two electrode surfaces are brought close to each other.

## VI. Gravitational Effects in Porous Media

The composition between electrodes in the cells of commercial batteries can, in general, be described as a two-phase porous structure; that is, the electrolyte is held in place by absorption in a battery separator or some other porous medium. Since gravitational or acceleration forces primarily affect natural or free convection, one might expect additional complications for a situation in which such free convection patterns were already disturbed by the presence of two-phase media.

Intuitively one might suspect that gravitational effects on the limiting current of a cell might be small or not important if the electrolyte were held in place by a porous matrix. It would seem that the capillary and surface tension forces might override density differences and thus make it difficult to notice gravity or acceleration forces.

As a test, Divine (Ref. 7) studied a model which consisted of two parallel electrodes separated by a space filled with small glass beads and electrolyte. Experimentally he found that the significant geometrical variables included the following: (1) the electrode length and spacing, (2) the concentration of the electrolyte, and (3) the diameter of the beads.

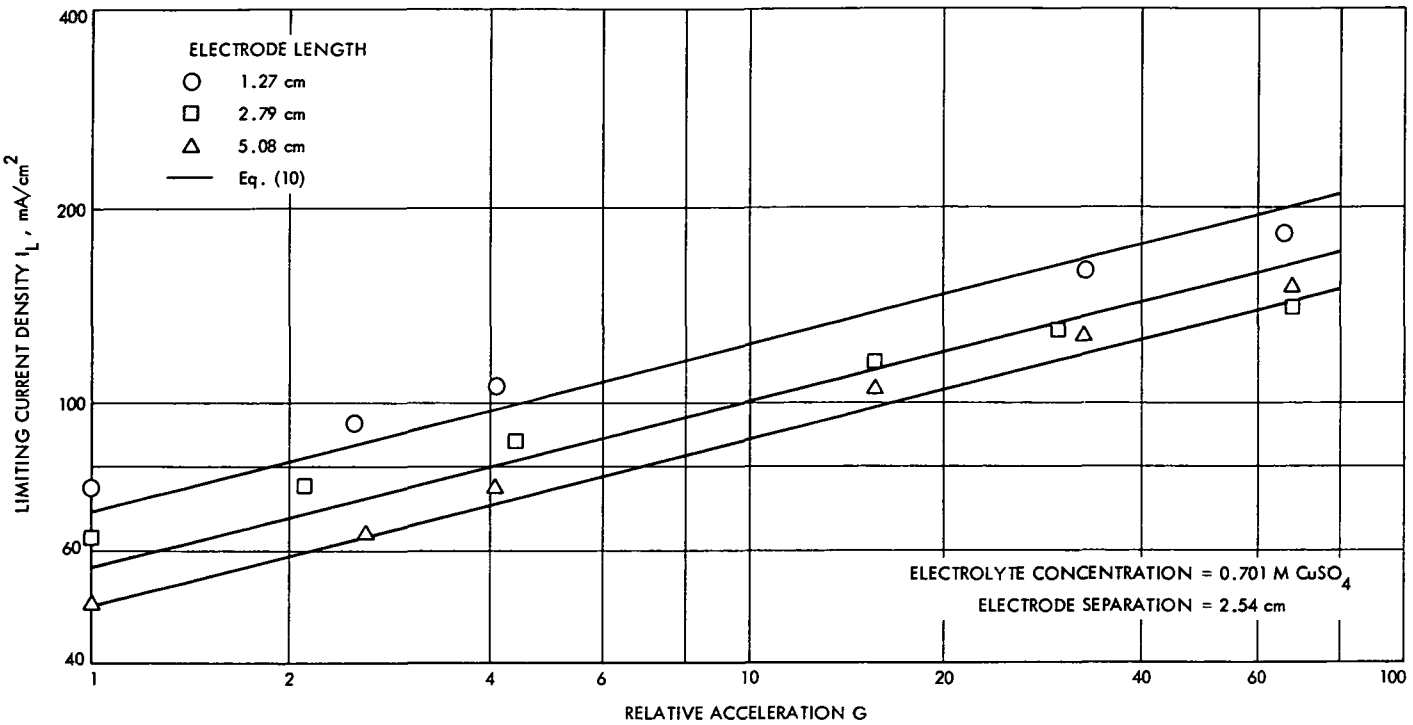


**Fig. 5. Limiting current density, corrected to 22°C, vs relative acceleration (2.54-cm electrode separation, 0.701 M $CuSO_4$ electrolyte concentration)**

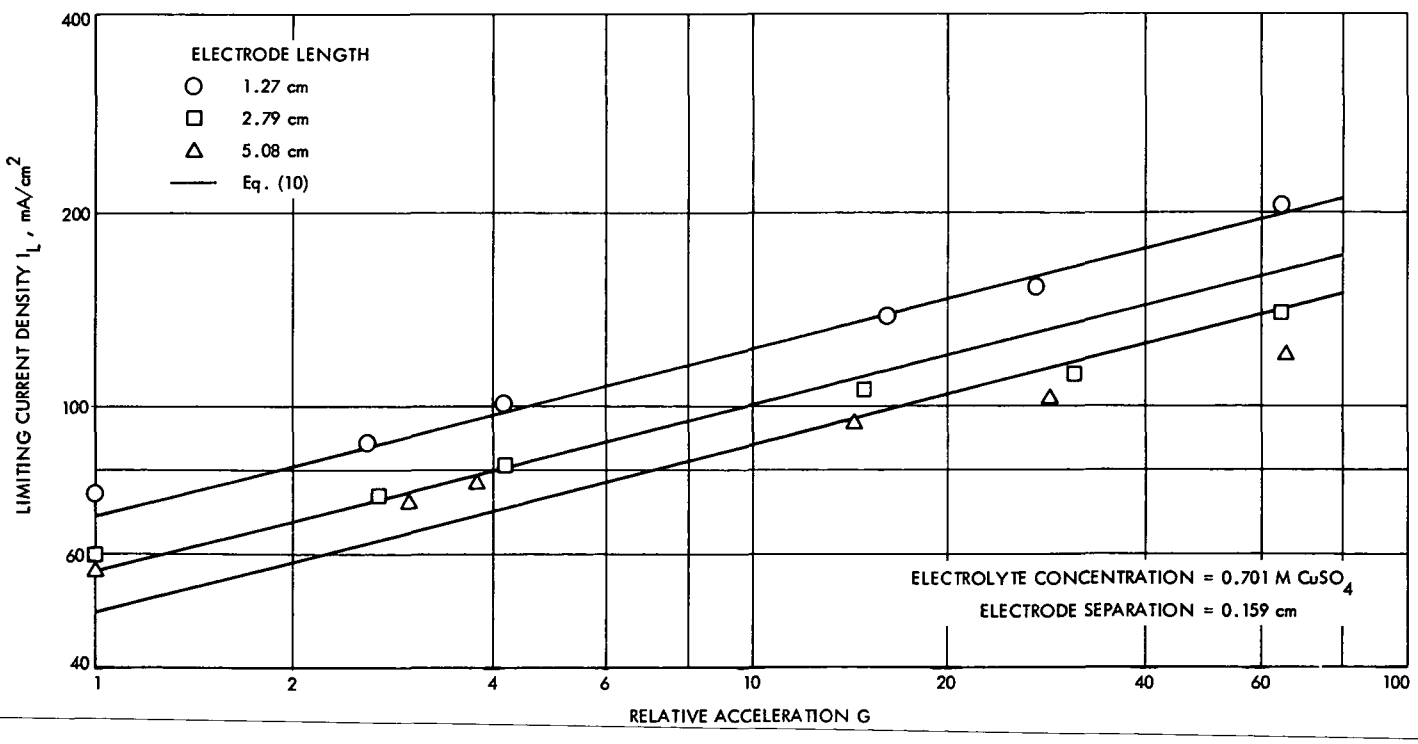


**Fig. 6. Limiting current density, corrected to 22°C, vs relative acceleration (0.159-cm electrode separation, 0.701 M $CuSO_4$ electrolyte concentration)**

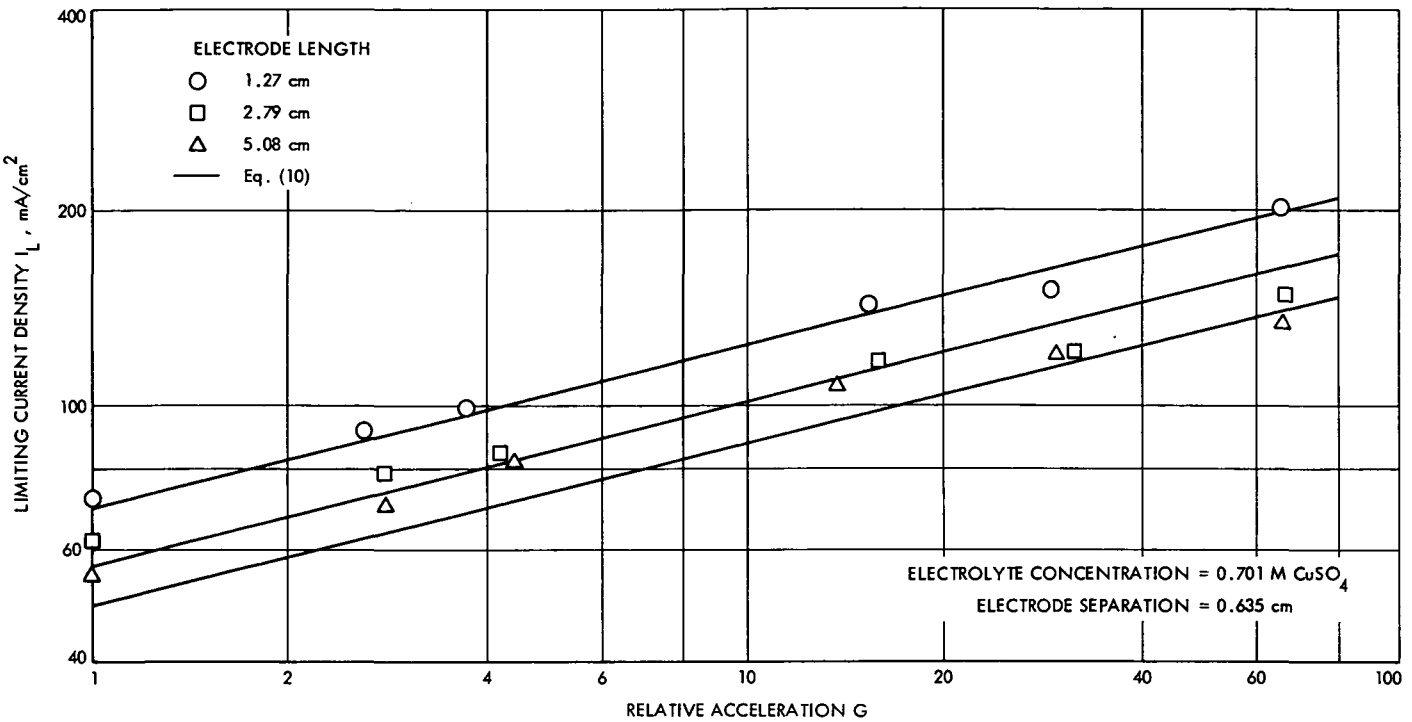


**Fig. 7. Limiting current density, corrected to 22°C, vs relative acceleration (0.635-cm electrode separation, 0.701 M $CuSO_4$ electrolyte concentration)**

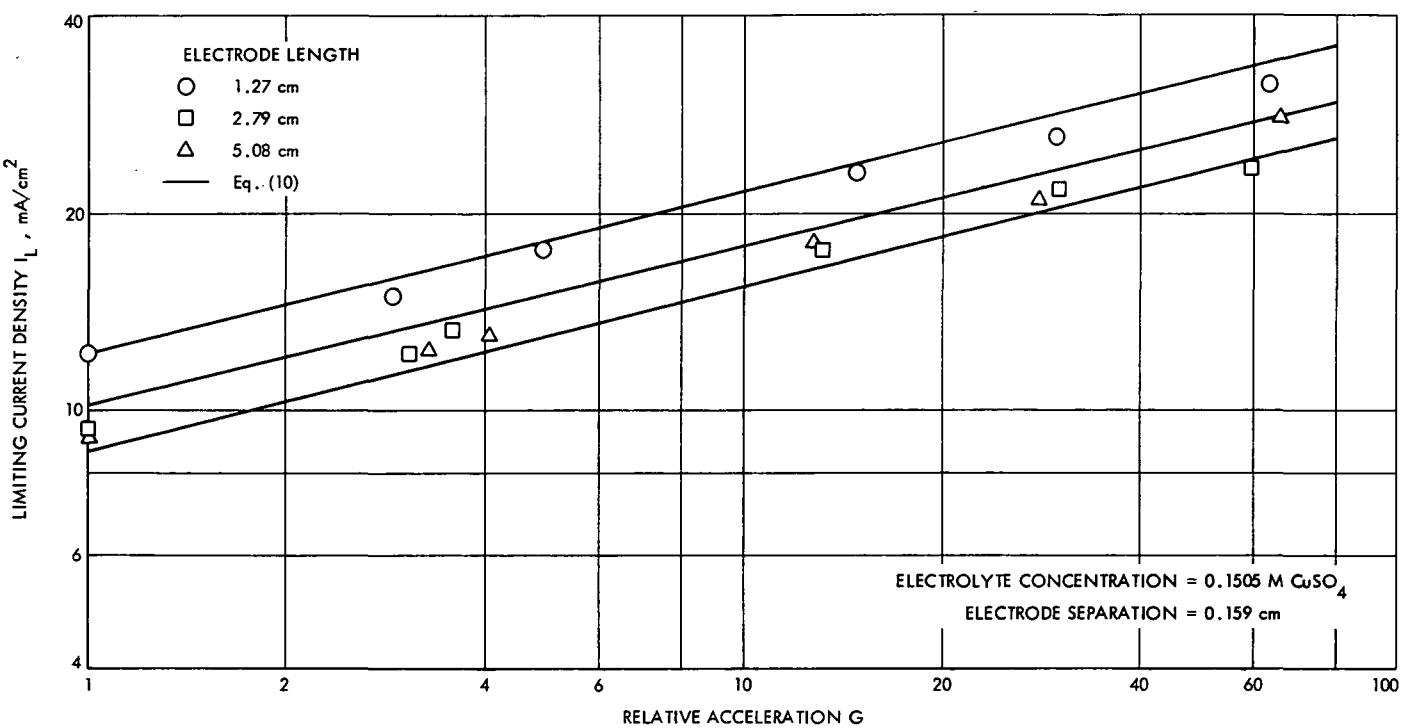


**Fig. 8. Limiting current density, corrected to 22°C, vs relative acceleration (0.159-cm electrode separation, 0.1505 M $CuSO_4$ electrolyte concentration)**

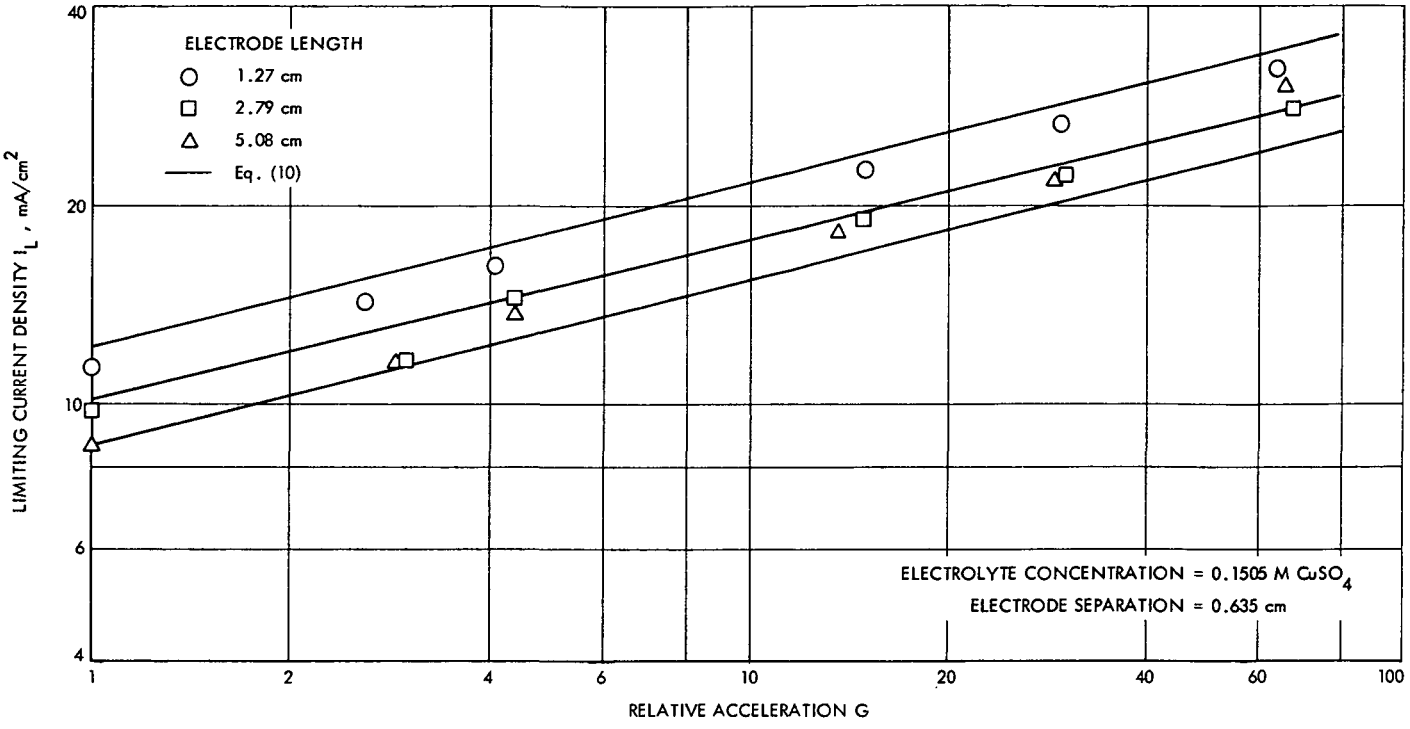


**Fig. 9. Limiting current density, corrected to 22°C, vs relative acceleration (0.635-cm electrode separation, 0.1505 M $CuSO_4$ electrolyte concentration)**

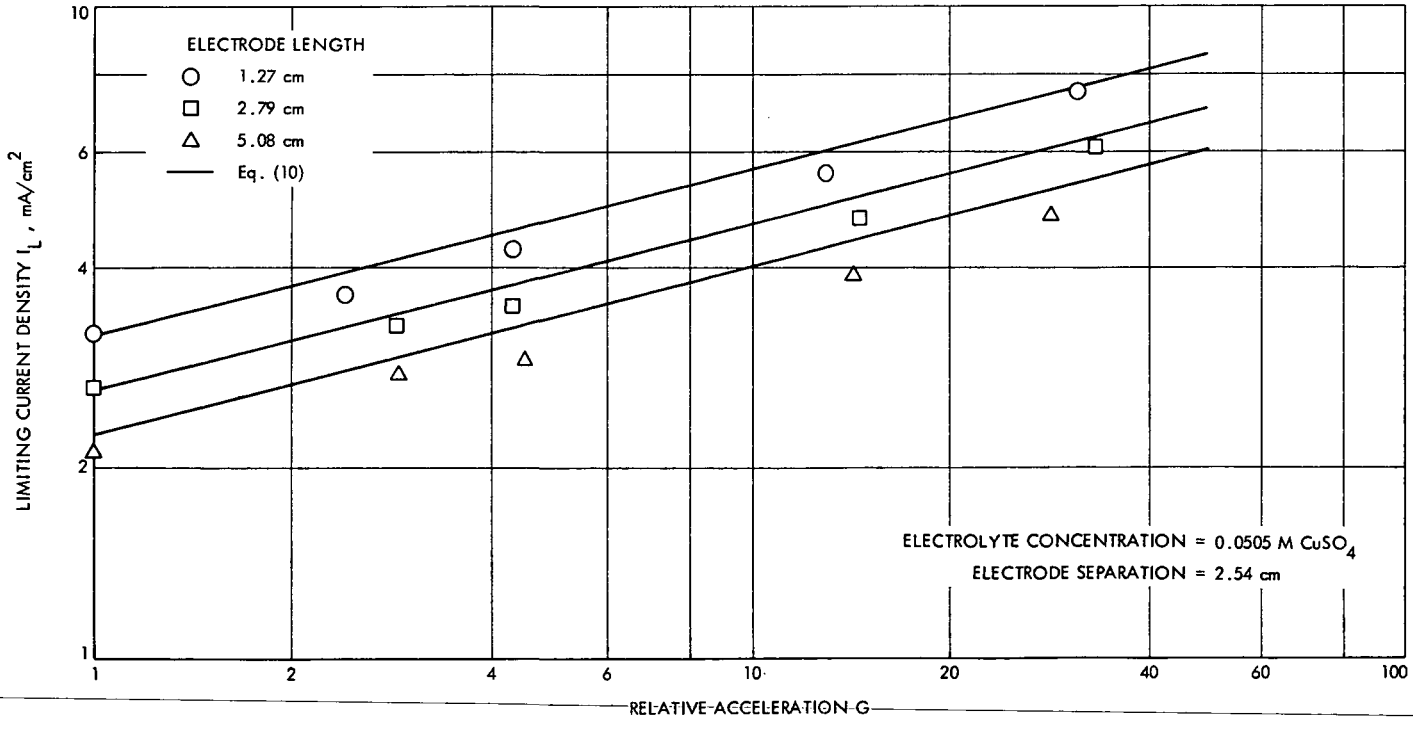


**Fig. 10. Limiting current density, corrected to 22°C, vs relative acceleration (2.54-cm electrode separation, 0.0505 M $CuSO_4$ electrolyte concentration)**

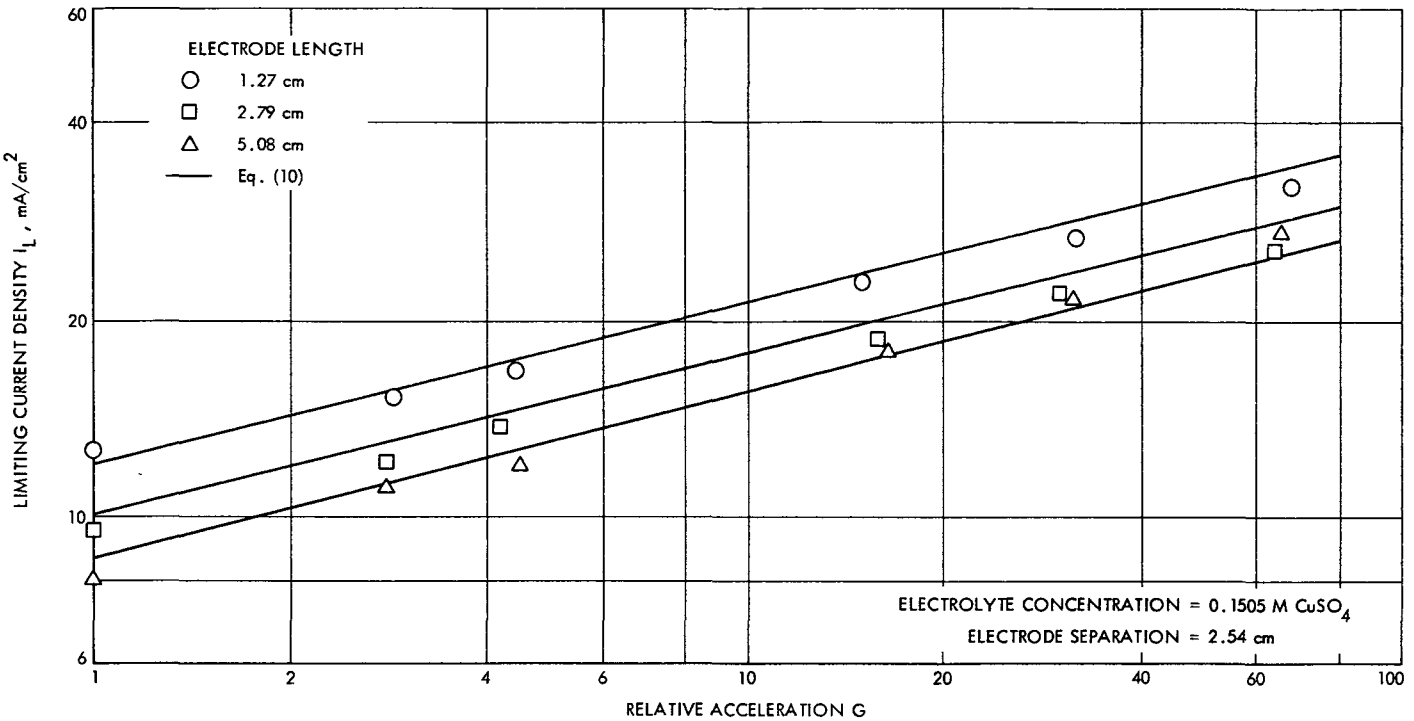


**Fig. 11. Limiting current density, corrected to 22°C, vs relative acceleration (2.54-cm electrode separation, 0.1505 M $CuSO_4$ electrolyte concentration)**

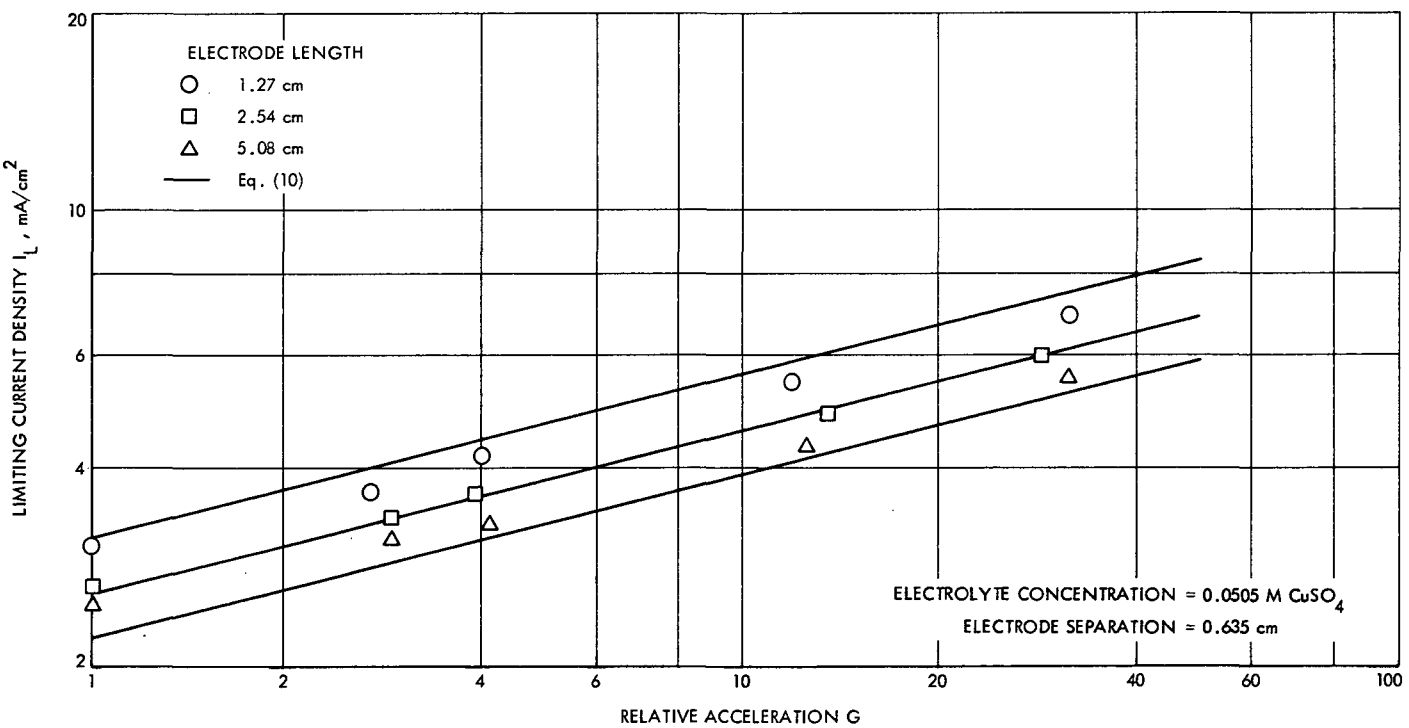


**Fig. 12. Limiting current density, corrected to 22°C, vs relative acceleration (0.635-cm electrode separation, 0.505 M $CuSO_4$ electrolyte concentration)**

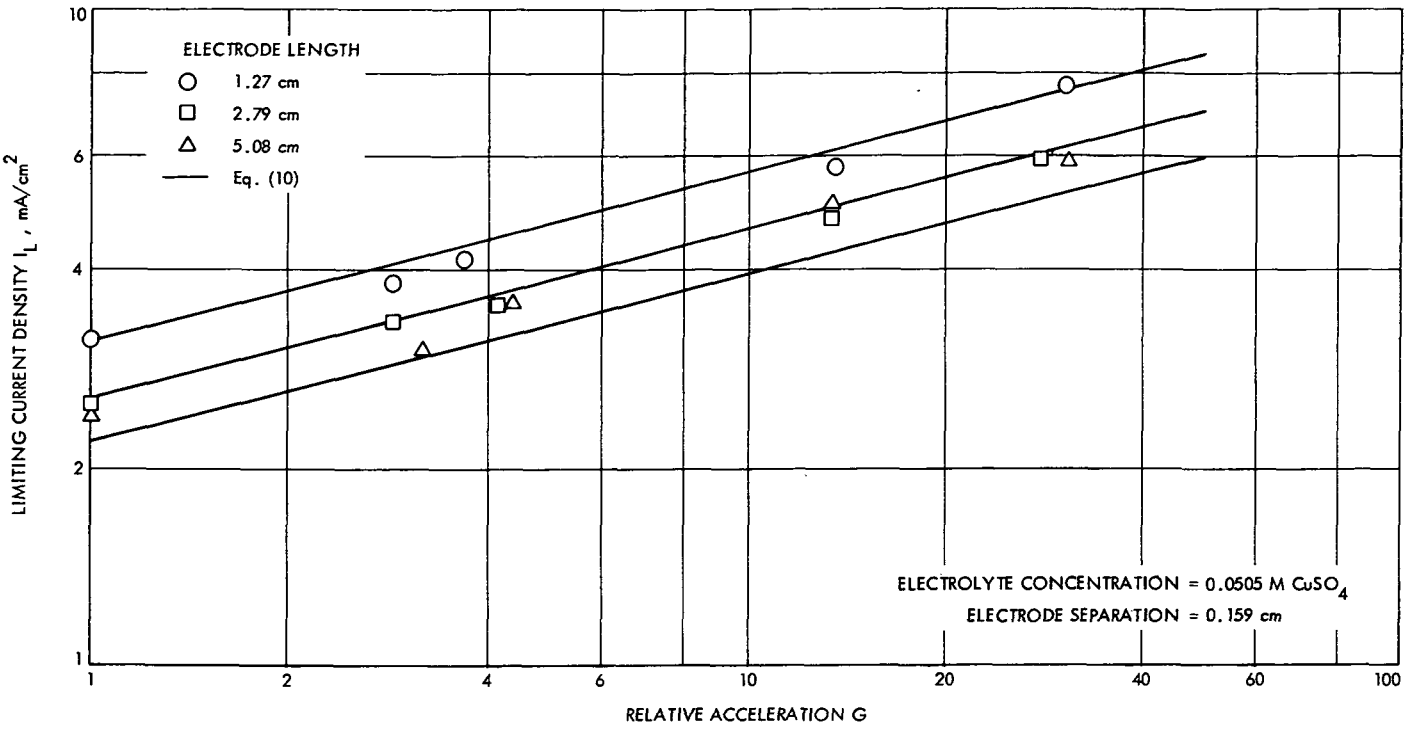


**Fig. 13. Limiting current density, corrected to 22°C, vs relative acceleration (0.159-cm electrode separation, 0.0505 M $CuSO_4$ electrolyte concentration)**

Just as in his studies on free electrolyte, Divine used copper electrodes and a copper sulphate electrolyte. By driving the electrodes with an external EMF while the cells were subjected to acceleration forces in a centrifuge, Divine measured the limiting current density that could be realized with each type of cell geometry.

Divine found that his porous structure behaved differently from a system which contained only free electrolyte between electrodes, as long as the diffusion boundary layer thickness was larger than about 1/15 of the diameter of the beads. If the boundary layer thickness was smaller than this factor, he found that the system behaved similarly to a cell containing only free electrolyte. Small effective values for the boundary layer thickness could be obtained by (1) increasing the concentration of the electrolyte, (2) increasing the size of the beads, and (3) increasing the acceleration forces.

For cases in which the boundary layer thickness was large compared with the diameter of the beads, i.e., greater than 1/15 of the diameter of the beads, it appeared that the limiting current was a rather complicated function of $G$ with a power dependence larger than the 1/4 factor predicted by Eq. (4). Indeed, the power dependence seemed to range upward from the 1/4 factor and approached a value as high as 2/3, depending upon a number of other system variables.

The data for this study are presented in Figs. 15–21. The parameters noted in these figures include the electrode length, the electrode spacing or separation, the electrolyte concentration, and the size of the beads.

A more detailed description of the apparatus and additional experimental details for this study are given in Appendix A.

## VII. Observed Battery Abnormalities in Zero-G Environment

Although many batteries have been employed in space flights during the past decade, seldom has any unusual battery behavior been attributed to zero-G effects, probably because most of these batteries have greater capacities than are actually required. Thus the batteries are not driven to anywhere near a point of limiting current where zero-G effects might be noted. Some interesting "space effects" did occur, however, with some of the batteries on the Apollo 7 flight, which orbited the earth in 1968. These anomalies are discussed below.

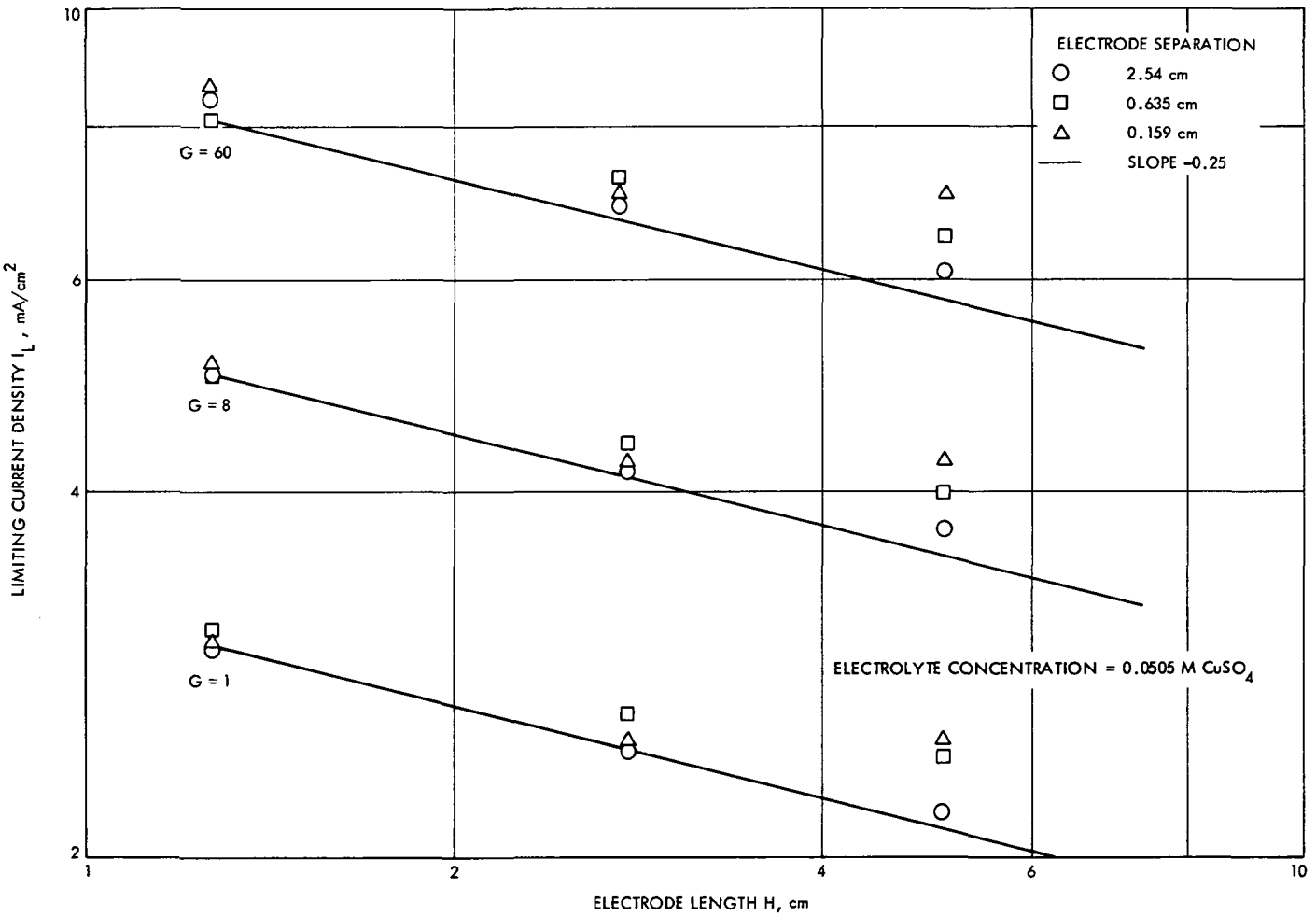


**Fig. 14. Limiting current density, corrected to 22°C, vs electrode length**

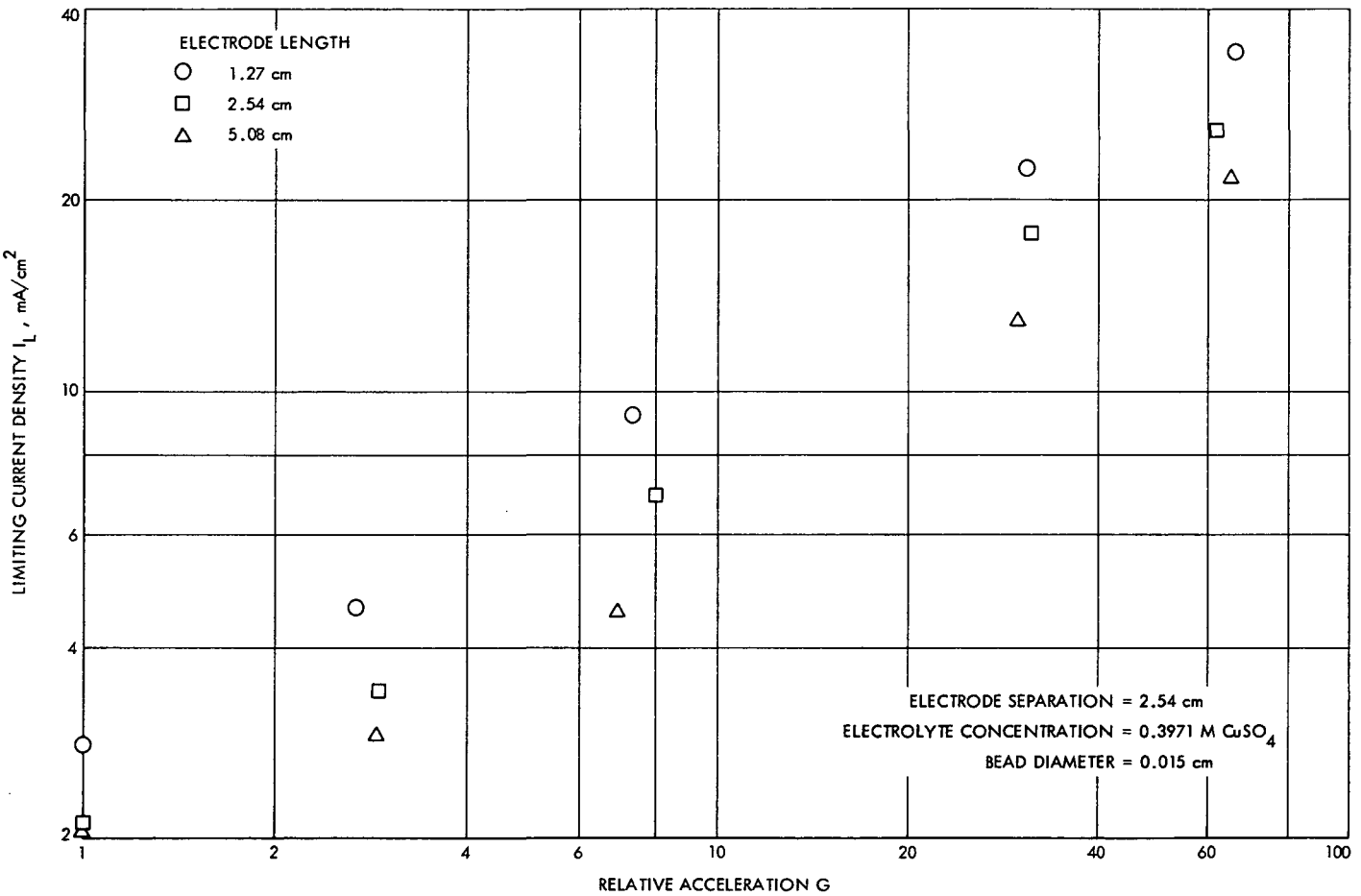


**Fig. 15. Limiting current density vs relative acceleration in porous media (2.54-cm electrode separation, 0.3971 M $CuSO_4$ electrolyte concentration, 0.015-cm-diameter beads)**

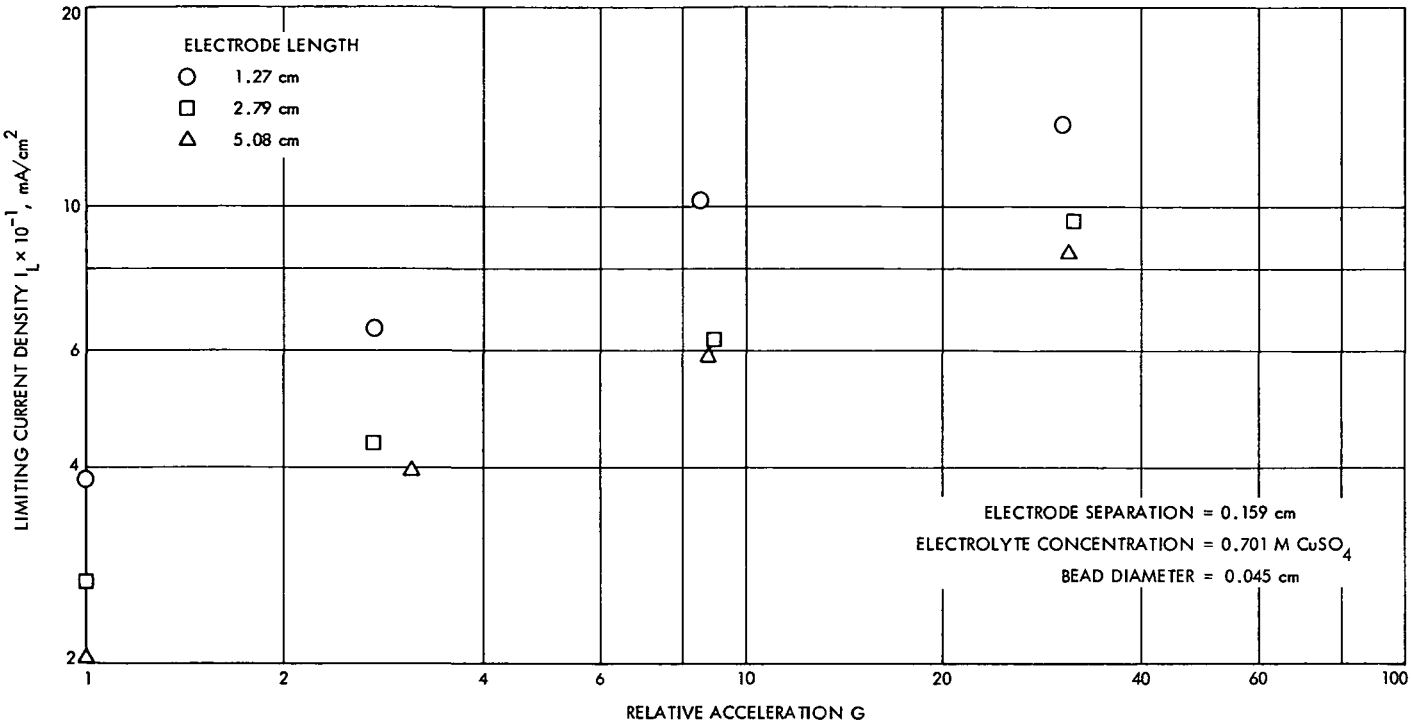


**Fig. 16. Limiting current density vs relative acceleration in porous media (0.159-cm electrode separation, 0.701 M $CuSO_4$ electrolyte concentration, 0.045-cm-diameter beads)**

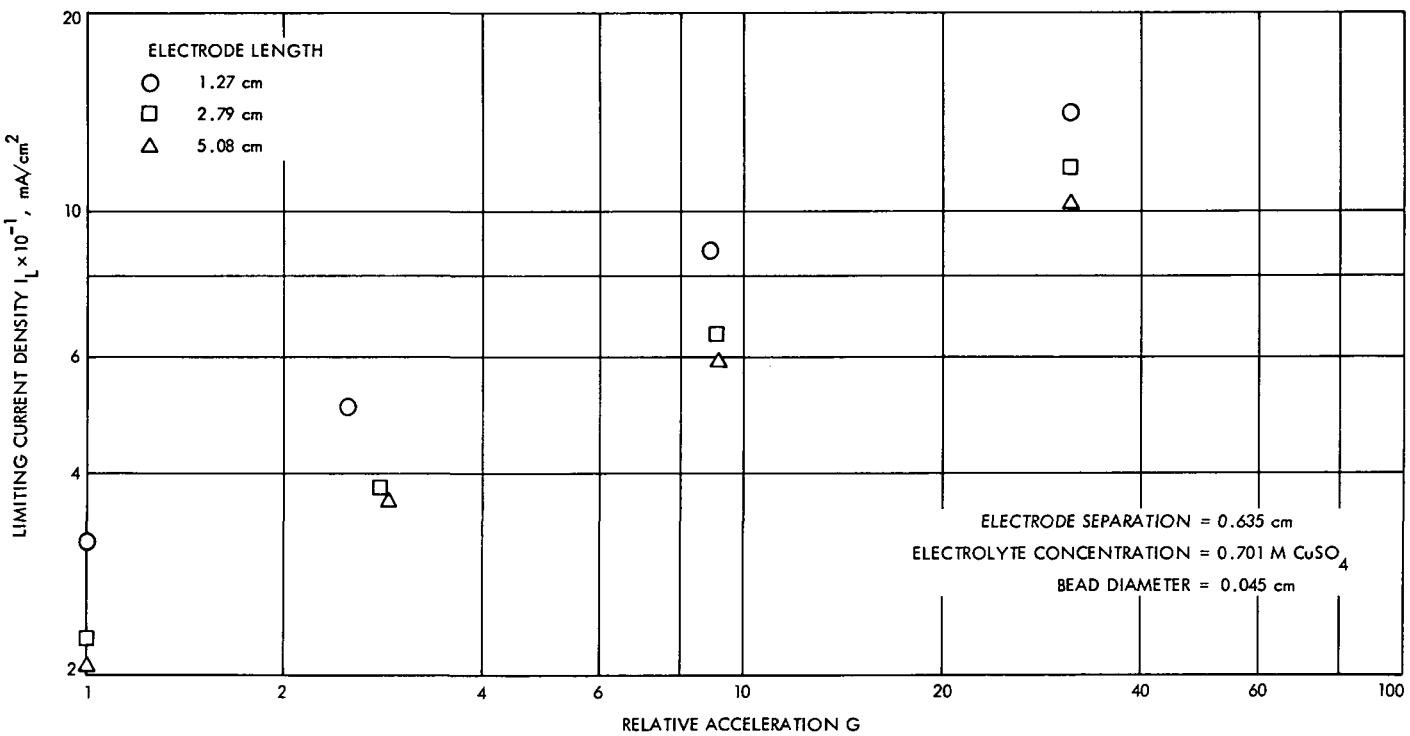


**Fig. 17. Limiting current density vs relative acceleration in porous media (0.635-cm electrode separation, 0.701 M $CuSO_4$ electrolyte concentration, 0.045-cm-diameter beads)**

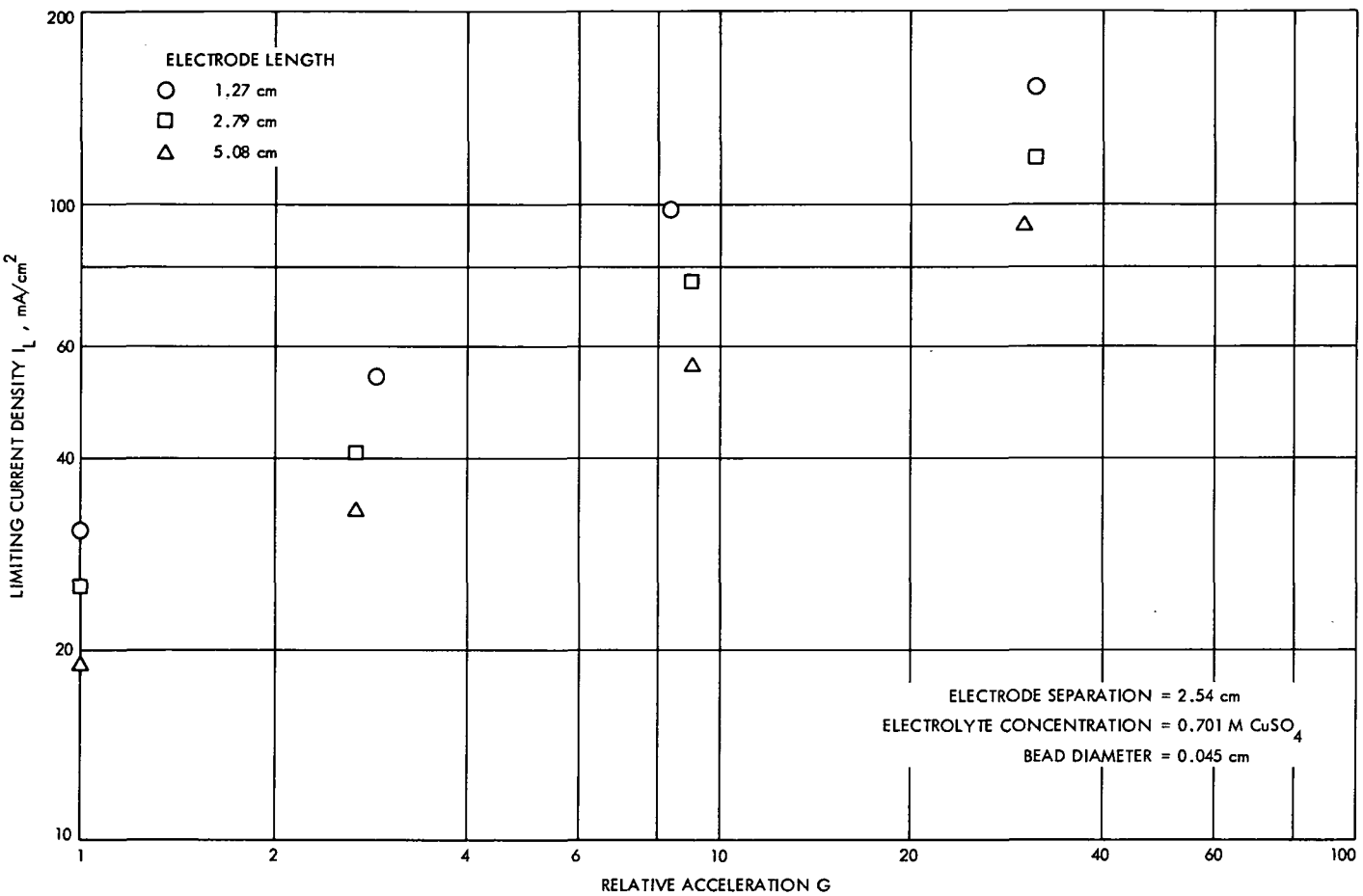


**Fig. 18. Limiting current density vs relative acceleration in porous media (2.54-cm electrode separation, 0.701 M $CuSO_4$ electrolyte concentration, 0.045-cm-diameter beads)**

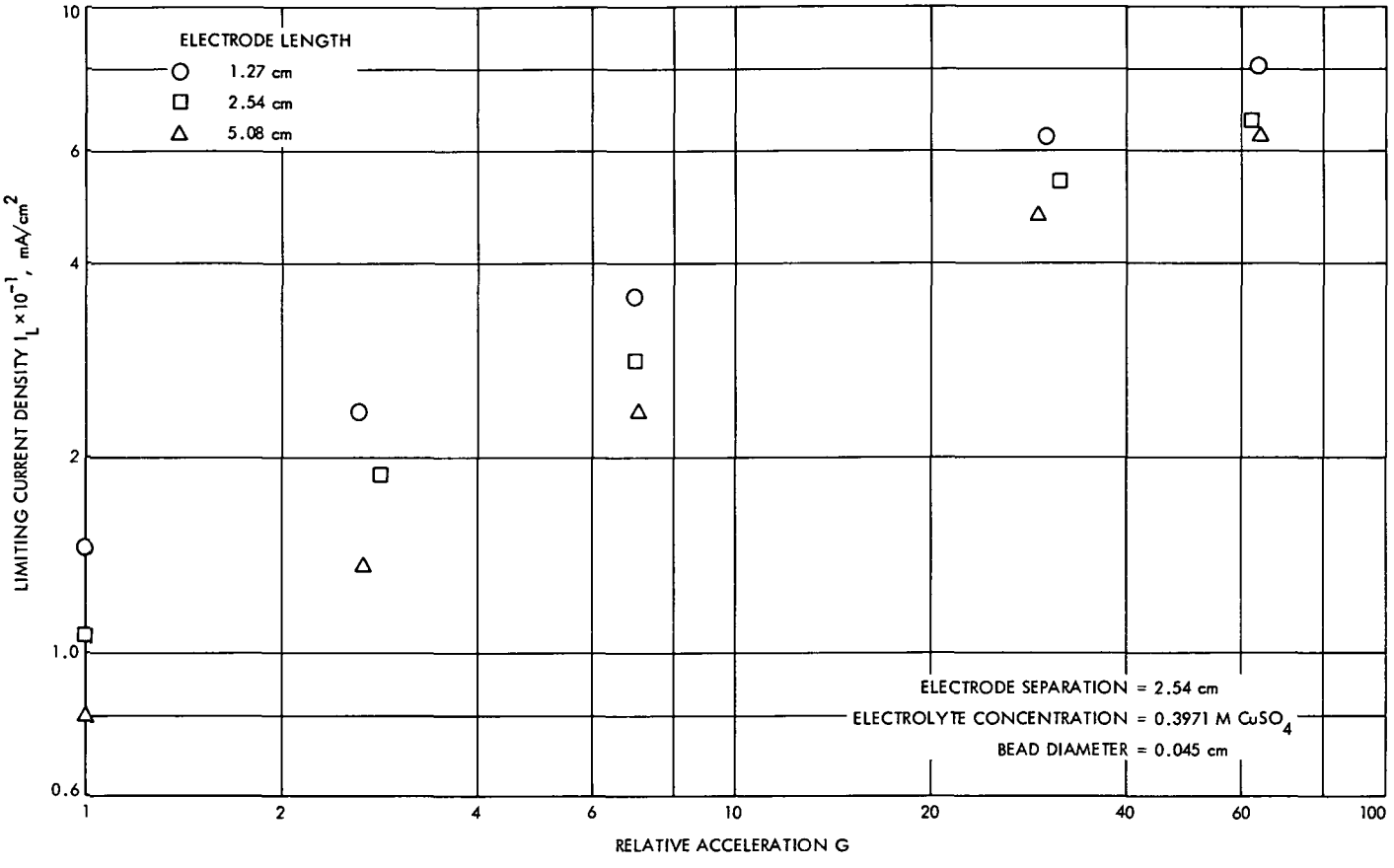


**Fig. 19. Limiting current density vs relative acceleration in porous media (2.54-cm electrode separation, 0.3971 M $CuSO_4$ electrolyte concentration, 0.045-cm-diameter beads)**

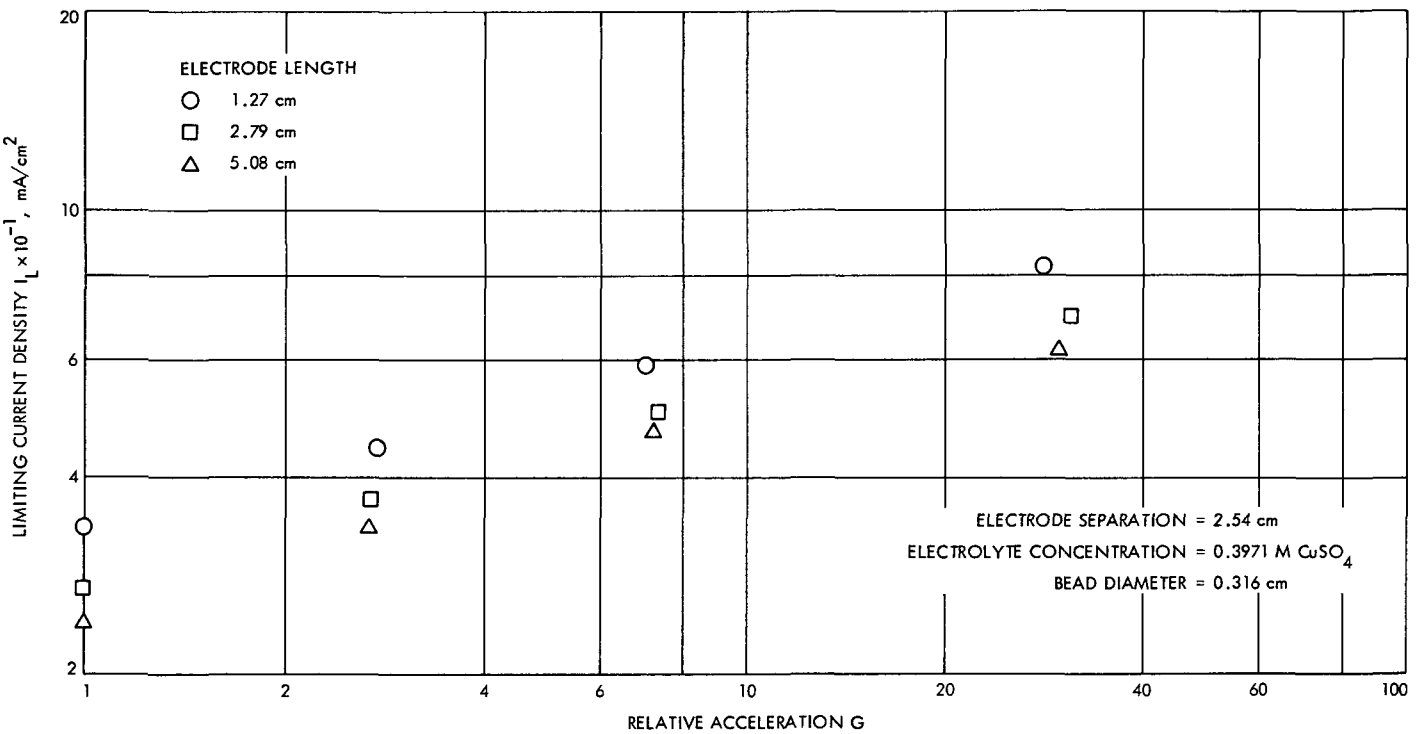


**Fig. 20. Limiting current density vs relative acceleration in porous media (2.54-cm electrode separation, 0.3971 M $CuSO_4$ electrolyte concentration, 0.316-cm-diameter beads)**

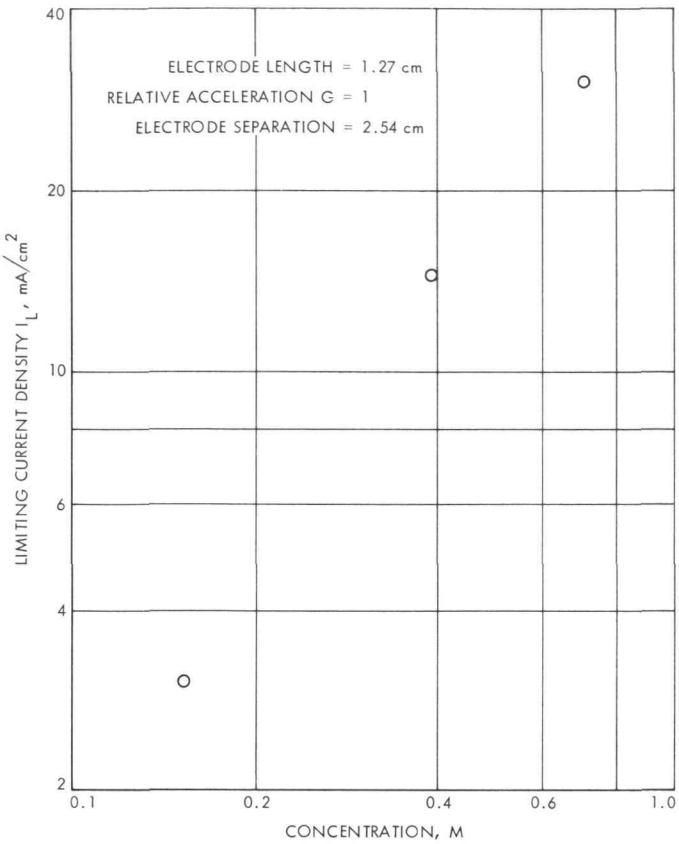


**Fig. 21. Limiting current density vs electrolyte concentration in porous media**

During the flight of the Apollo 7 capsule, five anomalies were noted in the performance of its batteries. In the postflight examination, some of the anomalies were either directly or indirectly attributed to zero-G effects. The situation, as revealed by I. K. Young of the North American Rockwell Corporation, is detailed in the following paragraphs.

In the space capsule of the Apollo 7 vehicle, there were three 40-A-h batteries, each yielding a nominal voltage of 29 V and each consisting of 20 silver–zinc cells. These units, called entry batteries, were designated as A, B, and C. Also aboard the capsule were two smaller batteries to supply power to various pyrotechnic devices. Each of these latter batteries had 20 silver–zinc cells, a capacity of 3/4 A-h, and an output of 29 V. These units were named pyro-batteries and, aside from the number and size, differed from entry batteries primarily in that the two sets of batteries employed different types of battery separators.

Each of the entry batteries had relief valves on each of their cells which were designed to open at a differential pressure of $2.069 \pm 0.345 \times 10^5$ N/m$^2$. Any discharge from the cells, when these valves were open, went into a manifold and to an overboard vent via a common pressure transducer and a normally closed valve. This same overboard vent also served the vehicle's waste management system via another normally closed valve.

At the beginning of the flight, the entry batteries were initially fully charged. At the time the capsule was inserted into the earth's orbit, batteries A and B would be discharged by 8 to 12 A-h, depending upon the energy required during the launch holds. Throughout the flight, batteries A and B would be discharged in supporting the capsule's fuel cell during peak energy demands and would also be used in low load sensing functions. These two batteries were to be recharged from the fuel cell between 8 and 24 h after launch. It was planned that battery C would be on standby during most of the mission and it would be connected to the other two batteries during re-entry when the capsule would be separated from the fuel cell. The three batteries would thus supply all of the power required by the capsule while it was awaiting pickup from the ocean.

The five anomalies observed on this flight affected only the entry batteries. In brief, they were as follows:

(1) Anomaly I. Batteries A and B were unable to be recharged adequately. After 48 h into the mission, only 4½ A-h of charge could be given to battery A, although by this time 9 A-h had been removed. In a like manner, battery B would accept only 2½ A-h after 70 h of operation, at which time it had given up 11 A-h.

(2) Anomaly II. After the command module had separated from the service module, a low voltage was shown by the commoned A, B, and C batteries. On a 70-A load the reading was 26.2 V. This reading should have been between 27.5 and 29.0 V.

(3) Anomaly III. Batteries A and B had capacity losses which could not be accounted for by their known charge and discharge cycles.

(4) Anomaly IV. The open-circuit voltage of battery C dropped from 37.0 to 36.0 V in approximately 11 days. The only drain on this battery was an occasional 2 mA needed to monitor its own readings. Such a voltage drop is not typical for silver–zinc batteries.

(5) Anomaly V. Fluid was found in the battery manifold after the flight. The liquid was a mixture of urine, from a misuse of the vehicle's waste management system, and potassium hydroxide solution from the electrolyte of the batteries. The fluid analyzed was 42% urine and 58% electrolyte.

A postflight examination of the batteries and charging unit revealed that there had been a gas leak from the cabin to the battery manifold and that the charger circuit resistance was greater than that used in establishing charging procedures. It was also found that the charger output voltage was at the low end of its specified tolerance.

Since silver–zinc batteries are known to gas under charge, discharge, or upon standing, it was postulated that such gas might have decreased the effective surface area of the active plates in the batteries, leading to an increased battery impedance. Such an event might explain anomalies I, II, and III. The fact that the pyro-batteries were not affected was attributed to their use of cellophane separator material which swells considerably, keeping the battery tightly packed and giving very little space for bubble growth. The entry batteries used Permion for separators and this material swells less than cellophane.

The investigators in this study concluded that the batteries did not accept a normal charge during the mission because of low charger output voltage. The consequent low state of charge and deficient capacity at command module–space module separation was considered to be the most likely cause of the voltage decay noted on Battery C. It was also concluded that the higher interval impedances might have been the result of a zero-G effect (Ref. 8).

## VIII. Test Equipment for Space Studies

Under a contract issued in 1968 by the Jet Propulsion Laboratory, the General Electric Research and Development Center untertook a one-year program which had the objectives of designing and fabricating a test system that would be capable of reporting the behavior of silver–zinc batteries during flight in a near-zero-G environment.

The assignment was broken down into the following three tasks:

(1) Measure the resulting limiting current densities on smooth zinc anodes so that a maximum correlation could be obtained with the 1- to 20-G data previously obtained by Arcand (Ref. 9).

(2) Investigate bubble formation on electrodes in near-zero-G flight and ascertain the effects on battery performance.

(3) Measure cell capacity in a secondary battery as a function of charge–discharge cycling in near-zero-G flight.

The resulting breadboard units were designed so that a minimal amount of change would be required in adapting the system to flight hardware. Typical elements are shown in photos of the complete system (Fig. 22) and cells employed for the first task are shown in Figs. 23 and 24.

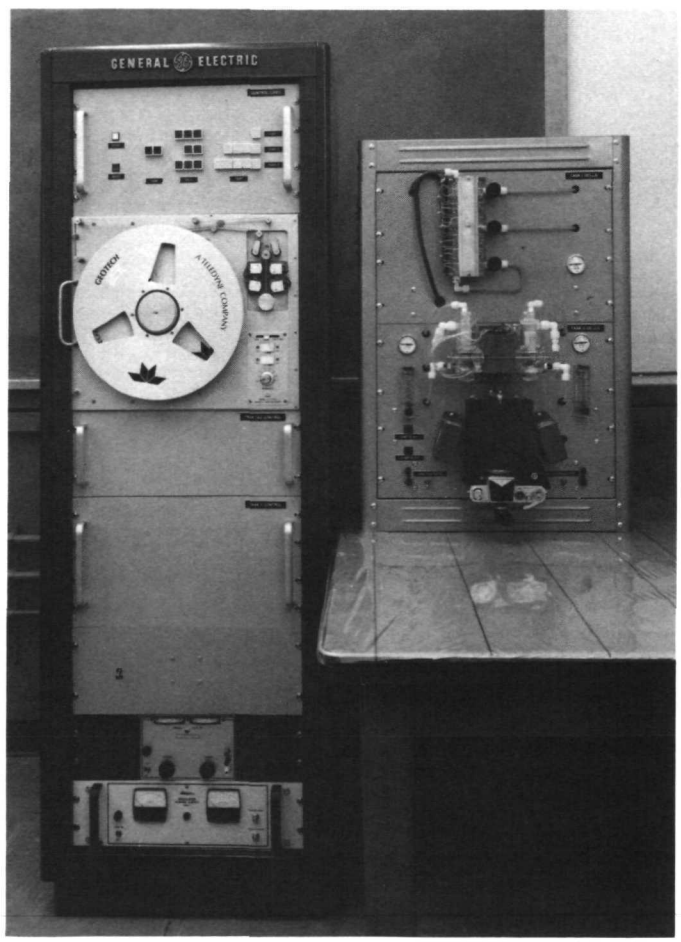


**Fig. 22. Complete breadboard unit, reduced gravity test equipment**

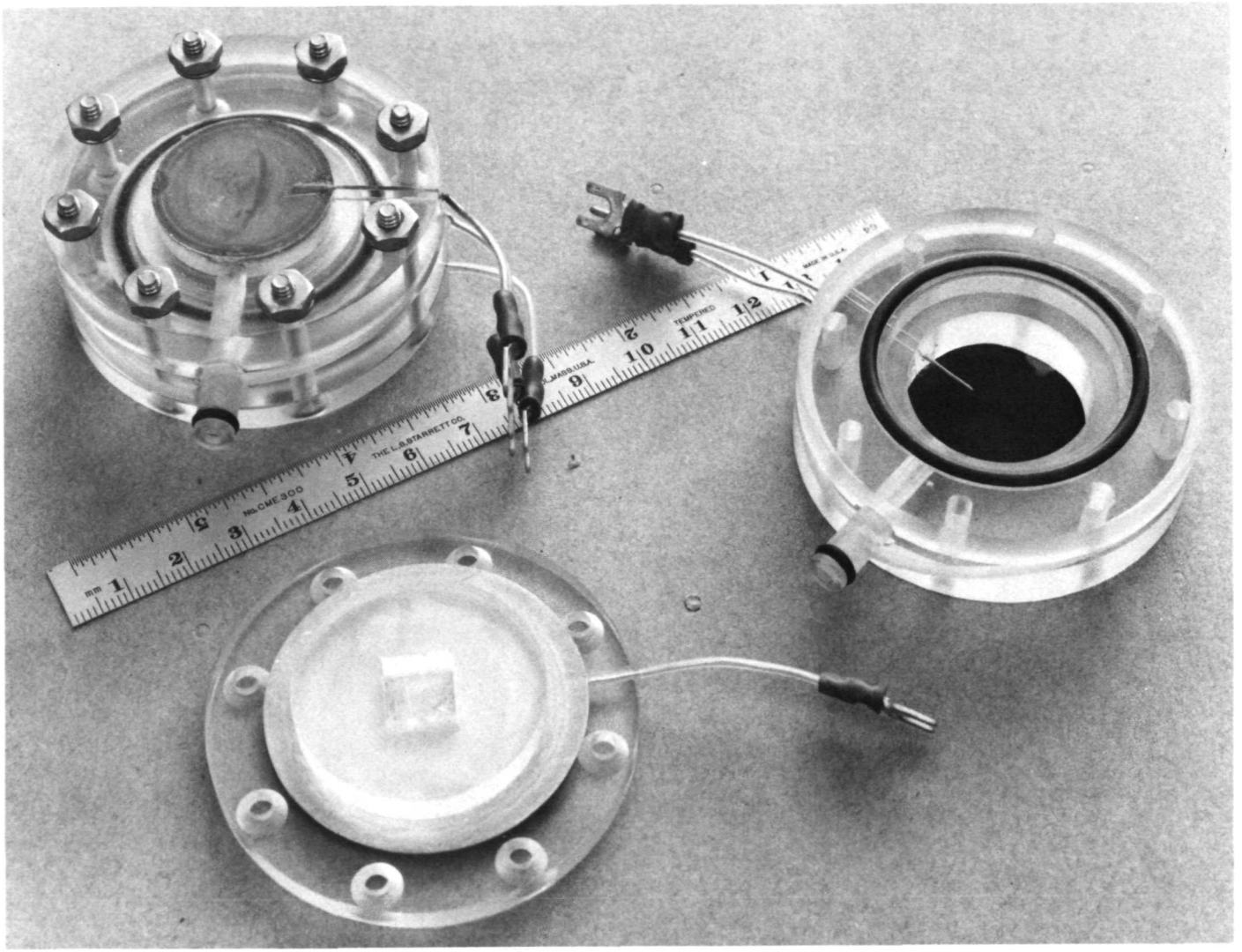


Fig. 23. Task 1 cell assembly

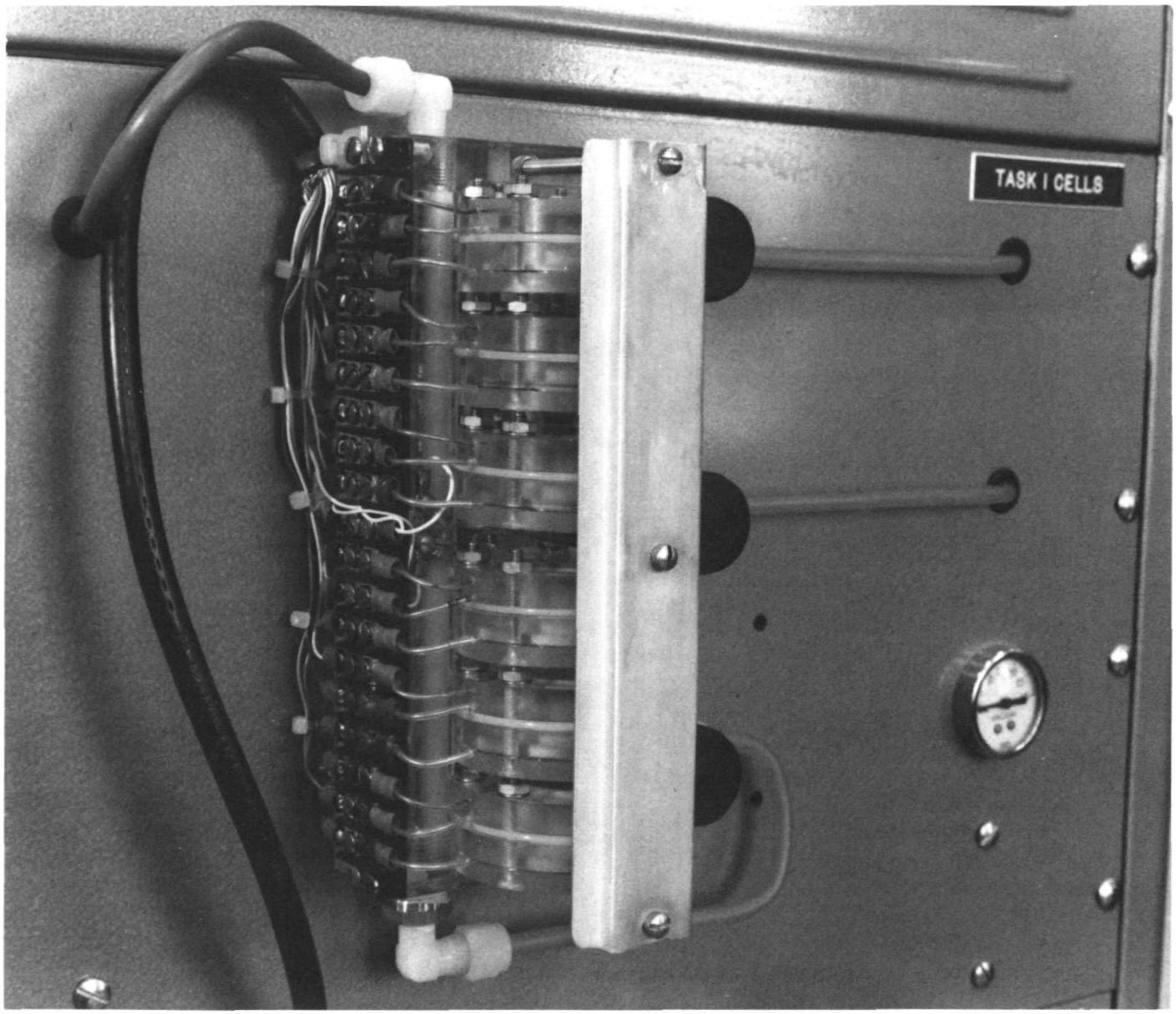


Fig. 24. Task 1 test panel showing cell-manifold assembly

Although this study does not include a space flight schedule, some of the measurements made during the construction and testing phases are of some significance. In particular, it should be noted that the limiting current data collected on vertical and horizontal electrode alignment at 1 *G* are in excellent agreement with the results obtained by Eisenberg (refer to the section on Pseudo-Zero-G Investigations of Cells). Studies at the General Electric Company indicate that the limiting current density for the silver–zinc anode is about 146 mA/cm² while the electrodes are mounted in a vertical position. When the battery is mounted in a horizontal position with the anode facing up (so as to achieve a minimum of convective mass transfer), the limiting current density is about 67 mA/cm². Eisenberg and his coworkers found these two measurements to be 143 and 67 mA/cm² respectively. The agreement is excellent considering the difference that must have existed in experimental equipment and technique (see Table 1 for test results).

At the end of this contract, Task 2 was not considered perfected. Specifically, troubles had been encountered in gas–electrolyte separation and bubble identification on electrode surfaces. Figures 25 and 26 show photographs of a zinc electrode at various states of charge and discharge. No conclusion was reached as to whether the light areas in the photographs were an indication of gas loading between the electrode and the cellophane separator or whether they were due to reflected light from metallic zinc particles on the electrode surface. The investigators concluded that the effect was most likely a combination of these two phenomena.

Task 3 was considered to be of successful design with little chance of difficulties being experienced in space flight. This section of the project was to investigate the degradation of commercial cells under stress. This study involved an initial capacity and polarization measurements, a series of five stress cycles, and a final polarization and capacity measurement. Cell degradation was to be assessed by comparing initial and final measurements of polarization and capacity. The layout for this study is shown in Fig. 27.

## IX. Gravitational Effects on Silver–Zinc Cells

In a series of studies conducted at the Jet Propulsion Laboratory, Arcand (Ref. 9) examined the electrical characteristics of a silver–zinc test cell while it was subjected to various acceleration forces.

**Table 1. Results of General Electric task 1**

| Test cell number | Limiting current density, mA/cm² | Time to polarization, min |
|---|---|---|
| | Vertical electrode position<br>Current ramp slope = 52.8 mA/min<br>Temperature = 24° C | |
| 1 | 141.4 | 2.68 |
| 2 | 139.0 | 2.60 |
| 3 | 149.0 | 2.80 |
| 4 | 156.2 | 2.93 |
| 5 | 141.3 | 2.68 |
| 6 | 151.3 | 2.85 |
| Mean | 146.4 | 2.76 |
| | Horizontal electrode position<br>Current ramp slope = 6.83 mA/min<br>Temperature = 24.5° C | |
| 1 | 65.8 | 9.3 |
| 2 | 65.8 | 9.3 |
| 3 | 69.5 | 10.1 |
| 4 | 69.5 | 10.2 |
| 5 | 65.8 | 9.5 |
| 6 | 65.8 | 9.7 |
| Mean | 67.0 | 9.7 |

A conventional cell employs a cathode of silver oxide (AgO or $Ag_2O_2$), which is produced by oxidizing silver beyond the intermediate oxide of $Ag_2O$, and an anode made of spongy or porous zinc. The electrolyte, which is approximately 40% aqueous potassium hydroxide saturated with potassium zincate, is held in a cellulosic material that is placed between the electrodes. The half-cell reactions for the discharge of this system are:

$$\text{Cathode: } AgO + H_2O + 2e = 2OH^- + Ag$$

$$\text{Anode: } Zn + 2OH^- = Zn(OH)_2 + 2e$$

giving an overall reaction of

$$AgO + H_2O + Zn = Ag + Zn(OH)_2$$

During discharge, the silver oxide paste is gradually converted to silver, which adheres to the cathode substrate. At this electrode, mass transfer problems are negligible during both charge and discharge. At the anode, however, the zinc hydroxide does not tend to adhere rigidly to the porous zinc substrate and it is

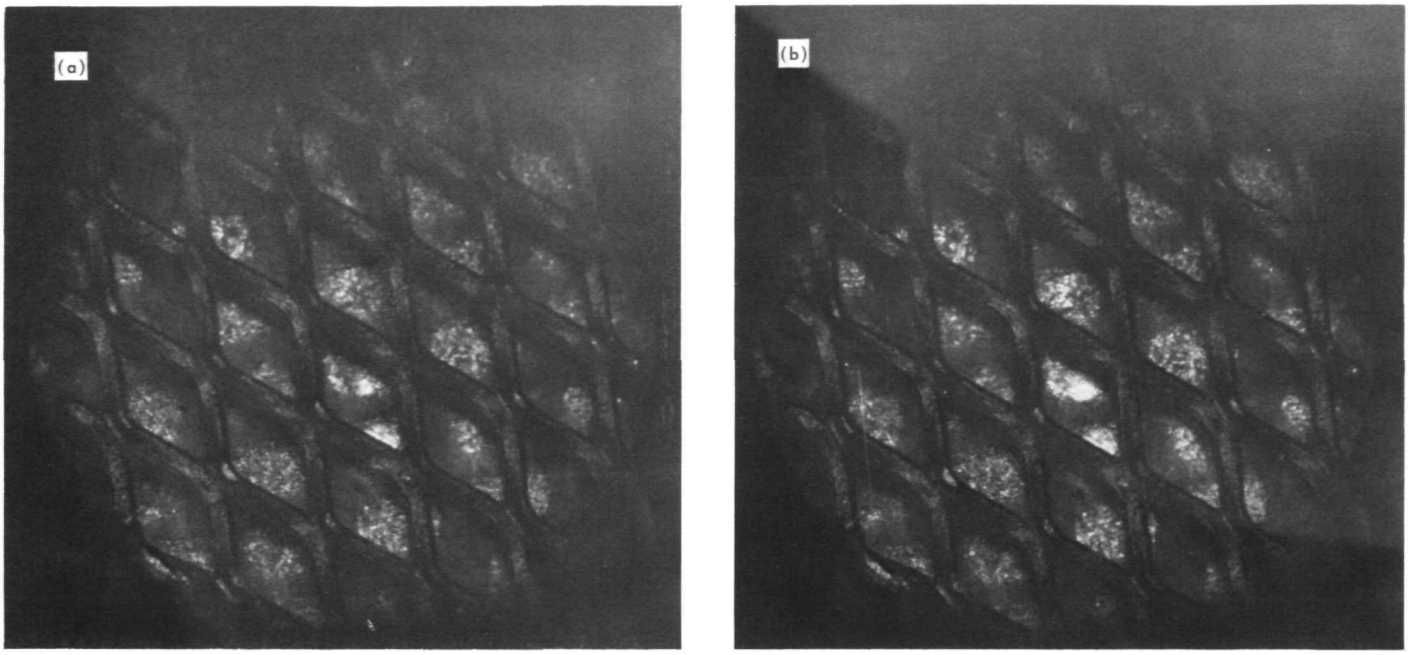


Fig. 25. Photographs of Zn test electrode: (a) start of test, (b) end of charge

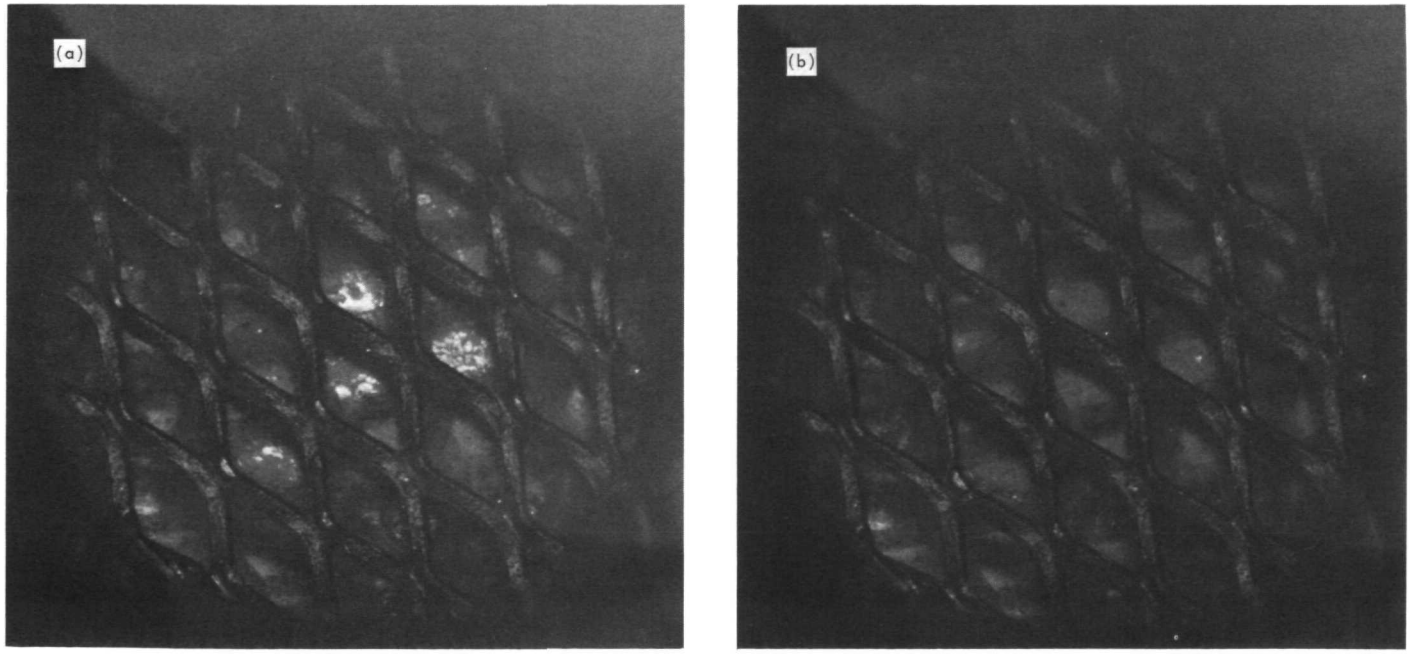


Fig. 26. Photographs of Zn test electrode: (a) end of first discharge, (b) end of second discharge

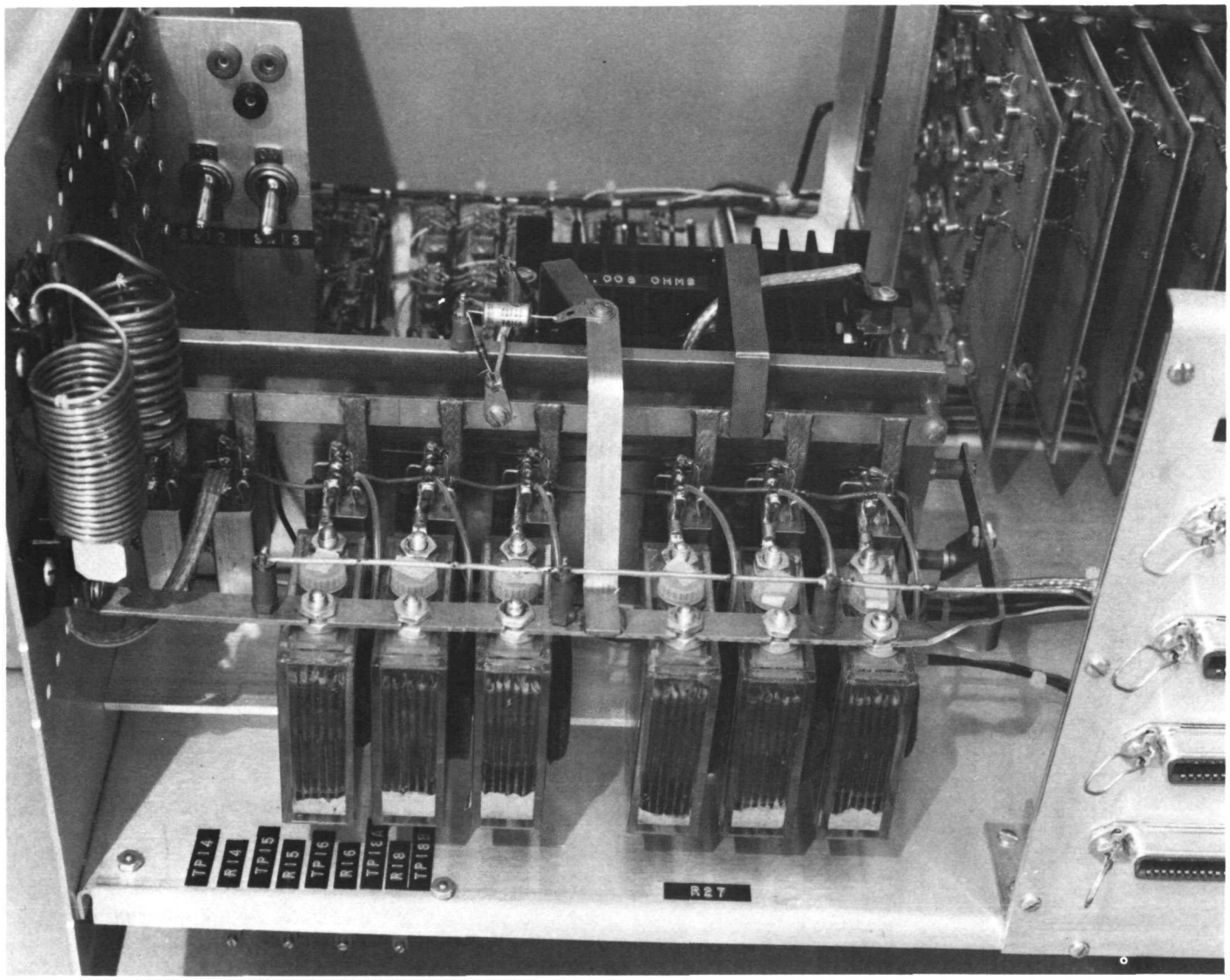


Fig. 27. Task 3 chassis, cell mounting arrangement

therefore possible to have a convective mass transfer of this material. Gravitational or acceleration effects of this cell, consequently, tend to be concentrated in physical phenomena which occur at the anode.

In order to better understand and control the chemistry and physics of the system, Arcand elected to examine only smooth zinc anodes. In particular, this type of anode made it possible to more accurately calculate effective electrode surface area and thus to ascertain current densities with greater exactness. The cell geometry employed in this study also provided for various spacings between the anode and the cellulose separator (see Appendix B).

Arcand collected data between 1 and 20 *G* by placing the cells in a large centrifuge. Most of the measurements were made with the electrodes parallel to the vector of acceleration; however, some tests were conducted with the electrodes aligned at a 10-deg angle to the vector. In this latter arrangement, a significantly different limiting current was obtained.

In order to make certain that the current was limited by the anode reaction, this electrode was masked down to be an order of magnitude smaller than the opposing cathode. In most studies the anode was a square surface 1 cm long on each side. Tests were conducted, however, to ascertain the effect of the anode height and width. At 20 *G*, Arcand found that there was no significant difference in the limiting current density between a 1 × 1-cm anode and one that had a height of 1 cm and a width of 2 cm. The result was different, however, if the height was varied while the width was kept the same. For example, it was found that a 20% reduction occurred in the limiting current if the height was increased to 2 cm while the width was kept the same at 1 cm.

The results of Arcand's studies are summarized in Figs. 28 and 29. In Fig. 28, a typical plot of overpotential versus current density is given. Such data are collected for each separator spacing and acceleration force to yield a limiting current density which, in turn, is reported in Fig. 29.

In these studies, the experiments consistently showed that the limiting current density increased with acceleration between 1 and 20 *G*. Also shown is the fact that the limiting current density decreased as the separator was moved closer to the anode. Empirical equations for each case are given in Table 2.

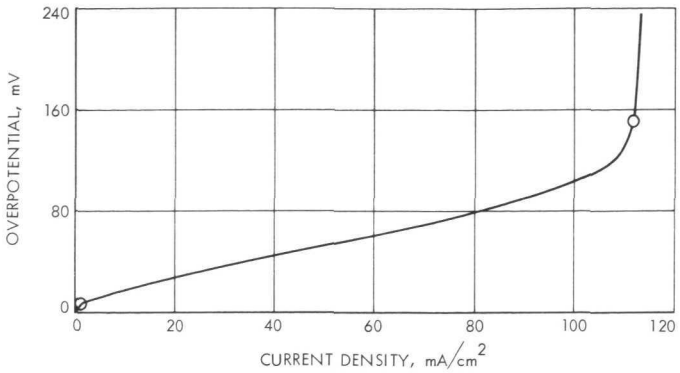


**Fig. 28. Typical overpotential curve for Zn/KOH, Zn(II) electrode**

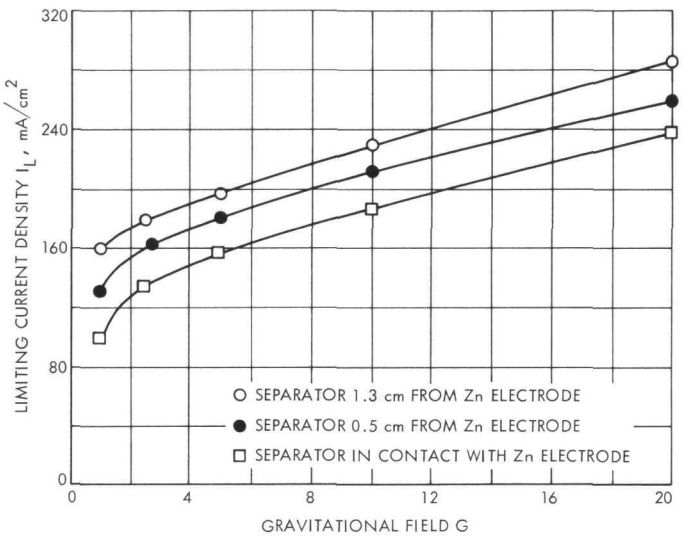


**Fig. 29. Limiting current density vs relative acceleration for various electrode separations**

For the case of the separator lying adjacent to the anode surface, the exponent on *G* is 0.28, which is only slightly greater than the theoretical value of 0.25. Such agreement may exist because only laminar flow occurs between the electrode and separator when the distance between the two surfaces is very small. The theory predicting a 0.25 dependence was based upon a model which assumed only a laminar flow.

The constants in each equation in Table 2 where obtained by a least-squares analysis. The standard deviations for the coefficients in the equations are 1.0 and, for the exponents, 0.01. The additive constants might be assumed to represent diffusion currents, but one should apply the results to a zero-*G* situation with caution since all of the tests performed in this

**Table 2. Arcand's empirical equations for limiting current density in the silver–zinc cell**

| Limiting current density $I^L$, mA/cm² | Separator–anode distance, cm |
|---|---|
| $I^L = 99\ G^{0.28} + 2$ | 0 |
| $I_L = 128\ G^{0.23} + 1$ | 0.5 |
| $I^L = 148\ G^{0.19} + 7$ | 1.3 |

study were for $G$ values greater than 1. It thus continues to remain questionable whether equations of this type can be employed to predict behavior between 0 and 1 $G$.

One might speculate, however, on the situation at zero $G$ if these equations are valid. For a tightly fitting separator, they would predict a limiting current density of only 2 mA/cm² at zero $G$ for the silver–zinc battery. This is only about 2% of the value realized at 1 $G$. A battery operating in free space would thus have a peak current much less than the value realized upon the surface of the earth.

## X. High-Acceleration Effects

In a study designed to ascertain whether acceleration forces affected commercially available silver–zinc and nickle–cadmium batteries, a series of tests was conducted in 1968 at the Naval Ammunition Depot in Crane, Indiana. The units examined were manufactured by the Yardney Electric Corporation, Pawcatuck, Conn., and the Gulton Battery Company, Metuchen, N.J.; the work was supported by JPL.

The experiments consisted of mounting the batteries in a high-impulse centrifuge with appropriate slip-ring connections and monitoring the current–voltage relations as a function of time and acceleration. Tests were conducted at 1, 10, 20, 30, 50, and 75 $G$.

In the case of the silver–zinc tests, several different types of cells were used in the study. Some were given an excess of electrolyte to create a "flooded" condition and others were supplied with only enough electrolyte to saturate the battery separators and thus create a "starved" environment. Each battery consisted of a package of 10 cells; the capacity of each cell was either 0.1 or 5 A-h. The small cell units were given one discharge to obtain voltage–time curves, but the 5-A-h cells were cycled four times and measurements were made on each of the 10 cells in the package. A new battery was used for each acceleration test.

A typical run on a 10-cell battery containing flooded 5-A-h cells consisted first of preconditioning each cell by the technique of discharging it at 5 A until the cell voltage dropped to one V, then recharging the cells at 0.35 A until the voltage rose to 2 V. The battery was then appropriately accelerated and operated through four 100%-charge–discharge cycles. The cell was discharged at 1 A until the voltage dropped to 1.25 V. The charge current was maintained at 0.35 A until the cell reached 2.10 V. Tables 3 and 4 are typical of the data collected on five of the cells in the unit. Data were also presented on other types of silver–zinc cells in the form of curves, as in Figs. 30 and 31. Similar tests were run on 0.08-A-h nickel–cadmium cells, in which no gravity effects were noted.

Various parameters have been examined by the authors in order to determine whether acceleration affected the performance of these cells. Table 5 shows the average ampere-hour capacity realized for each value of acceleration on one type of battery. Each entry in this table is an average of 40 values (4 cycles on 10 cells) and, although no trend appears obvious, the following statistical analysis was applied to the data.

Student $t$ values were computed for various pairs of data sets in order to judge whether the ampere-hour values for one run were significantly different from those for another. For instance, the data for 1 $G$ were compared with the values obtained at 75 $G$, while 10-$G$ data were compared with 50-$G$, and 20-$G$ compared with 30-$G$. The $t$ values obtained were 0.6333, 1.125, and 2.223 respectively. From statistical tables these $t$ values should lie outside the interval of $\pm 2.64$ for 99% confidence that a significant difference exists in these sets of data, or, stated in a different way, these data do not permit one to conclude, with 99% confidence, that acceleration forces affect the ampere-hour capacity.

As a further check on the significance of the variations realized in this study, the 20 data values for the first two cycles in the 1-$G$ series were compared with the 20 values obtained in the last two cycles. In this comparison, a $t$ value of 1.832 was calculated. For 99% confidence that there is significant difference in the first two and last two cycles, statistical tables indicate that the $t$ value should lie outside the range $\pm 2.712$. The conclusion is that the values obtained for the first and last cycles were not significantly differ-

**Table 3. Format for sample data page, charge data**

| HR-5 DC-10 CELLS Cycle 3 10 G test<br>CHARGE AT 350 MILLIAMPERES to 2.10 VOLTS | | | | | |
|---|---|---|---|---|---|
| HR. MIN. | 1 | 2 | 3 | 4 | 5 |
| OCV | 1.58 | 1.58 | 1.58 | 1.58 | 1.58 |
| 30 | 1.60 | 1.60 | 1.60 | 1.60 | 1.60 |
| 2 | 1.61 | 1.61 | 1.61 | 1.61 | 1.61 |
| 4 | 1.62 | 1.62 | 1.62 | 1.62 | 1.62 |
| 6 | 1.62 | 1.62 | 1.63 | 1.62 | 1.62 |
| 8 | 1.89 | 1.89 | 1.89 | 1.89 | 1.89 |
| 10 | 1.90 | 1.90 | 1.90 | 1.90 | 1.90 |
| 12 | 1.93 | 1.93 | 1.93 | 1.93 | 1.92 |
| 14 | 1.92 | 1.92 | 1.92 | 1.92 | 1.92 |
| 16 | 1.92 | 1.92 | 1.93 | 1.92 | 1.92 |
| 18 | 1.93 | 1.93 | 1.94 | 1.93 | 1.93 |
| 20 | 1.95 | 1.93 | 1.97 | 1.94 | 1.94 |
| 22 | | 1.95 | | 1.98 | 1.98 |
| | | | | | |
| | | | | | |
| | | | | | |
| | | | | | |
| | | | | | |
| | | | | | |
| | | | | | |
| TIME TO 2.10 VOLTS IN HOURS AND MINUTES | | | | | |
| ah | 7.65 | 8.24 | 7.44 | 8.12 | 8.22 |
| CHARGE TIME | 21:51 | 23:33 | 21:17 | 23:13 | 23:30 |

**Table 4. Format for sample data page, discharge data**

| HR-5 DC-10 CELLS Cycle 3 10 G test<br>DISCHARGE AT 1 AMPERE TO 1.25 VOLTS | | | | | |
|---|---|---|---|---|---|
| TIME | 1 | 2 | 3 | 4 | 5 |
| OCV | 1.86 | 1.86 | 1.86 | 1.86 | 1.87 |
| 01 | 1.79 | 1.79 | 1.7 | 1.79 | 1.78 |
| 30 | 1.54 | 1.54 | 1.55 | 1.54 | 1.54 |
| 1 | 1.53 | 1.53 | 1.53 | 1.53 | 1.53 |
| 30 | 1.53 | 1.53 | 1.53 | 1.53 | 1.53 |
| 2 | 1.53 | 1.53 | 1.53 | 1.53 | 1.53 |
| 30 | 1.53 | 1.53 | 1.53 | 1.53 | 1.53 |
| 3 | 1.53 | 1.53 | 1.53 | 1.53 | 1.53 |
| 30 | 1.53 | 1.53 | 1.53 | 1.53 | 1.53 |
| 4 | 1.53 | 1.53 | 1.53 | 1.53 | 1.53 |
| 30 | 1.53 | 1.53 | 1.53 | 1.53 | 1.53 |
| 5 | 1.53 | 1.53 | 1.53 | 1.53 | 1.53 |
| 30 | 1.53 | 1.53 | 1.52 | 1.53 | 1.53 |
| 6 | 1.52 | 1.53 | 1.52 | 1.52 | 1.53 |
| 30 | 1.52 | 1.52 | 1.51 | 1.52 | 1.52 |
| 7 | 1.51 | 1.52 | 1.50 | 1.51 | 1.51 |
| 30 | 1.50 | 1.50 | 1.45 | 1.50 | 1.49 |
| 8 | 1.26 | 1.40 | | 1.34 | |
| 30 | | | | | |
| 9 | | | | | |
| DISCHARGE TIME IN MINUTES AND SECONDS TO 1.25 VOLTS | | | | | |
| ah | 8.00 | 8.06 | 7.78 | 8.01 | 7.95 |
| DISCHARGE TIME | 8:00 | 8:04 | 7:47 | 8:01 | 7:57 |

ent. The same type of examination was also performed on the 75-$G$ data and the same conclusions were obtained.

Finally, two attempts were made to fit the data of Table 5 to equations. The first form tried was

$$Ah = A + BG \tag{12}$$

where $Ah$ is the ampere-hour capacity of the cells, $A$ and $B$ are constants, and $G$ is the value of the acceleration. With this equation a correlation coefficient of $-0.216$ was obtained, which indicates a very poor fit.

The second equation tried was of the form

$$Ah = AB^{B} \tag{13}$$

for which a correlation coefficient of $-0.109$ was obtained, indicating, once again, a poor correlation.

**Table 5. Average ampere-hour capacity for flooded 5-A-h Yardney silver–zinc cells**

| Acceleration, G | Capacity, A-h |
|---|---|
| 1 | 7.78 |
| 10 | 7.79 |
| 20 | 7.97 |
| 30 | 7.74 |
| 50 | 7.87 |
| 75 | 7.73 |

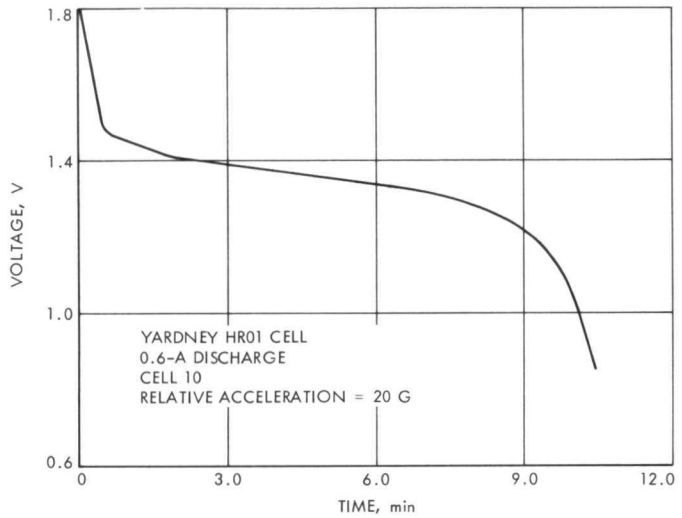


**Fig. 30. Typical voltage vs time curve for Yardney HR01 cell, 20-G relative acceleration**

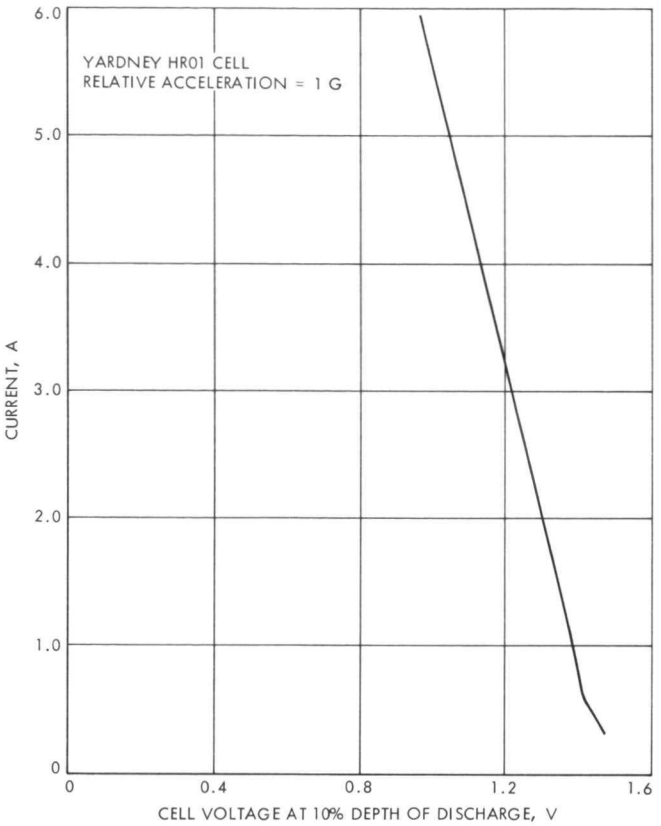


**Fig. 31. Typical current vs voltage curve for Yardney HR01 cell, 1-G relative acceleration**

## XI. Photographic Evidence of Gravitational Effects

A series of tests was performed at the U.S. Naval Depot in Crane, Indiana, to obtain photographic evidence of the effects of sustained acceleration. Figures 32-49 show zinc anode behavior in Ag-Zn cells subjected to various acceleration forces. Three different types of cells are depicted in these photographs:

(1) Flooded 5-A-h cells manufactured by the Yardney Electric Company and designated as model HR5DC-10. Each cell consisted of seven anode plates adjacent to six positive electrodes. These electrodes were connected in parallel, and the dimensions of each plate were 4.29 cm × 3.57 cm × 0.13 cm. Each cell was cycled four times, and 10 new cells were used in each gravitational test.

(2) Cells identical in description and treatment to those described above, except that they were electrolyte-starved.

(3) Mariner-type cells manufactured to Jet Propulsion Laboratory specifications, which were identical to flight cells. Each of the silver–zinc cells was electrolyte-starved and contained 25 plates (13 anodes and 12 positive electrodes). These cells had a nominal capacity of 50 A-h at a 10-A discharge rate at 25°C. The cells were manufactured by ESB, Inc.

The photographs presented herein are representative of a number of pictures taken after each test. A summary of the types of cells tested and the acceleration levels used is given in Table 6.

**Table 6. Guide to figure numbers of photographs of zinc electrodes**

| Relative acceleration G | Figure numbers | | |
|---|---|---|---|
| | Yardney flooded cells | Yardney starved cells | Mariner-type cells[a] |
| 1 | 32 | 38 | 44 |
| 10 | 33 | 39 | 45 |
| 20 | 34 | 40 | 46 |
| 30 | 35 | 41 | 47 |
| 50 | 36 | 42 | 48 |
| 75 | 37 | 43 | 49 |

[a]The Mariner cells were manufactured by the Electric Storage Battery Company, Raleigh, North Carolina.

**Table 7. Ratios of the bottom to top zinc electrode thickness on Ag–Zn Yardney cells after acceleration tests**

| Relative acceleration G | Ratio of bottom to top electrode thickness | |
|---|---|---|
| | Flooded cells | Starved cells |
| 1 | 1.38 | 1.03 |
| 10 | 1.48 | 1.09 |
| 20 | 1.40 | 1.06 |
| 30 | 2.33 | 1.11 |
| 50 | 2.86 | 2.25 |
| 75 | 3.05 | 3.41 |

In examining the pictures, it is evident that, during the tests, the zinc deposit moved from the top of the electrode (the long edge with the terminal connection) to the bottom portion of the electrode. For example, in Fig. 35, a relatively large amount of the substrate is visible at the top edge of each electrode, indicating a significant shift of the zinc from the top to the bottom of the electrode.

Another measure of this zinc migration is given in Table 7, in which the ratio of the bottom to top electrode thickness is given after the acceleration tests on the Yardney cells. Here, with the exception of the 20-*G* data, there is a gradual increase in this ratio as the acceleration progresses from 1 to 75 *G*. Whether the cell is flooded or starved seems to be of little consequence in this test.

This same type of migration of material is also indicated for the Mariner-type cells, as shown in Fig. 50. The lines shown in this figure were computed using a least-squares analysis of the data given in Appendix C. No evidence was found that the silver electrode was affected in any way, on either make of battery, by acceleration forces.

The conclusion that one might reach concerning the zinc migration would be that as the cells continued to be cycled under high acceleration forces, the effective zinc surface area would be significantly reduced since the upper portion of the electrode would become depleted in active electrode material. This would ultimately mean that the anodes would have to work at higher current densities on the remaining active surface in order to deliver the same power. Thus, problems arising from gas formation will be made more acute if the zinc migration is not controlled.

Certain implications for the design of silver–zinc batteries to operate in high-gravity fields arise from the zinc migration data. Since the migration of zinc is quite sharply affected by the moderate acceleration forces used in these experiments, one might infer that the zinc is leaving the electrode in relatively large aggregates of material. Consequently, providing mechanical support for the zinc electrodes in cells fabricated for use where acceleration forces are to be encountered for extended periods of time appears to be an important design consideration. Some mechanical support could readily be achieved by utilizing thin negative plates so that a larger proportion of the active material is more rigidly attached to the current collector grid, and by ensuring that the cell construction provides for adequate pack tightness. The latter provision appears to be the more important of the two.

Design work is also required on the separator system, with particular emphasis on the absorber, so that the cells could meet desired discharge and charge capability requirements while conforming to the pack tightness criterion stated above.

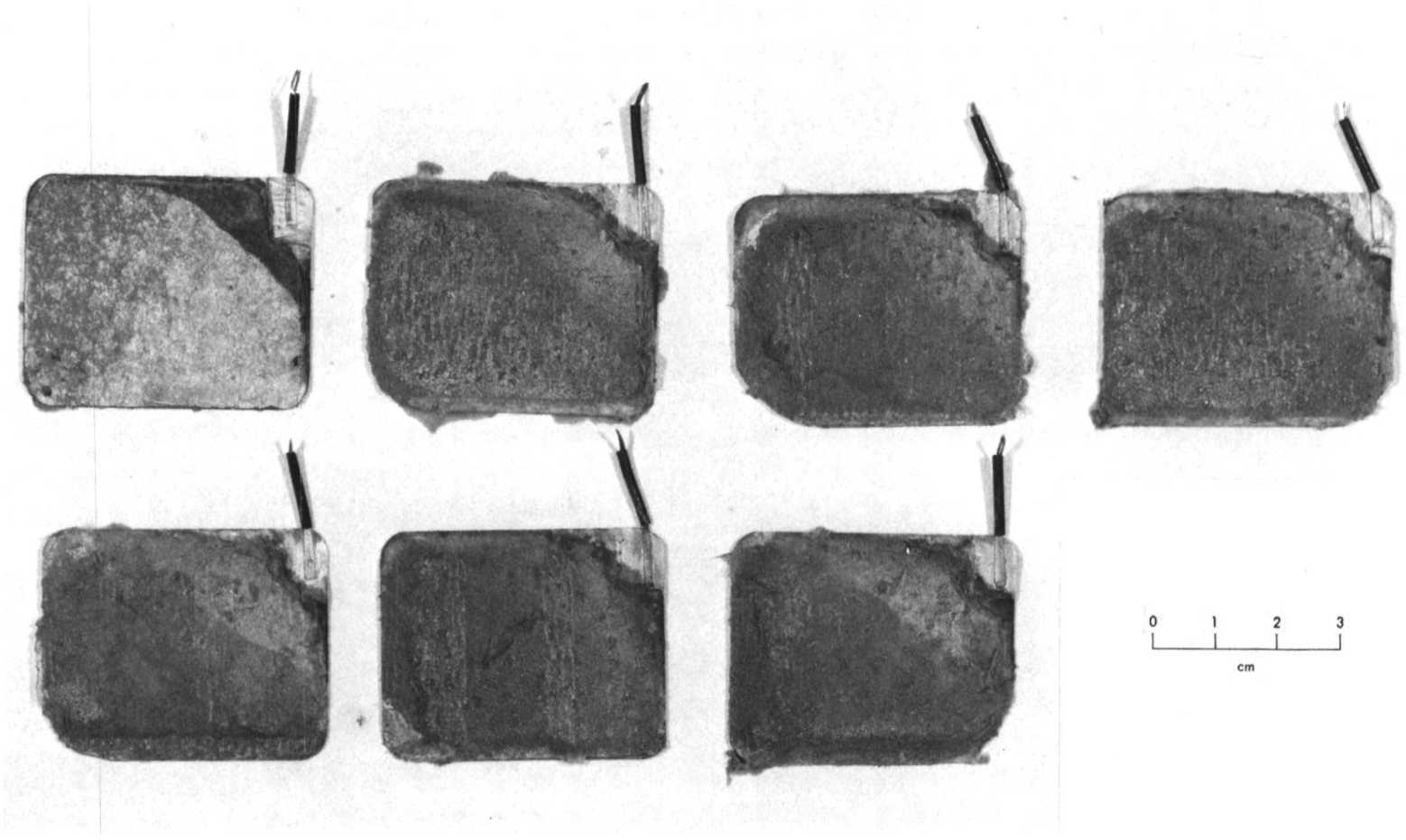


Fig. 32. Yardney electrolyte-flooded cell, 1-G relative acceleration, zinc electrodes

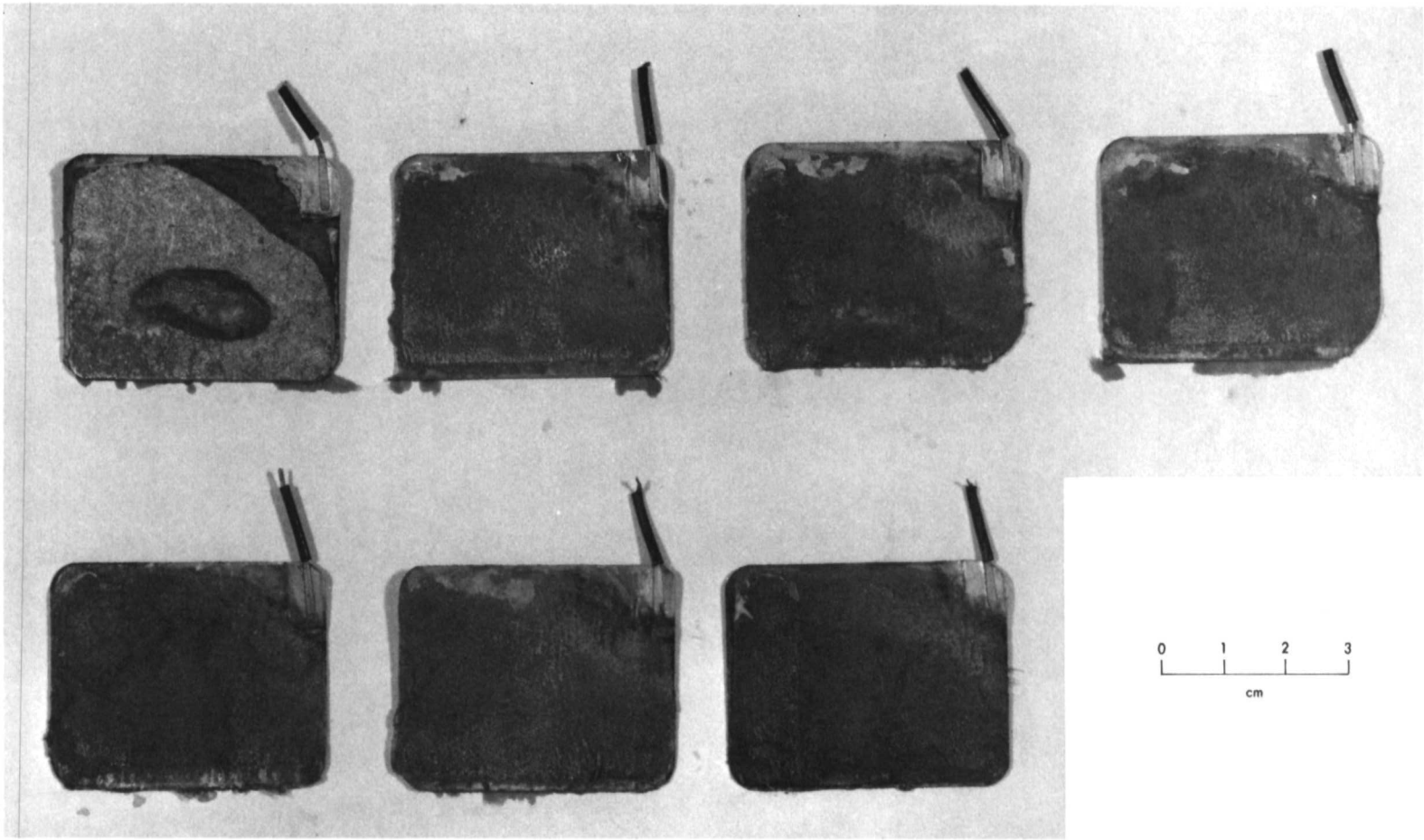


Fig. 33. Yardney electrolyte-flooded cell, 10-G relative acceleration, zinc electrodes

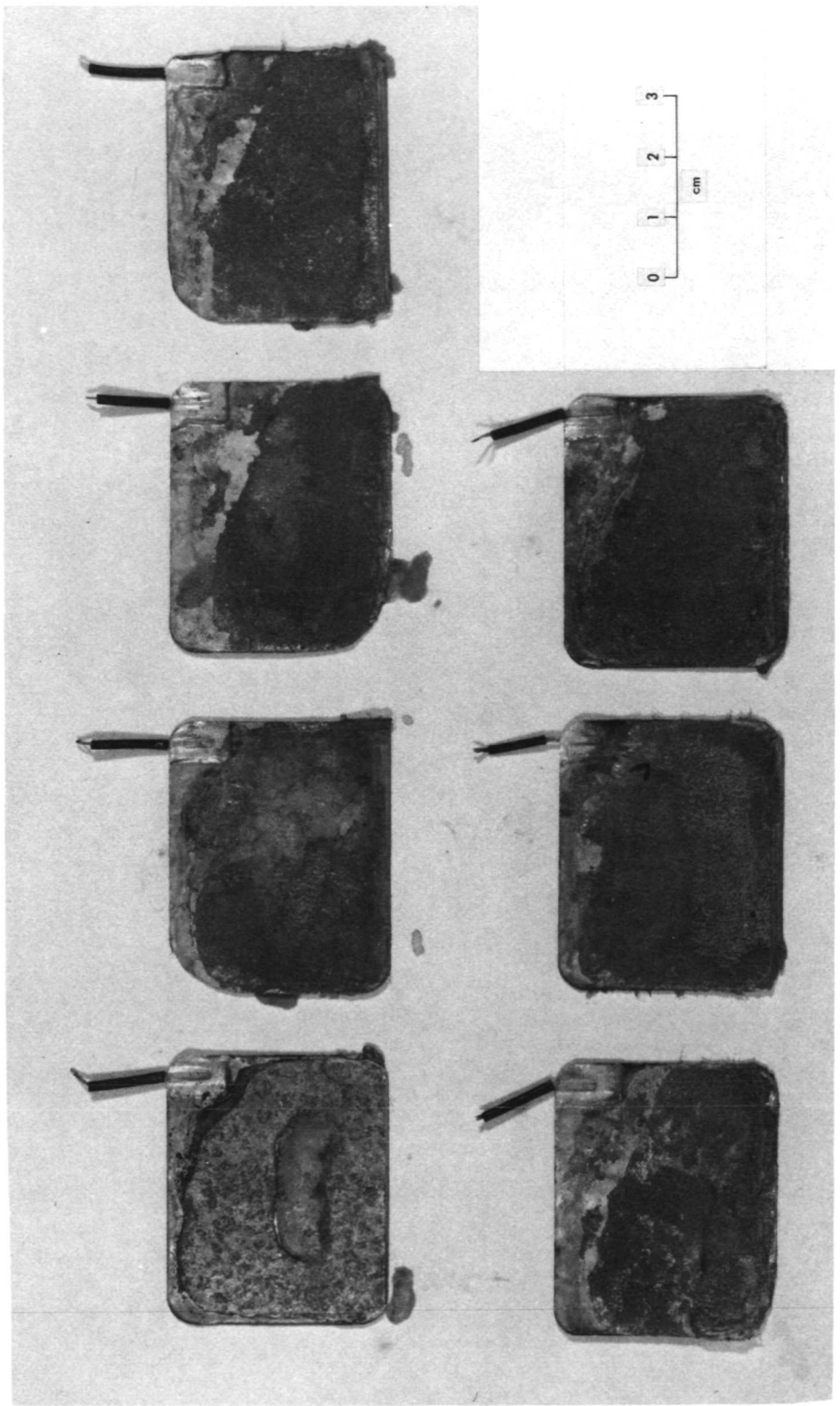


Fig. 34. Yardney electrolyte-flooded cell, 20-G relative acceleration, zinc electrodes

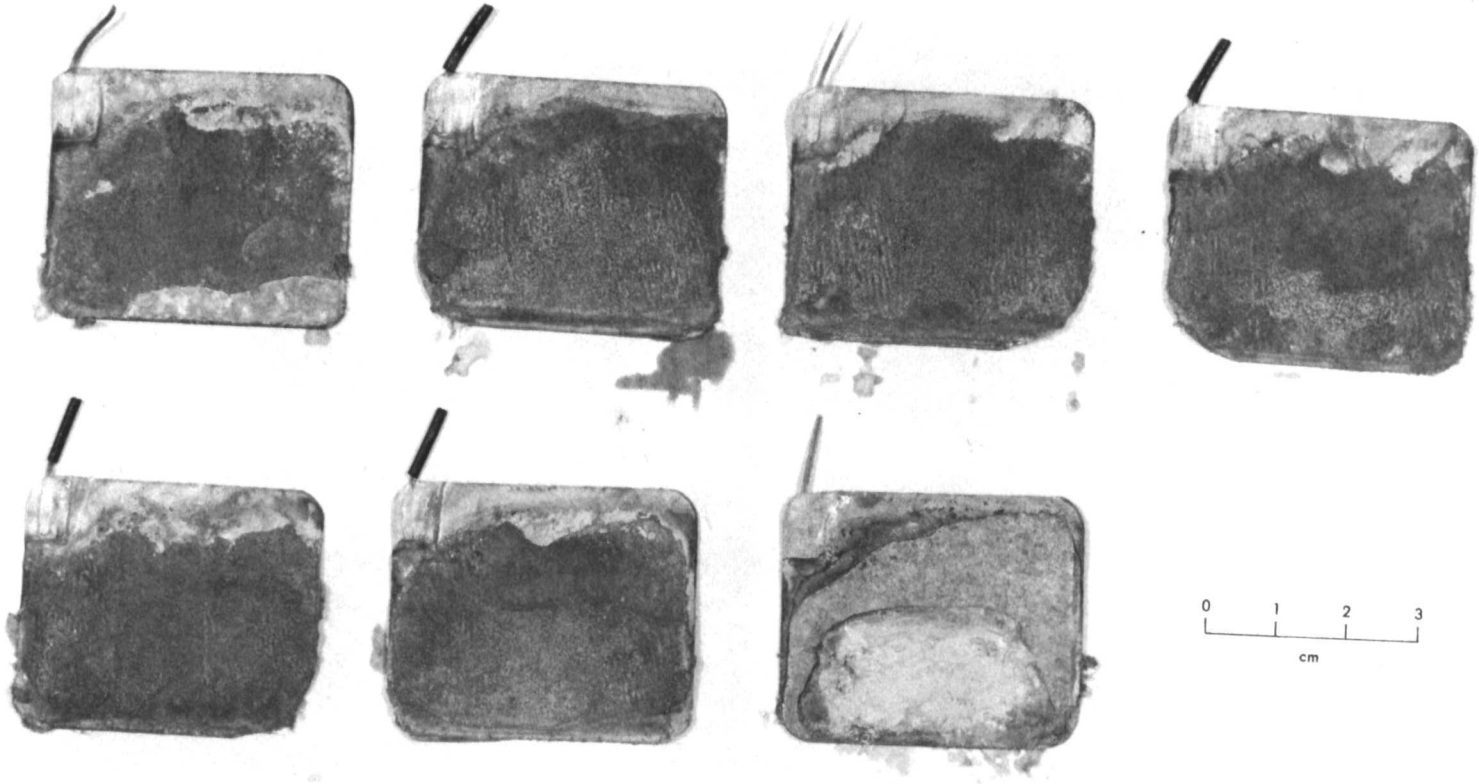


Fig. 35. Yardney electrolyte-flooded cell, 30-G relative acceleration, zinc electrodes

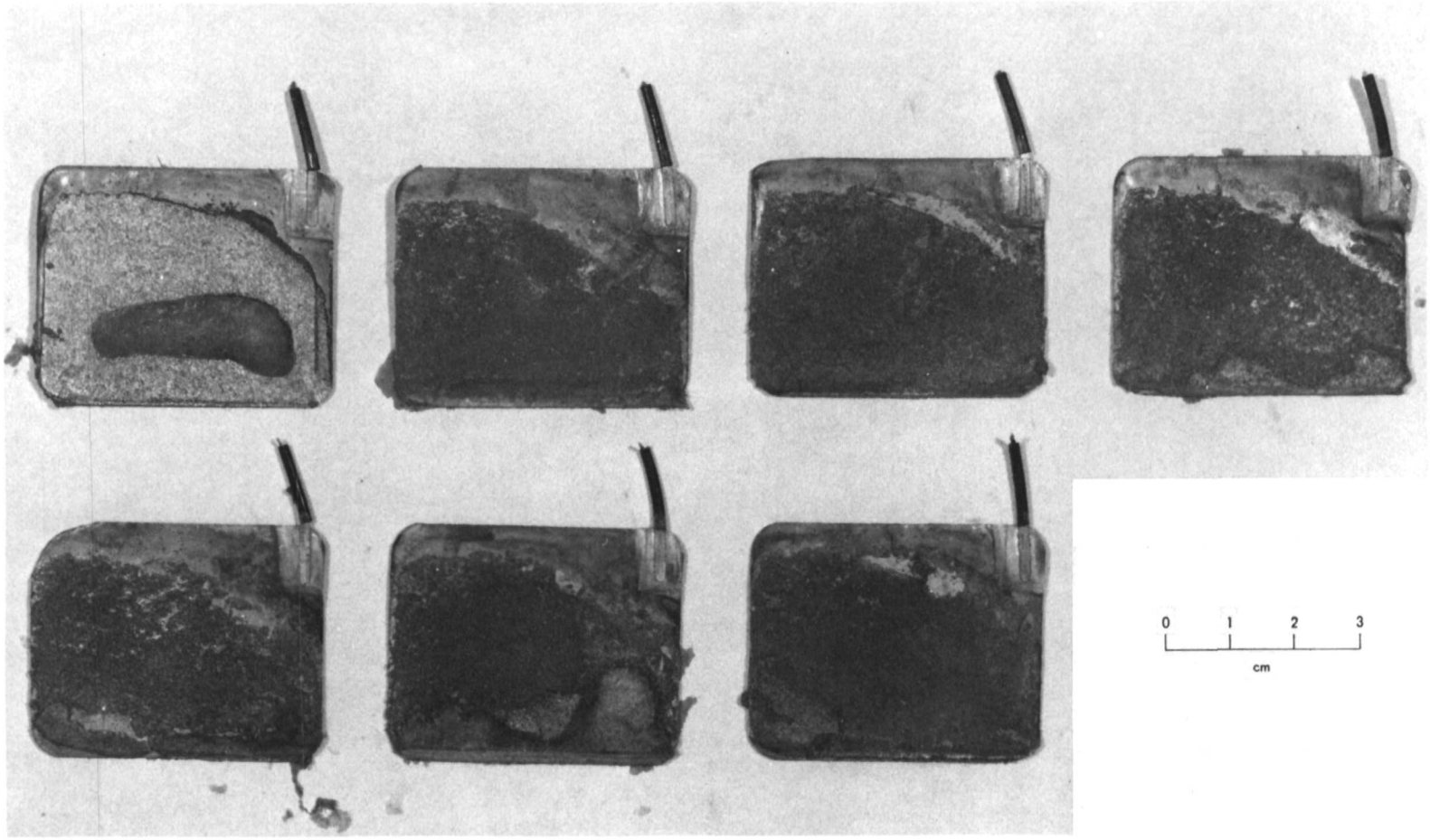


Fig. 36. Yardney electrolyte-flooded cell, 50-G relative acceleration, zinc electrodes

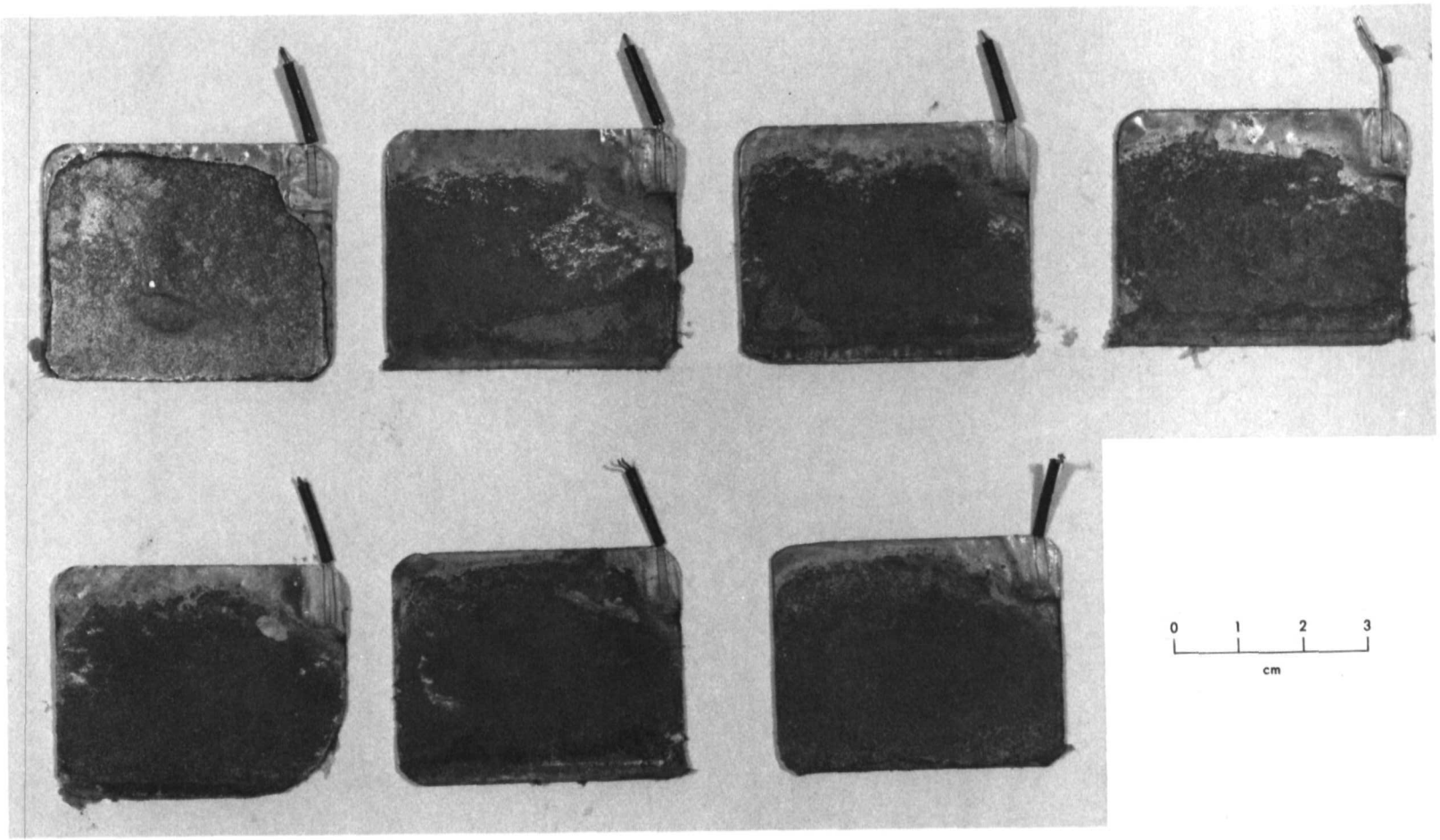


Fig. 37. Yardney electrolyte-flooded cell, 75-G relative acceleration, zinc electrodes

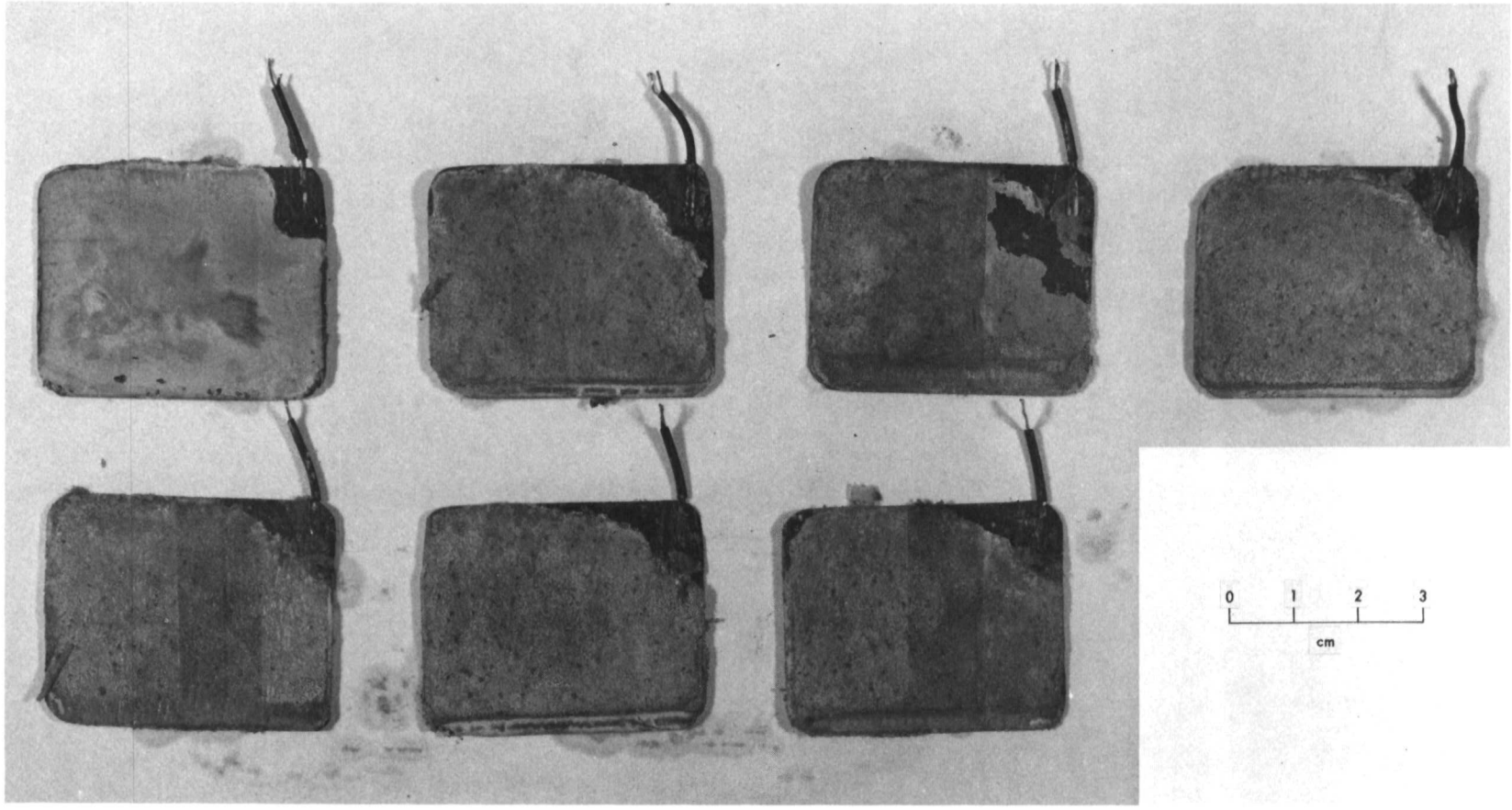


Fig. 38. Yardney electrolyte-starved cell, 1-G relative acceleration, zinc electrodes

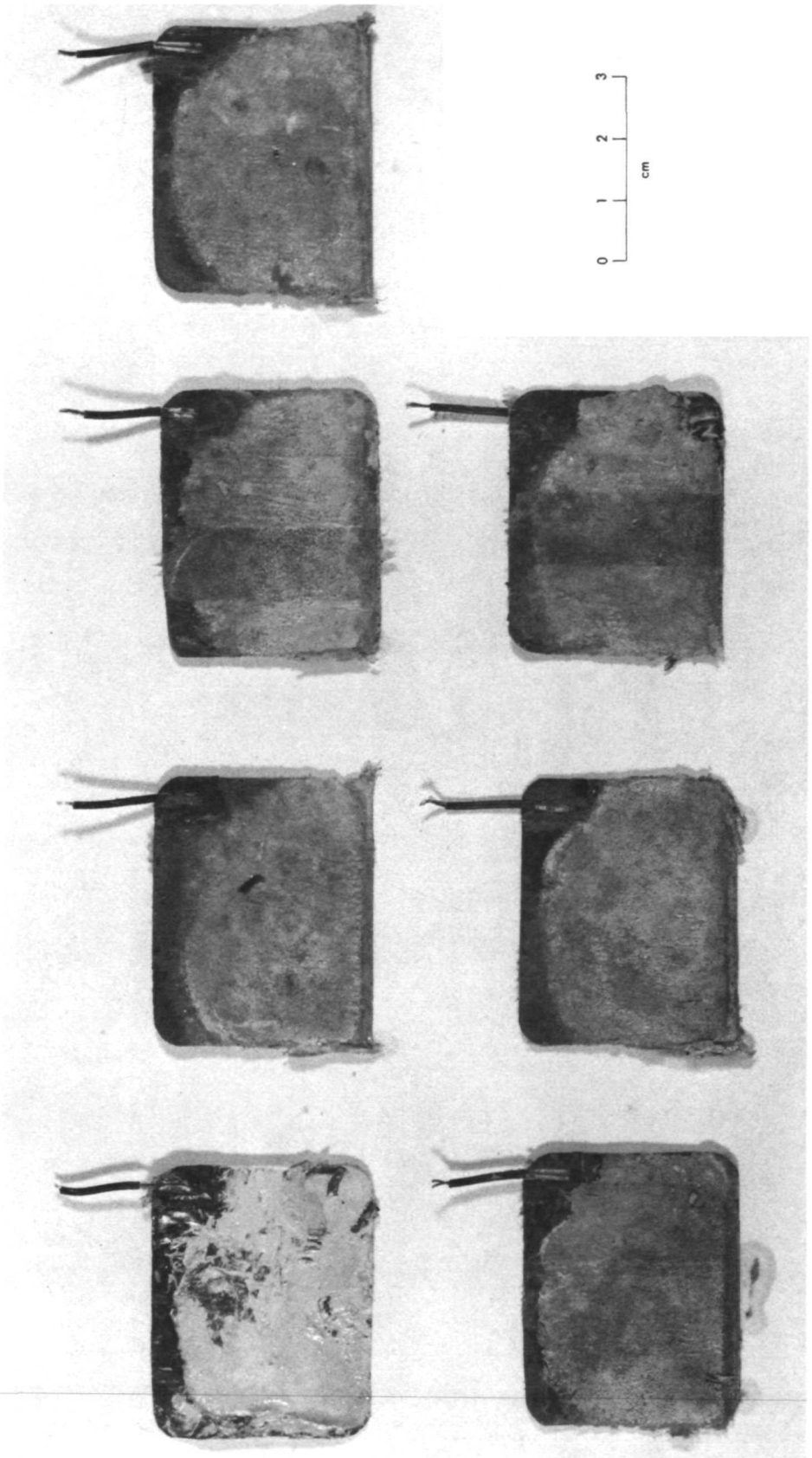


Fig. 39. Yardney electrolyte-starved cell, 10-G relative acceleration, zinc electrodes

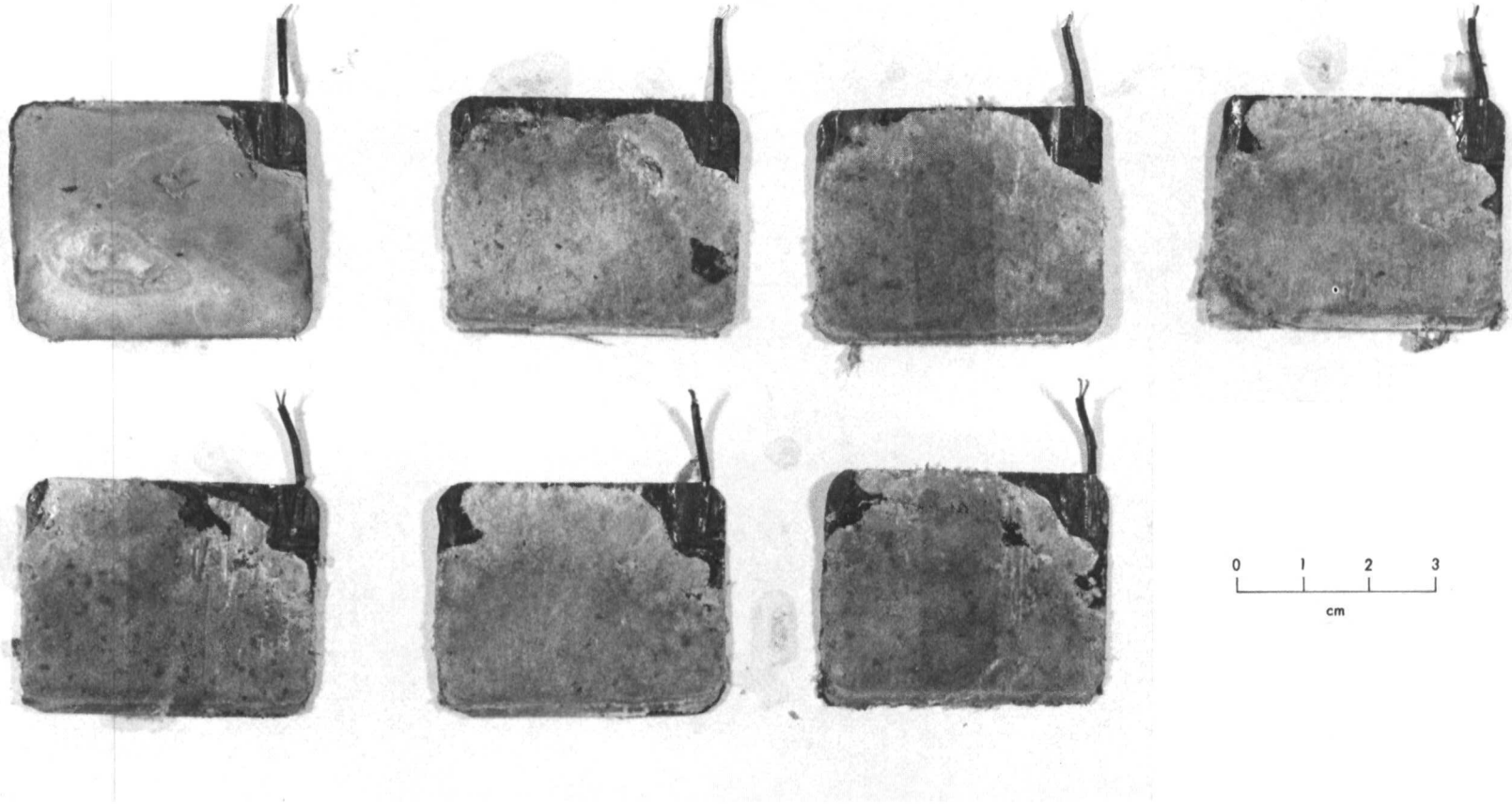


Fig. 40. Yardney electrolyte-starved cell, 20-G relative acceleration, zinc electrodes

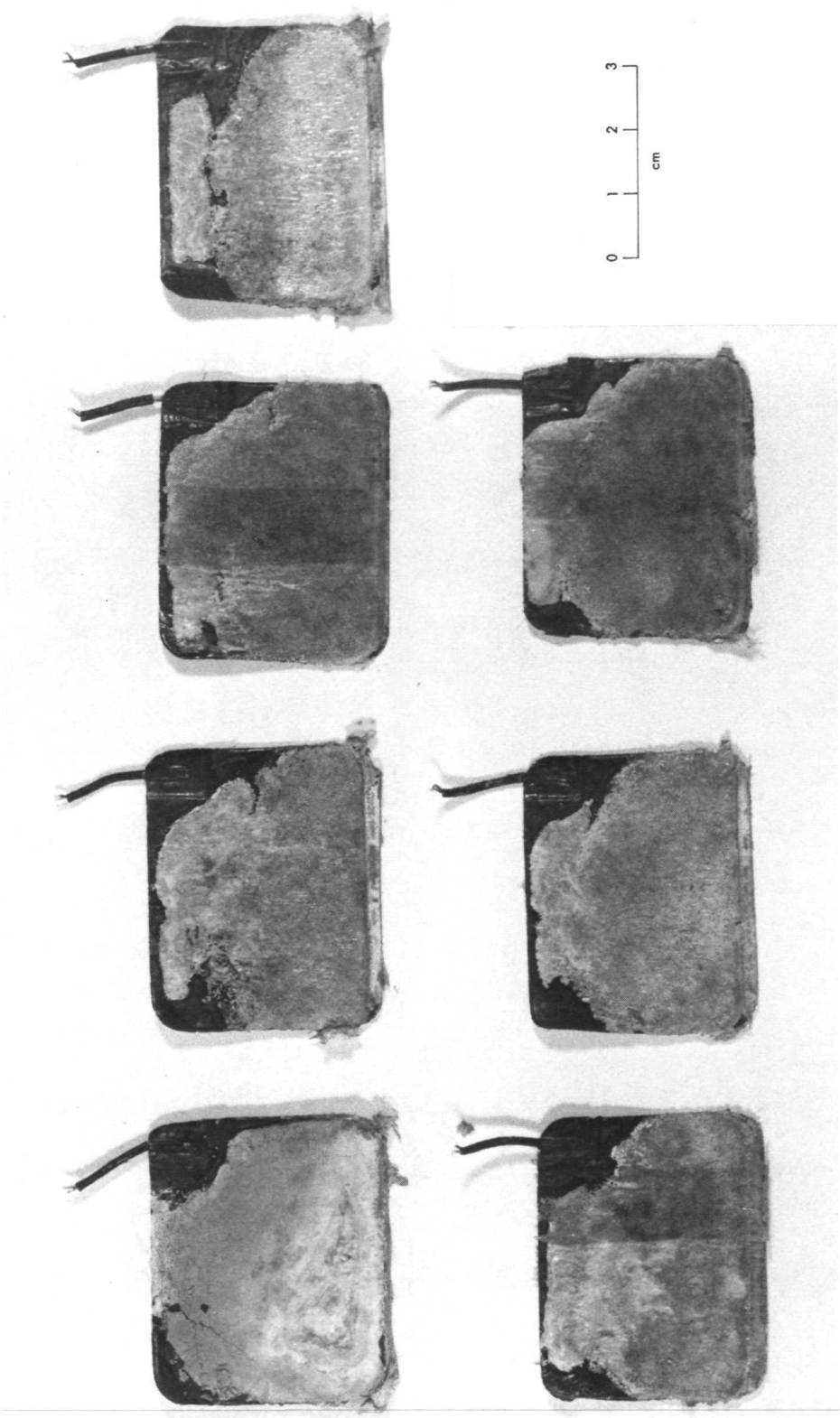


Fig. 41. Yardney electrolyte-starved cell, 30-G relative acceleration, zinc electrodes

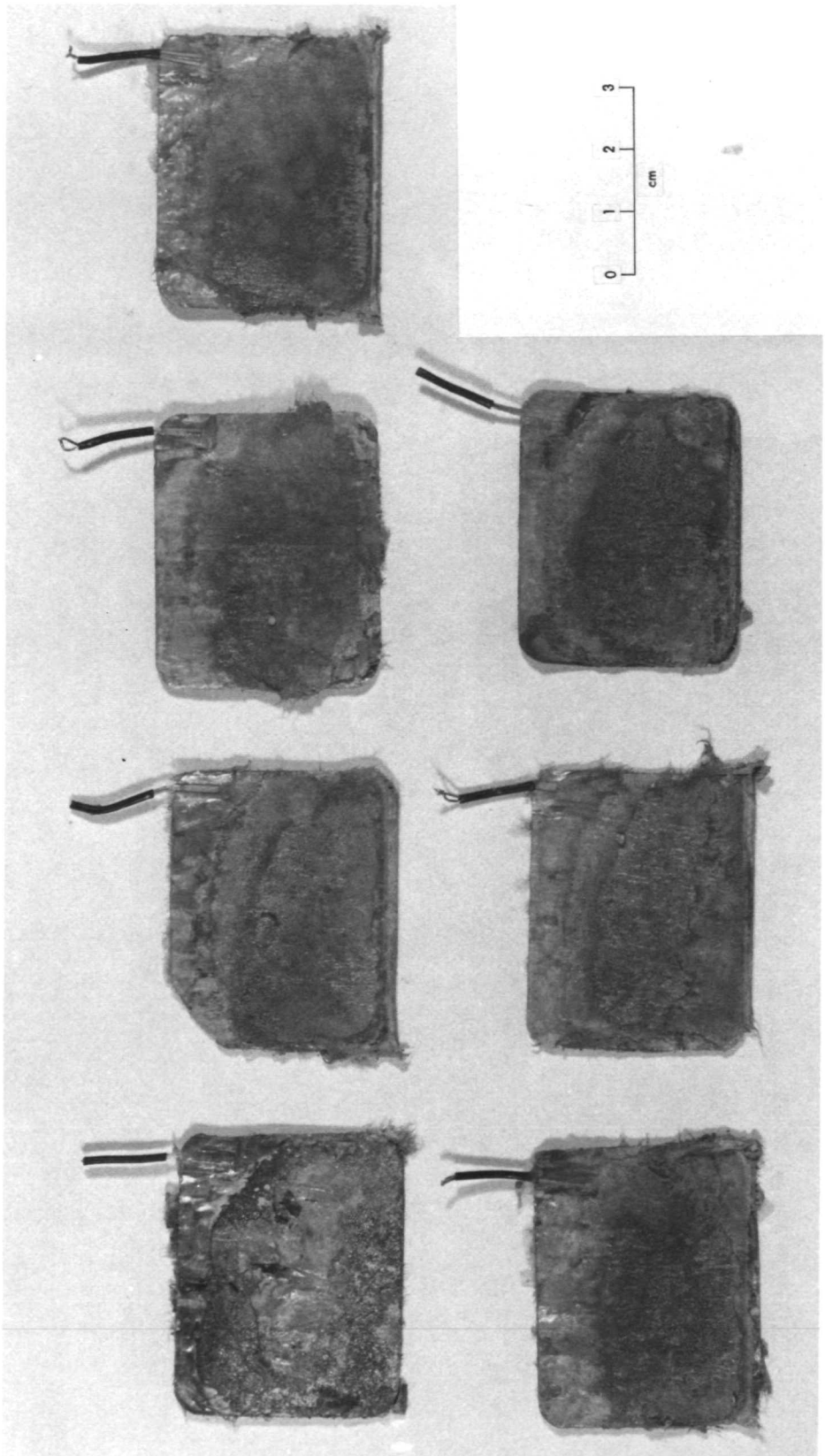


Fig. 42. Yardney electrolyte-starved cell, 50-G relative acceleration, zinc electrodes

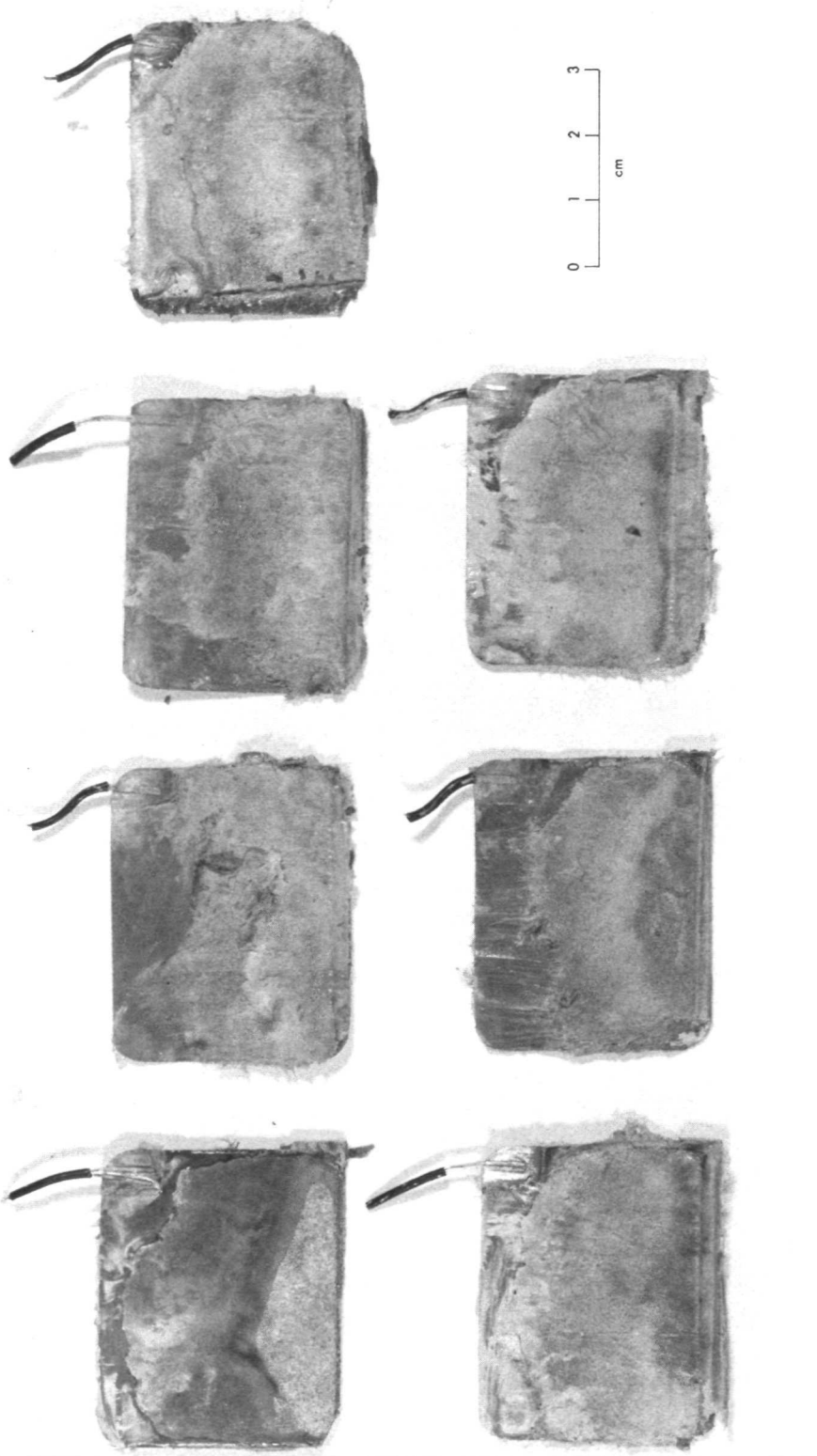


Fig. 43. Yardney electrolyte-starved cell, 75-G relative acceleration, zinc electrodes

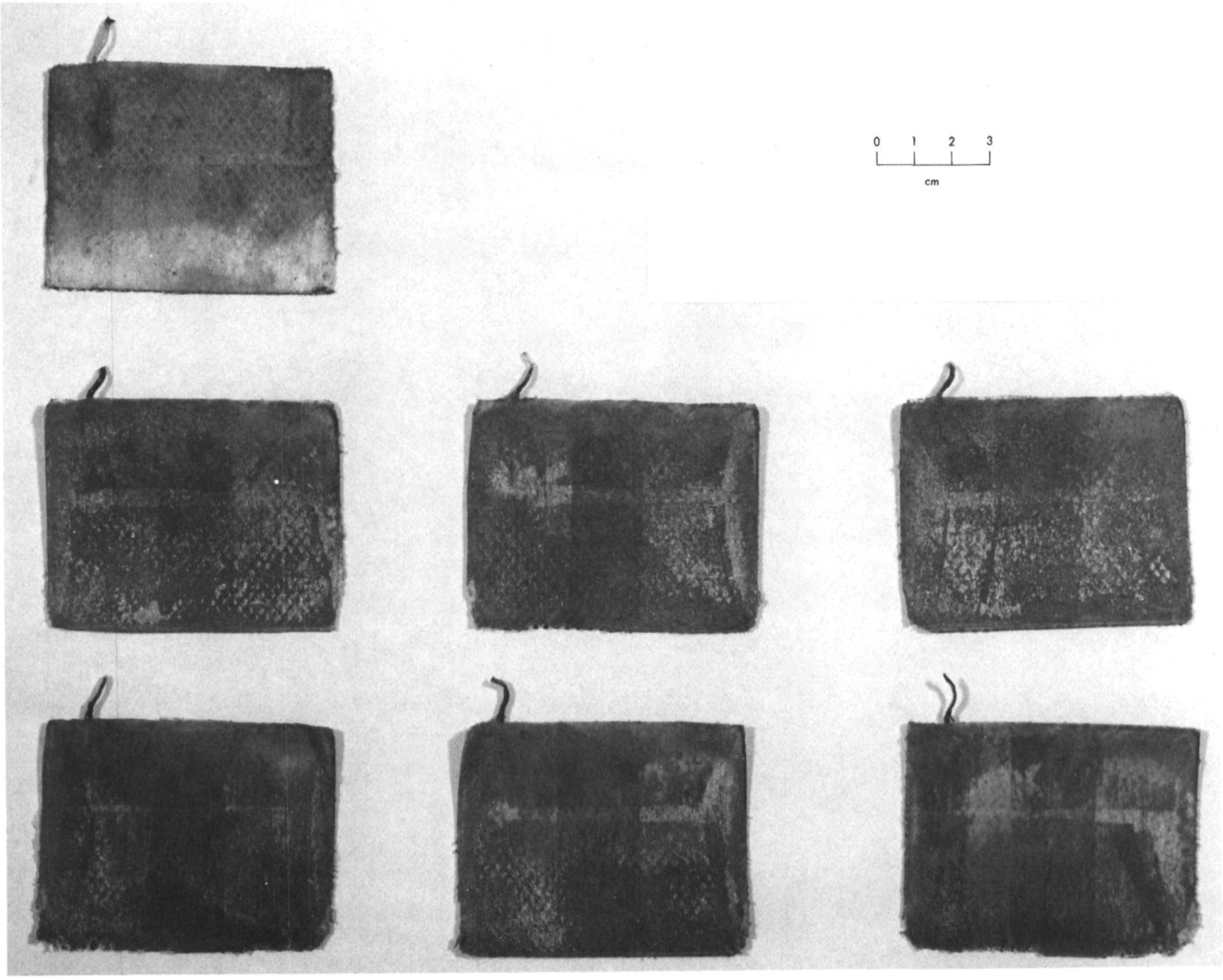


Fig. 44. Mariner-type cell, 1-G relative acceleration, zinc electrodes

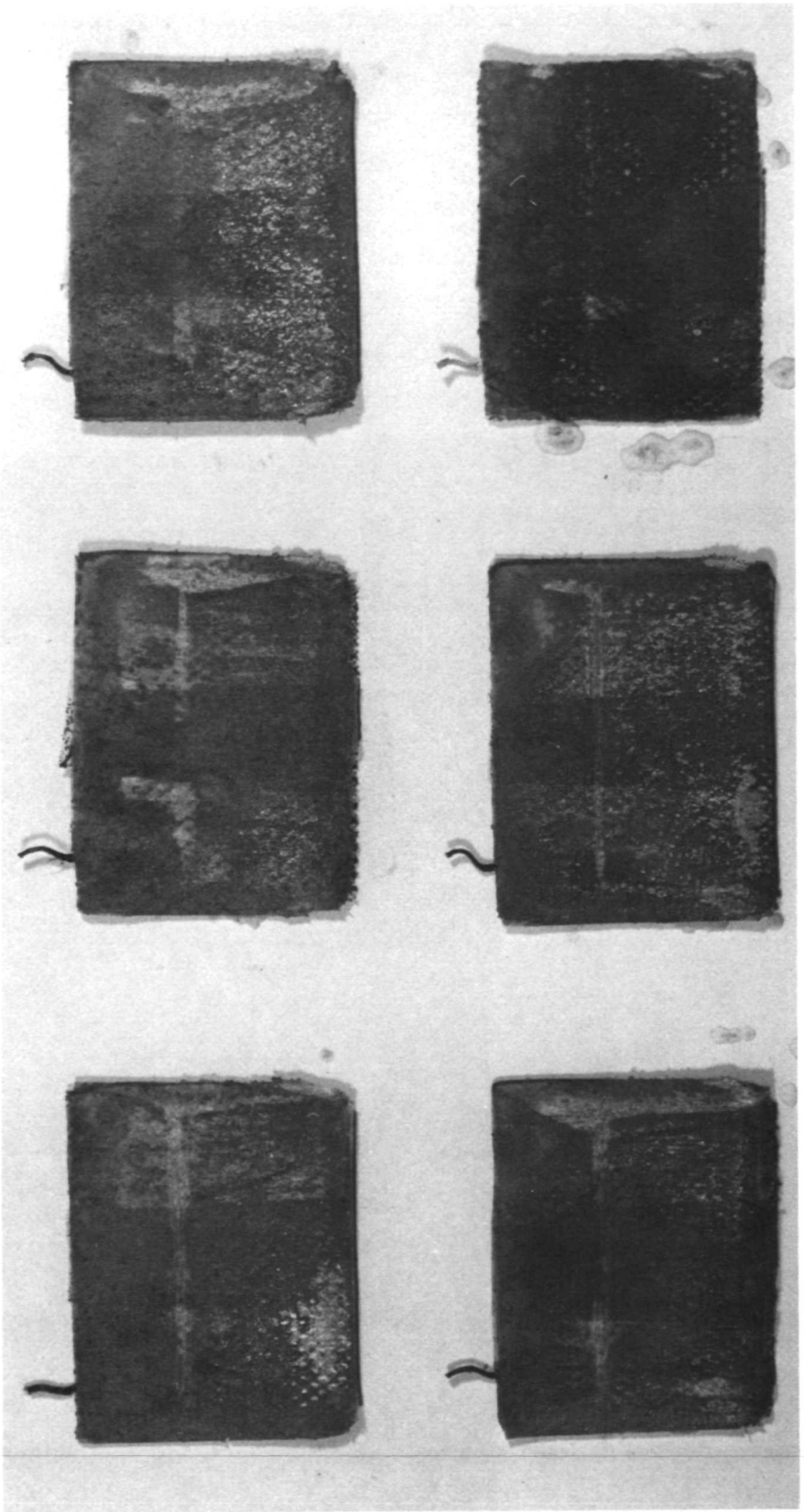

Fig. 44 (contd)

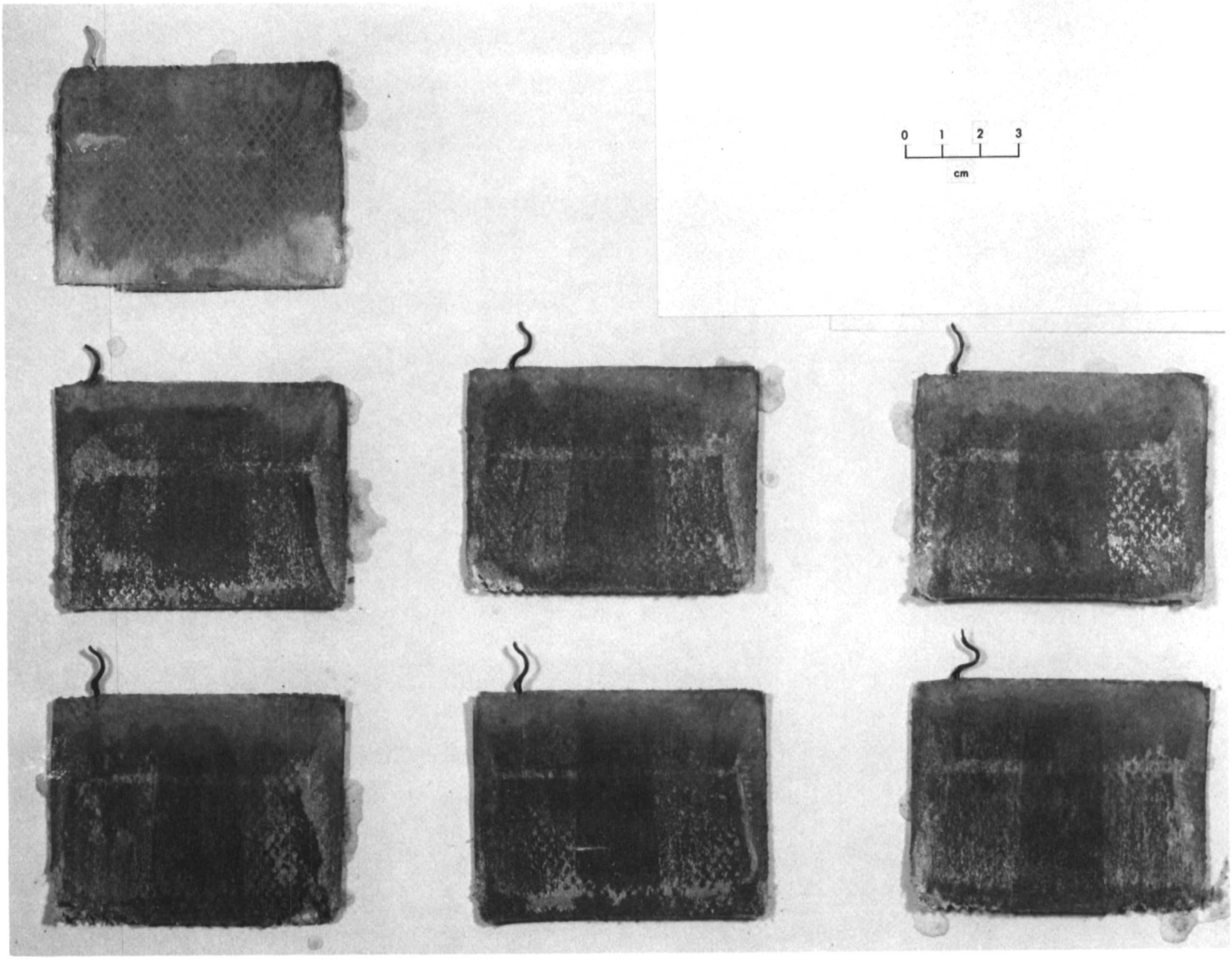


Fig. 45. Mariner-type cell, 10-G relative acceleration, zinc electrodes

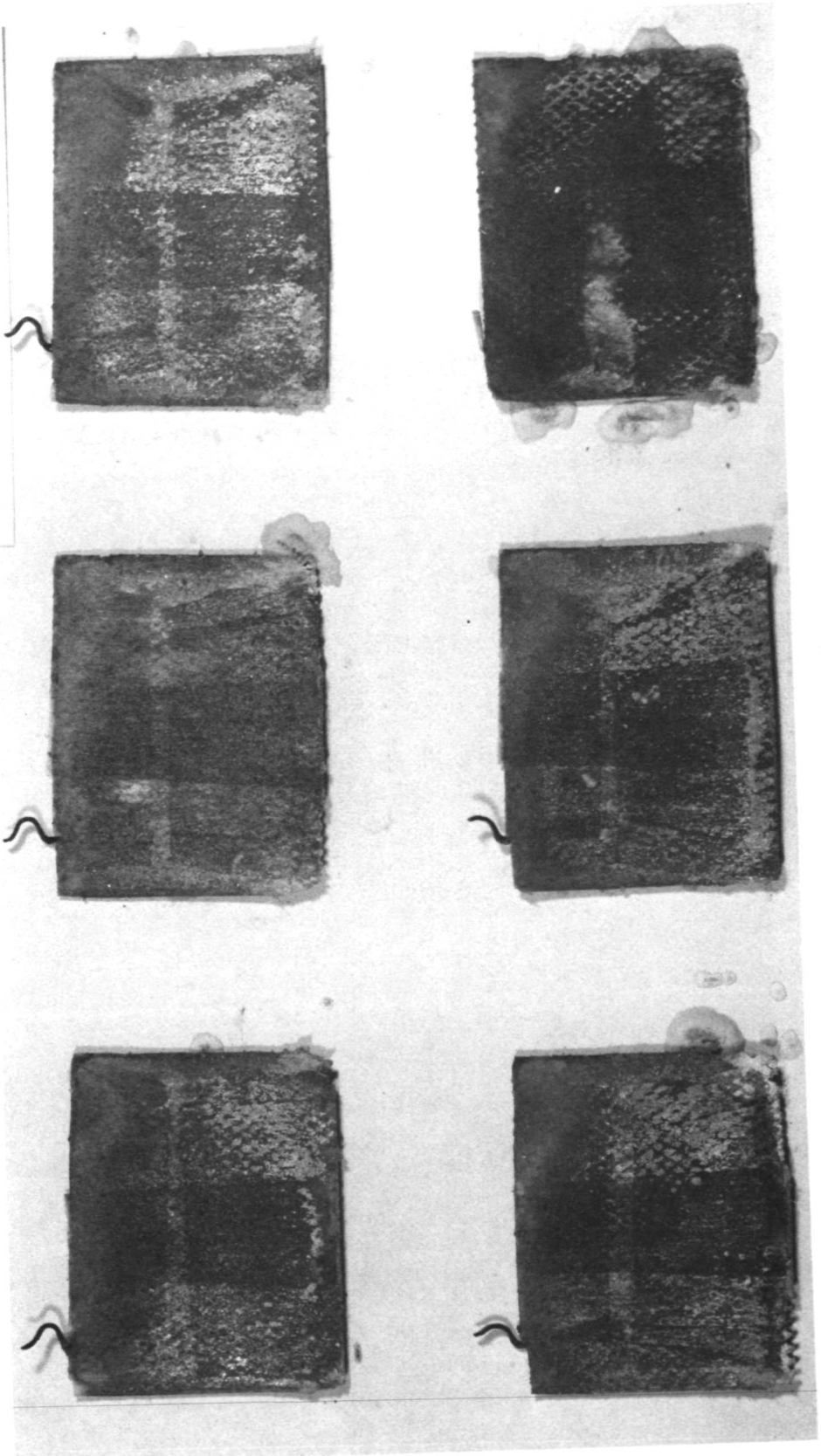

Fig. 45 (contd)

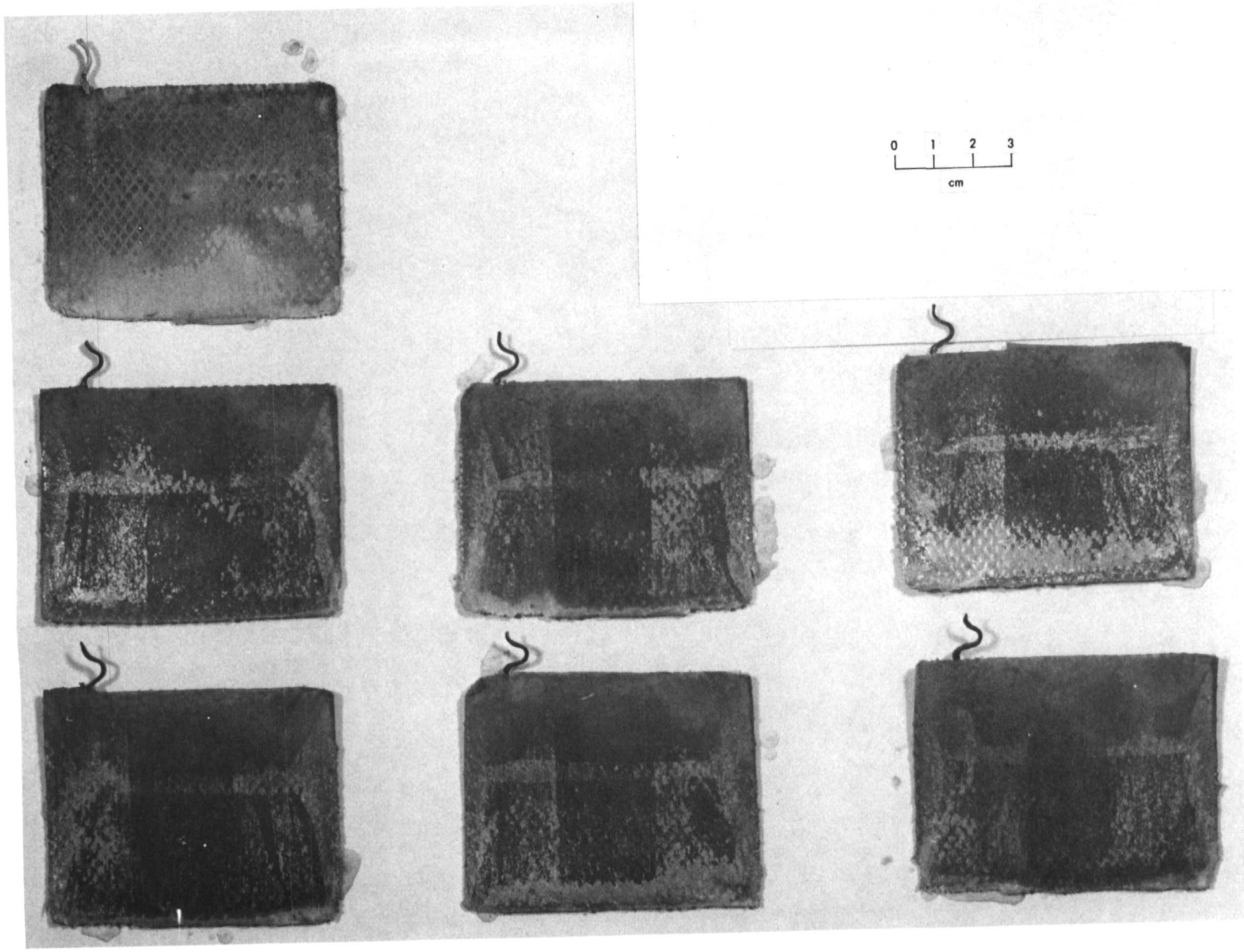


Fig. 46. Mariner-type cell, 20-G relative acceleration, zinc electrodes

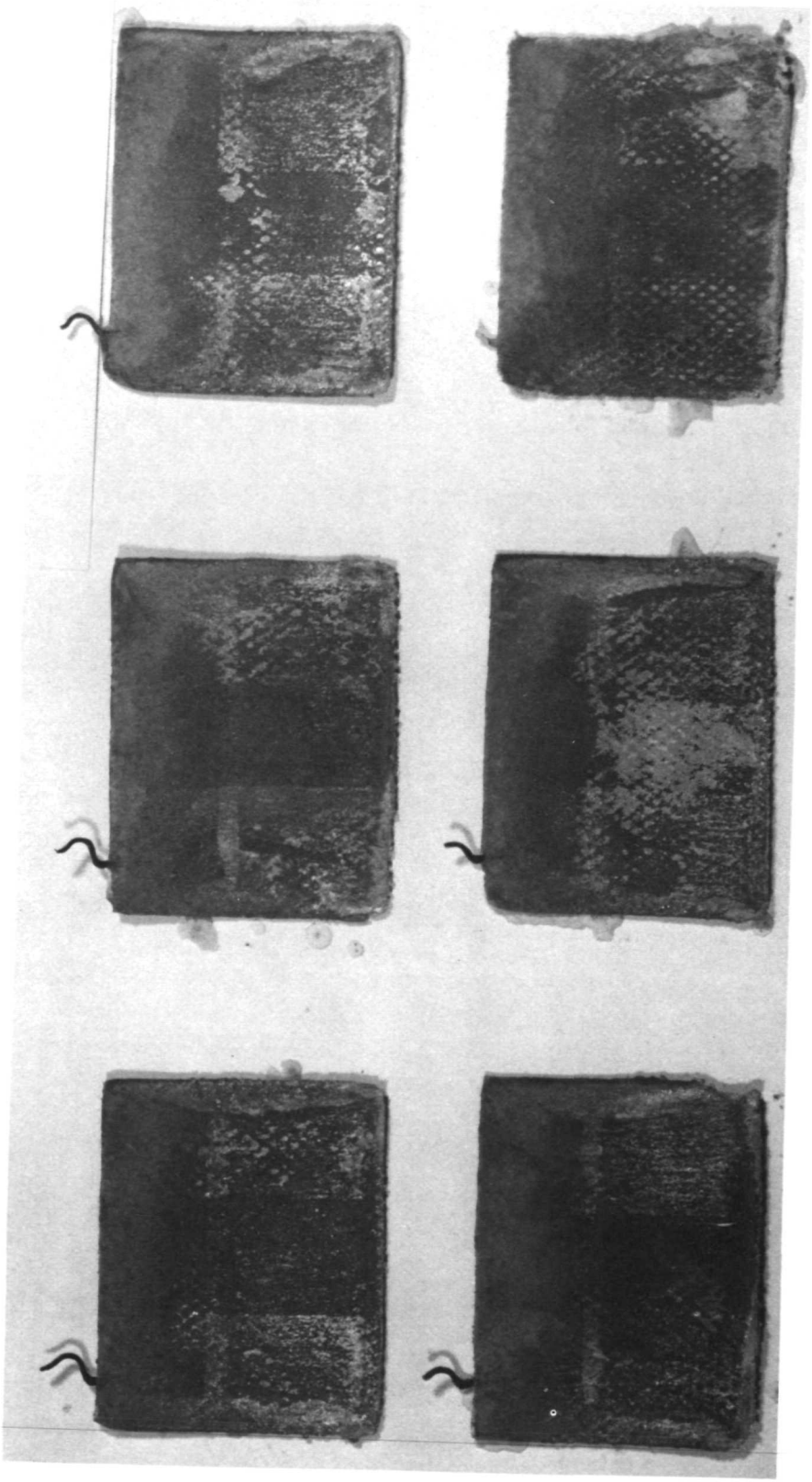

Fig. 46 (contd)

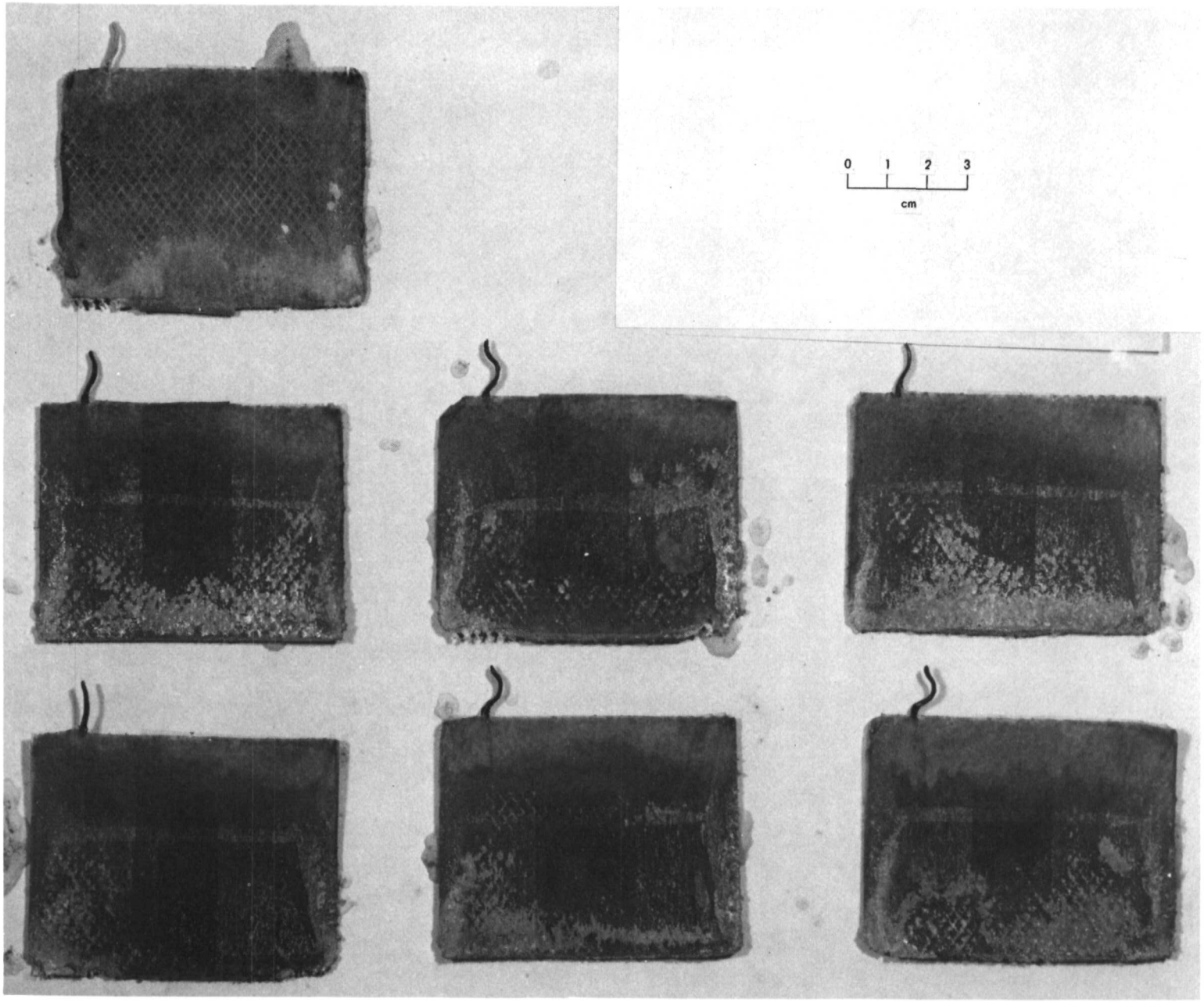


Fig. 47. Mariner-type cell, 30-G relative acceleration, zinc electrodes

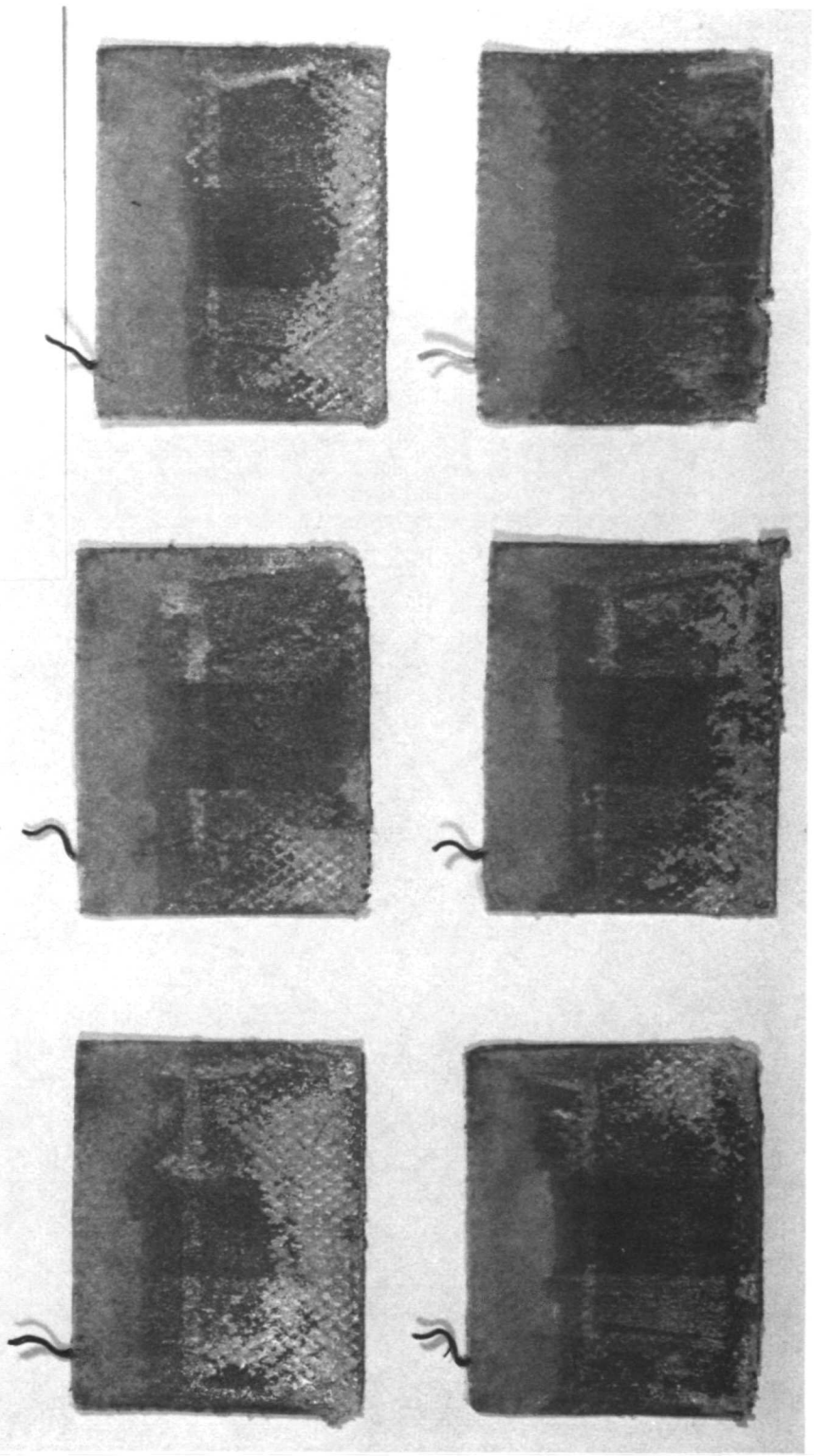

Fig. 47 (contd)

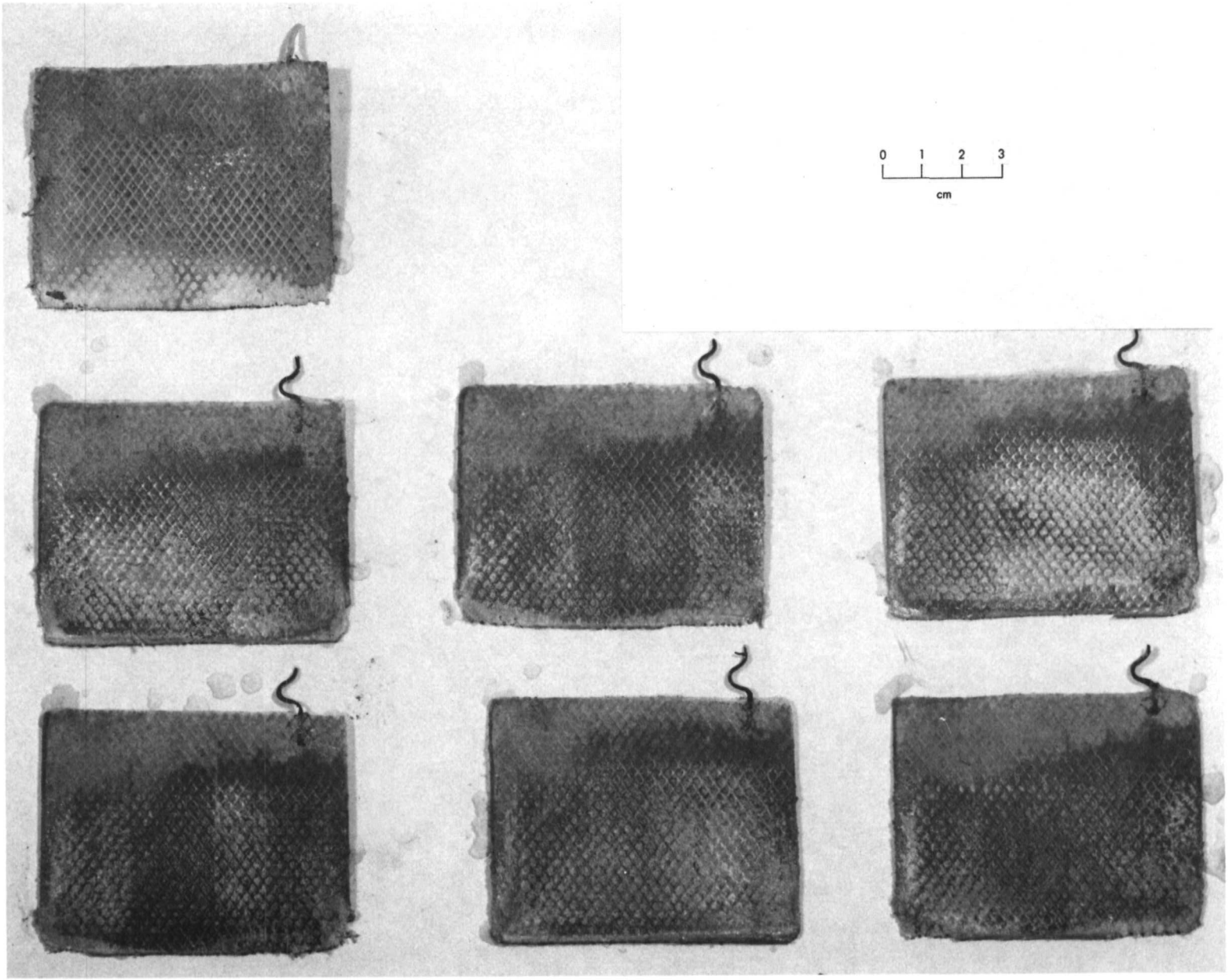


Fig. 48. Mariner-type cell, 50-G relative acceleration, zinc electrodes

Fig. 48 (contd)

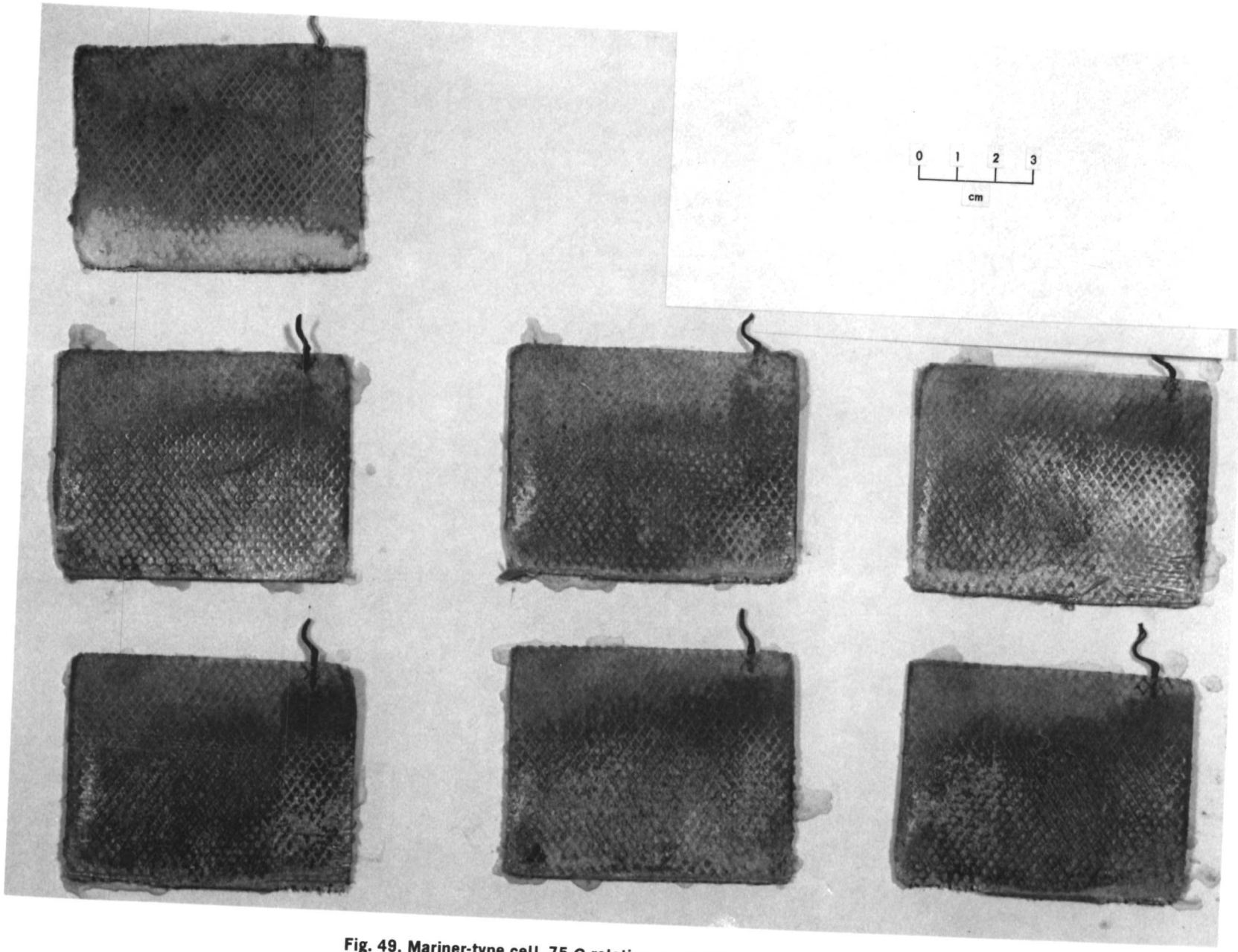


Fig. 49. Mariner-type cell, 75-*G* relative acceleration, zinc electrodes

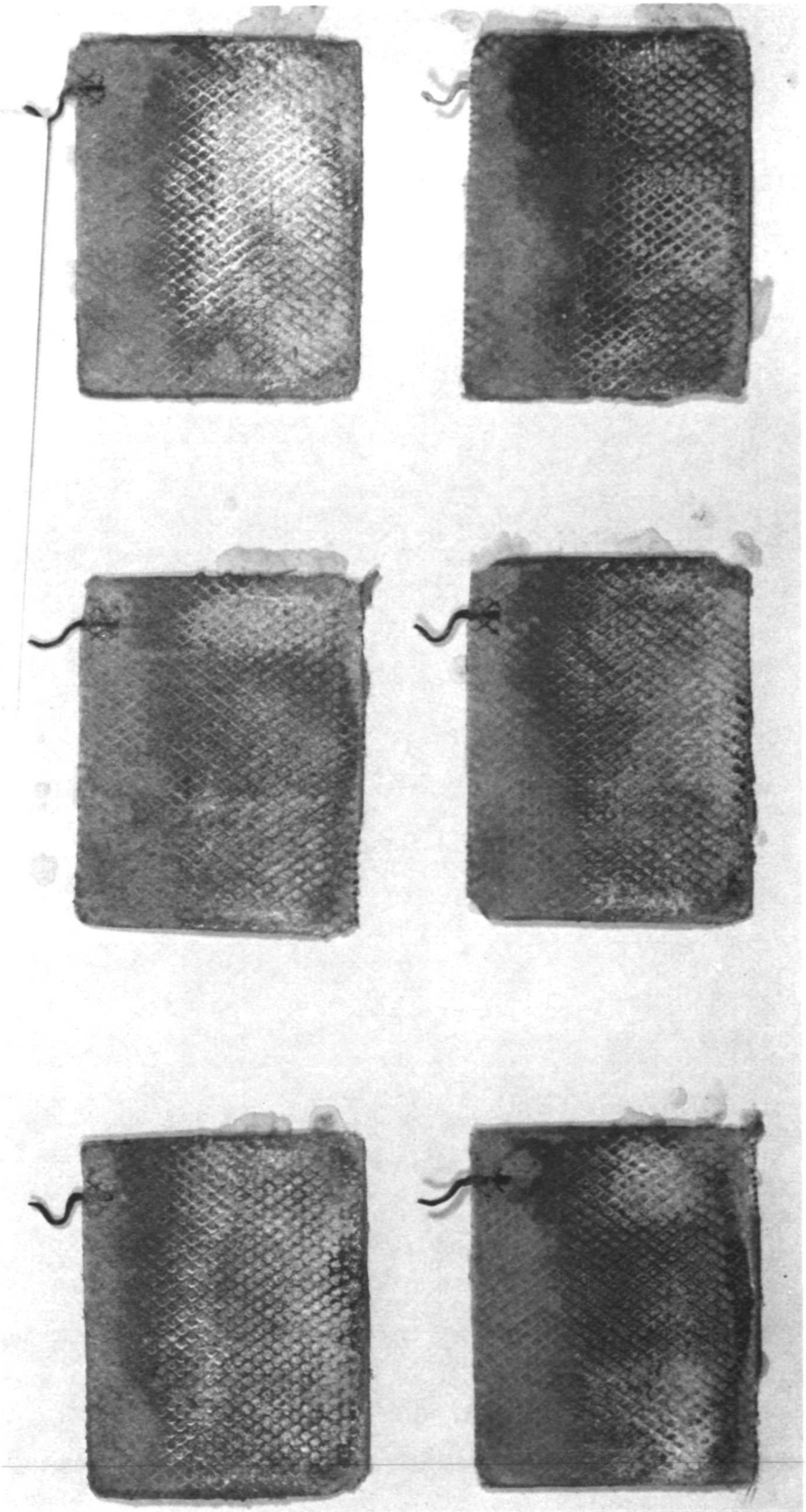

Fig. 49 (contd)

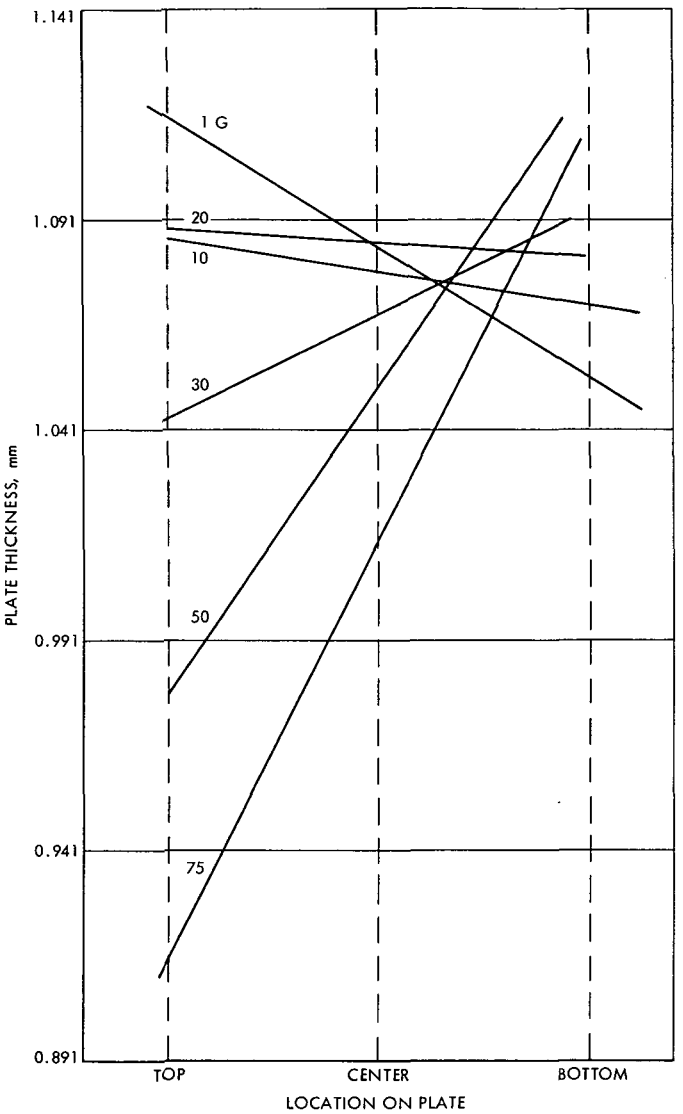


**Fig. 50. Zinc electrode thickness profile after acceleration tests on starved Mariner-type cells**

## XII. Observed Current Densities for Batteries in Space

As of the date of this writing, no information is available on limiting current densities from any batteries involved in space flight. Indeed, most indications are that such batteries are generally overdesigned to the extent that when they are working properly there is still considerable reserve at times of peak demand.

In spite of the lack of these data, some observations on past space flights give information on current densities that have actually been realized in environments of less than 1 *G*. A few of these accounts are listed below.

(1) Mariner 7. The battery on the Mariner 7 probe was a starved silver–zinc unit of 50-A-h capacity. While operating in space at zero *G*, it delivered 12.54 A on 1200 $cm^2$ of electrode surface under routine conditions. This is equivalent to 10.5 $mA/cm^2$ (Ref. 10).

(2) Mariner 9. The battery on Mariner 9 is a sealed nickle–cadmium system with 1290.3 $cm^2$ of anode surface. It was known to deliver 2 A in zero-*G* application. This is approximately 1.5 $mA/cm^2$ (Ref. 10).

(3) Apollo 15 ascent battery. On the flight of Apollo 15, a 296-A-h, silver–zinc battery was utilized in the lunar module. This battery had 20 cells, with 12 positive and 13 negative plates per cell. The plates were 11.11 × 14.29 cm in size. A drain of 32.7 A was incurred after the vehicle left the surface of the moon and after the lift-off engines had ceased firing. The *G* value was thus somewhere between 1/6 and zero. The apparent current density at this rate was 8.6 $mA/cm^2$ (Ref. 11).

(4) Apollo 15 lunar rover battery. The battery which propelled the lunar rover of Apollo 15 was a 23-cell flooded silver–zinc battery with a capacity of 121 A-h. Each cell contained 11 positive and 12 negative plates. The plates were 15.24 × 6.98 cm in size. During use, the maximum current drain was 10 A, resulting in a peak current density of 4.3 $mA/cm^2$ (Ref. 12).

(5) Apollo 15 entry battery. On this flight, the battery used in the earth re-entry vehicle was a 20-cell, 40-A-h, starved silver–zinc battery containing 8 positive and 9 negative plates per cell. The plates were 5.24 × 10.32 cm in size. After the parachutes had been deployed (which means that the value of *G* was somewhat less than 1) the battery delivered 33 A at a voltage of 28.5 V. This is equivalent to a current density of 38 $mA/cm^2$. The battery had been in use approximately 1/2 h, delivering a current of about 20 A, when the 33-A pulse was observed (Ref. 11).

## XIII. The Generation of EMF by Gravitational Effects

It has long been observed that an EMF may be generated within an electrochemical cell merely by separating the electrodes along the direction of a gravitational field. These effects should not be confused with the more serious disturbance which occurs due to chemical mass transfer influences by gravitational fields and which is the main topic of this report. Although the EMF generated by gravitational forces is very small, the subject merits some discussion in order to avoid confusion between the two types of physical phenomena.

One may generate an EMF with the use of a gravitational field by taking an electrochemical cell consisting of two chemically identical electrodes in contact with a uniform solution of electrolyte and merely arranging that the electrodes are parallel to each other and perpendicular to the gravitational field. The strength of the EMF that is generated is proportional to the separation between the electrodes and the strength of the gravitational field. In the common electrochemical cell, the EMF that is generated is due to a difference in chemical potential between the pair of electrodes. In the "gravity cell" the EMF that is generated is due to a difference in gravitational potential between the electrodes.

The early work on the study of the gravity cell dates back to a series of experiments by Des Coudres (Ref. 13) between 1893 and 1896. Des Coudres found the EMF generated by gravitational fields to be of the order of a few microvolts per meter and showed that the potential generated was a function of the transference numbers of the chemical components in the cell.

In a later study, Tolman (Ref. 14) conducted experiments with a powerful centrifuge and obtained potentials about 150 times the values measured by Des Coudres. Tolman utilized the technique to measure the transference number for potassium iodide, and the value he obtained agrees with the best modern values to well within 1%.

Ensanian (Ref. 15) reportedly observed a significant gravitational potential effect in a 5.2-m free-fall experiment with a thermocell. He questioned his own findings, however, and reasoned that the observed deflections in EMF might have been due to unknown mass transfer phenomena. Kaimakov and Varshavskaya (Ref. 16) asserted that the gravitational EMF reaches a limiting value after $10^{-8}$ s, and that changes which occur after that can be traced to concentration EMFs. A summary of the effects of gravity and centrifugal force in generating EMF in galvanic cells has been presented by MacInnes (Ref. 17).

## XIV. Conclusions

Theories developed for cases of natural convection seem only partly adequate in helping predict gravitational or acceleration effects on batteries. Such theories generally predict that the limiting current density that one can realize will vary with the relative acceleration to the 1/4 power and are based upon a model that does not consider electrode separation, separator material, or electrode length as parameters. These latter variables are certainly significant as demonstrated in the studies by Arcand (Ref. 9) and Divine (Ref. 7), and the power dependence on the relative acceleration may vary from 1/3 to 1/5 depending upon how the cell is constructed. The difference between these two fractions may appear small, but they predict greatly different results when the value of $G$ is very small or very large. Eisenberg et al. (Ref. 5) demonstrated that natural convection is a very important mode of mass transfer in an experimental silver–zinc cell and that one loses much of the ability to draw current from a system if this type of fluid flow is absent.

For batteries used in space applications, it is desirable to have some design information concerning performance in a near-zero gravitational field. There are still very few satisfactory correlations that will predict limiting current behavior in such environments, chiefly because (1) one can not obtain the time needed to perform an experiment by the presently available methods of low-gravity simulation while being subjected to the earth's gravitational field and (2) the cost of properly performing such experiments in an earth-orbiting vehicle is very high.

With regard to high-$G$ information, the studies performed to date appear to give consistent results, and there is no apparent need for additional research in this area at present. The research performed at the U.S. Naval Depot in Crane, Indiana, indicates severe zinc migration in the secondary silver–zinc cell, which one might not have predicted at high-$G$ levels. Such phenomena could shorten the life of these cells in that type of environment and should be taken into consideration by those designing batteries for exploration vehicles on large planets.

Continued research appears necessary for zero- or <1-*G* battery applications. The problem of extrapolating data from >1-*G* experiments to <1-*G* situations is easily seen by noting that the work of Arcand (see Table 2) would predict that a limiting current density of no greater than 7 mA/cm$^2$ could be achieved in zero *G* by a silver–zinc cell, yet the same type of system easily gave a current density of 10.5 mA/cm$^2$ on the Mariner 7 probe in deep space. Conflicts also appear to be evident by the rather large current densities obtained in <1-*G* environments by the batteries on the Apollo 15 flight (see Section XII).

In spite of the funds devoted to various types of battery studies during the past decade, the technology still seems to fall far short of providing the type of information necessary for low-*G* battery design. Considering that all batteries have poor energy–weight ratios and that the cost of putting a probe into space is directly related to weight, it is apparent that a 2.3-kg (5-lb) experimental package put aboard one of the space vehicles to determine how hard a battery may be worked in zero-*G* environments would yield valuable data for future battery designers. An ammeter and a small silver–zinc battery that would be set to discharge at high load in a sounding rocket, or a similar system that would be designed to undergo charge and discharge cycles in free space, would provide more pertinent information than that which can be obtained in the laboratory.

## References


1. Levich, V. G., *Physicochemical Hydrodynamics.* Prentice-Hall, Inc., Englewood Cliffs, N.J., 1962.
2. Wagner, C. "The Role of Natural Convection in Electrolytic Processes," *J. Electrochem. Soc.*, Vol. 95, pp. 161–173, 1949.
3. Keulegan, G. H., "Hydrodynamics of Cathode Films," *J. Res. NBS*, Vol. 47, pp. 156–169, 1951.
4. Kotake, S., "Effects of Reduced Gravity on Nucleate Boiling, *Jap. Soc. Mech. Eng. Bull.*, Vol. 12, pp. 1459–1466, Dec. 1969.
5. Eisenberg, M., Bauman, F., and Brettner, D. M., "Gravity Field Effects on Zinc Anode Discharge in Alkaline Media." *J. Electrochem. Soc.*, Vol. 108, pp. 909–915, 1961.
6. Fenech, E. J., *Ionic Mass Transport by Free Convection to Horizontal Electrodes,* Ph.D. Thesis. University of California, Berkeley, Calif., 1960.
7. Divine, J. *Mass Transfer at Vertical Plane Electrodes as Affected by Electrode Separation, Porous Separators and Acceleration,* Ph.D. Thesis. Oregon State University, Corvallis, Ore., 1965.
8. Young, I. K., Space Division, North American Rockwell Corporation, personal communication.

## References (contd)


9. Arcand, G. M., and Uchiyama, A. A., "Gravity Effects on Batteries," in *Supporting Research and Advanced Development*, Space Programs Summary 37-23, Vol. IV, pp. 23–24, Oct. 31, 1963; Arcand, G. M., "Gravity Effects on Batteries," in *Supporting Research and Advanced Development*, Space Programs Summary 37-26, Vol. IV, pp. 40–41, Apr. 30, 1964; Arcand, G. M., and Uchiyama, A. A., "Gravity Effects on Batteries," in *Supporting Research and Advanced Development*, Space Programs Summary 37-30, Vol. IV, pp. 28–29, Dec. 31, 1964. Jet Propulsion Laboratory, Pasadena, Calif.

10. Krause, S., Jet Propulsion Laboratory, Pasadena, Calif., personal communication.

11. Trout, J. B., NASA Manned Spacecraft Center, Houston, Tex., personal communication.

12. Stanley, D., Eagle-Picher Industries, Inc., Joplin, Mo., personal communication.

13. Des Coudres, T., *Ann. Phys. und Chem.*, Vol. 49, p. 284–294, 1893.

14. Tolman, R. C., *Proc. Am. Acad.*, Vol. 46, p. 109–146, 1910; *J. Am. Chem. Soc.*, Vol. 33, p. 121, 1911.

15. Ensanian, M., *J. Electrochem. Soc.*, Vol. 113, p. 516–518, 1966.

16. Kaimakov, E. A., and Varshavskaya, N. L., Elektrokhimia, Vol. I, p. 585, 1965.

17. MacInnes, D. A., *The Principles of Electrochemistry*, pp. 174–180. Reinhold Publishing Corp., New York, 1939.

# Appendix A
# Equipment Used by Divine (Ref. 7)

## I. Cell and Electrodes

The cell used for this work was machined from a cast Lucite[2] rod 6.35 cm in diameter. The external dimensions of the assembled cell are 6.35 cm in diameter by 13.02 cm in length. The internal dimensions are shown in Fig. A-1.

Nine pairs of vertical electrodes were constructed. This group of nine was then subdivided into three groups of three pairs. Group I, designated by $s = 1$, consisted of three anodes, occupying the entire exposed face of the electrode holder, and three cathodes. Each of the cathodes was centered on and inserted in a groove in the face of its electrode holder. The three pairs of group I were designated by $d = 1$, 2, and 3, where the cathodes are 1.27, 2.79, and 5.08 cm long, respectively. For the study of the effects of the porous separator, two more sets of these electrodes were constructed. The only difference between the three sets of $s = 1$ electrodes was that in the second two sets the cathode length was 2.54 cm rather than 2.79 for $d = 2$.

Groups II, $s = 2$, and III, $s = 3$, were each separated into similar pairs with $d = 1$, 2, and 3; the lengths were again 1.27, 2.79, and 5.08 cm. For $s = 1$, the cathode–anode separation was 2.54 cm; for $s = 2$, the separation was 0.635 cm; and for $s = 3$, it was 0.159 cm.

The individual electrodes are designated by their name (for example, "cathode") and the classification number *sd*. That is, if $sd = 11$, then the electrode pair of interest is in the group with an electrode separation of 2.54 cm and a cathode length of 1.27 cm. Thus, the three groups are 11, 12, 13; 21, 22, 23; 31, 32, and 33. This shorthand notation is used throughout this work. (see Table A-1).

The electrodes themselves were constructed from electrolytic copper sheet and were attached to the machined electrode holders with black Glyptal paint. The cathodes were mounted so that the copper surface was flush with the plastic surface.

## II. Reference Electrode

A reference electrode of the Luggin capillary type, consisting of a copper wire in a glass tube, was used to measure the polarization of the cathode. In the case of $s = 1$, the reference electrode was situated in

[2]Universal Plastics Company, Seattle, Washington.

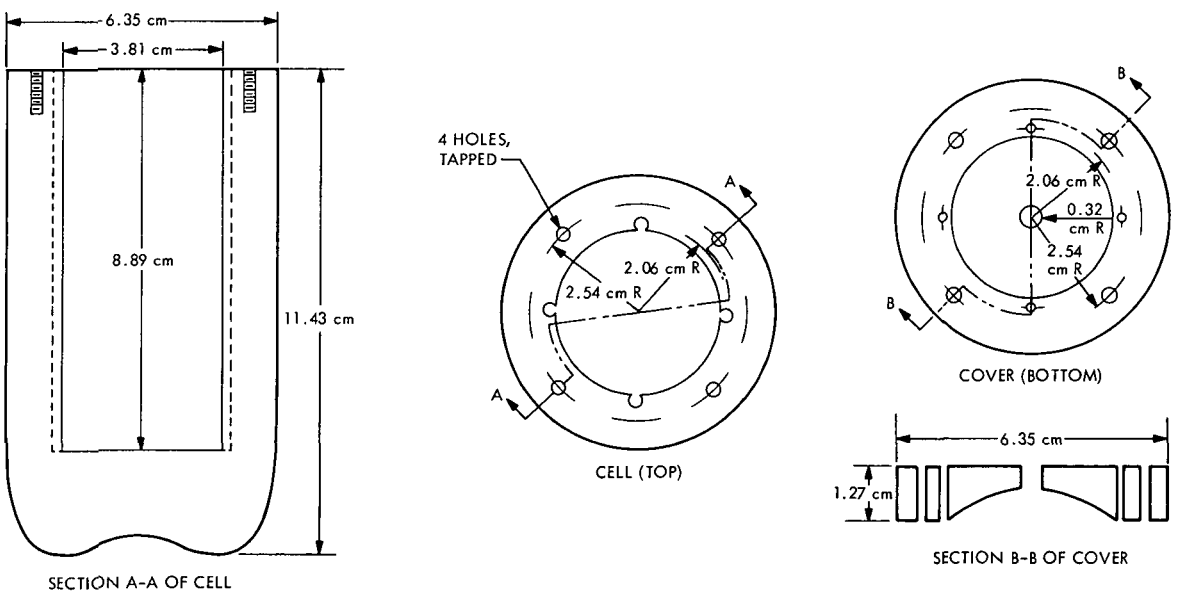


**Fig. A-1. Cell and cell cover design (Divine)**

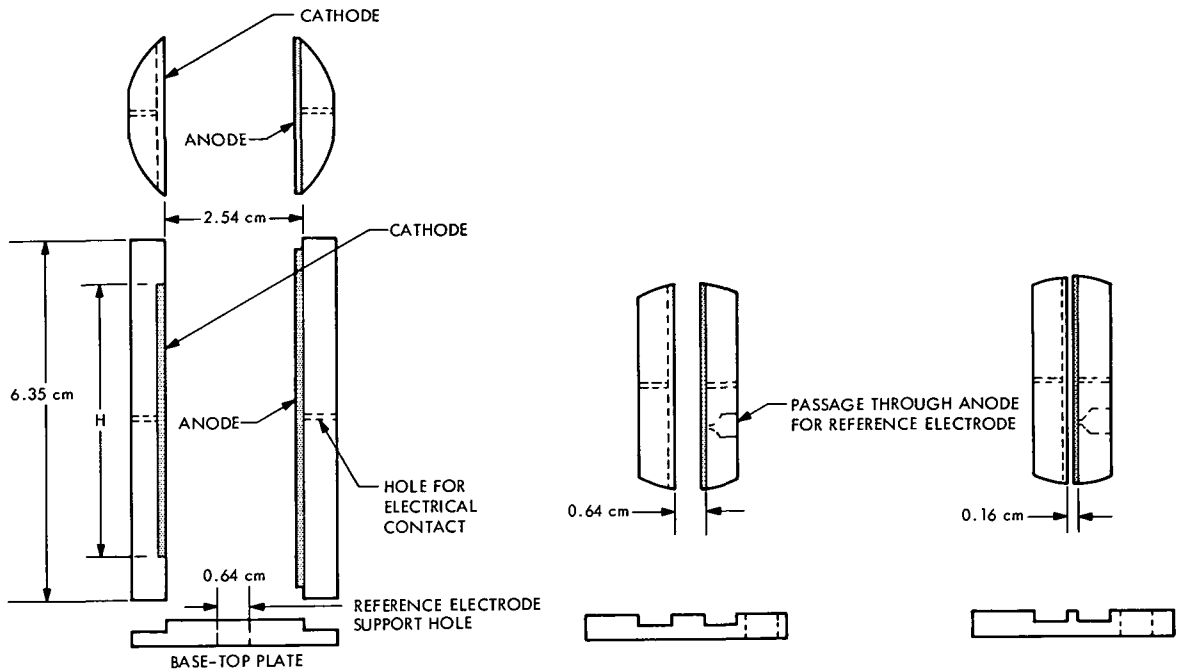


**Fig. A-2. Electrode and base plate design (Divine)**

the region between the electrodes. With $s = 2$ and 3, owing to the lack of space, it was necessary to place the reference electrode behind the anode. Thus the capillary tube had to pass through the anode to reach the cathode. Figures A-2 and A-3 illustrate the two arrangements.

## III. Mercury Contact

The rotating mercury contact used in this work is different from the type conventionally used. Whereas the usual practice is to have the mercury pool stationary and the immersed contacts rotating, it was found convenient to do the reverse.

The mercury channels were four equally spaced grooves in a section of Lucite rod (Fig. A-4). This plastic component had platinum-plated brass screws inserted into each channel from the underside. Wires from these screws made contact with the cell, while mercury completed the connection to the stationary contacts.

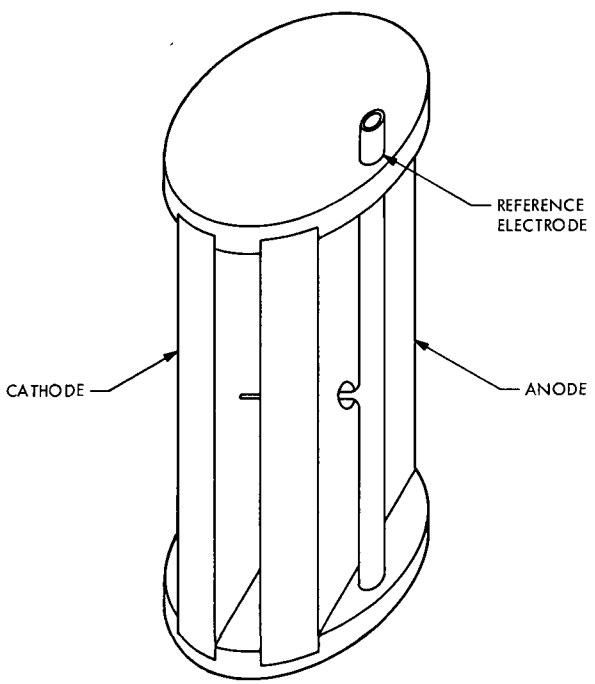


**Fig. A-3. Assembled electrodes with top, base, and Luggin capillary, for spacings $s = 2$ and 3 (Divine)**

Copper wires were used for the stationary contacts because of their wettability by the mercury and the consequent behavior in the moving mercury stream. It was learned late in the experimental work that very satisfactory results could be obtained by using carbon brushes on stainless steel rings. Only the mercury contact was used in this work, however.

**Table A-1. Electrode classification**

| Electrode classification[a] | Length, cm | Geometric surface area, cm² |
|---|---|---|
| 11 or 11B1 | 1.27 | 3.44 |
| 12 or 12B1 | 2.79 | 7.66 |
| 13 or 13B1 | 5.08 | 14.4 |
| 21 | 1.27 | 4.69 |
| 22 | 2.79 | 10.1 |
| 23 | 5.08 | 18.6 |
| 31 | 1.27 | 4.66 |
| 32 | 2.79 | 10.69 |
| 33 | 5.08 | 18.88 |
| 11B2 | 1.27 | 3.52 |
| 12B2 | 2.54 | 7.05 |
| 13B2 | 5.08 | 14.4 |
| 11B3 | 1.27 | 3.58 |
| 12B3 | 2.54 | 7.16 |
| 13B3 | 5.08 | 14.4 |

[a]The letter B indicates that the electrode was used in the porous separator experiments and the number following denotes the size of particles used.

## IV. Instrumentation

The calibration and experimental equipment is described below.

### A. Calibration

The following equipment was used for calibration of the instruments used in the experimental work:

(1) A 0 to 1.6-V precision potentiometer.[3]

(2) A high-sensitivity, 0.48-$\mu$V/mm galvanometer.[4]

(3) A 0 to 999.9-Ω precision resistor.[5]

(4) A precision resistance bridge.[6]

[3]Model K2, Leeds and Northrup Company, Philadelphia, Pennsylvania.

[4]Catalog No. 2430-A, Leeds and Northrup Company, Philadelphia, Pennsylvania.

[5]Catalog No. 4776, Leeds and Northrup Company, Philadelphia, Pennsylvania.

[6]Catalog No. 4725, Leeds and Northrup Company, Philadelphia, Pennsylvania.

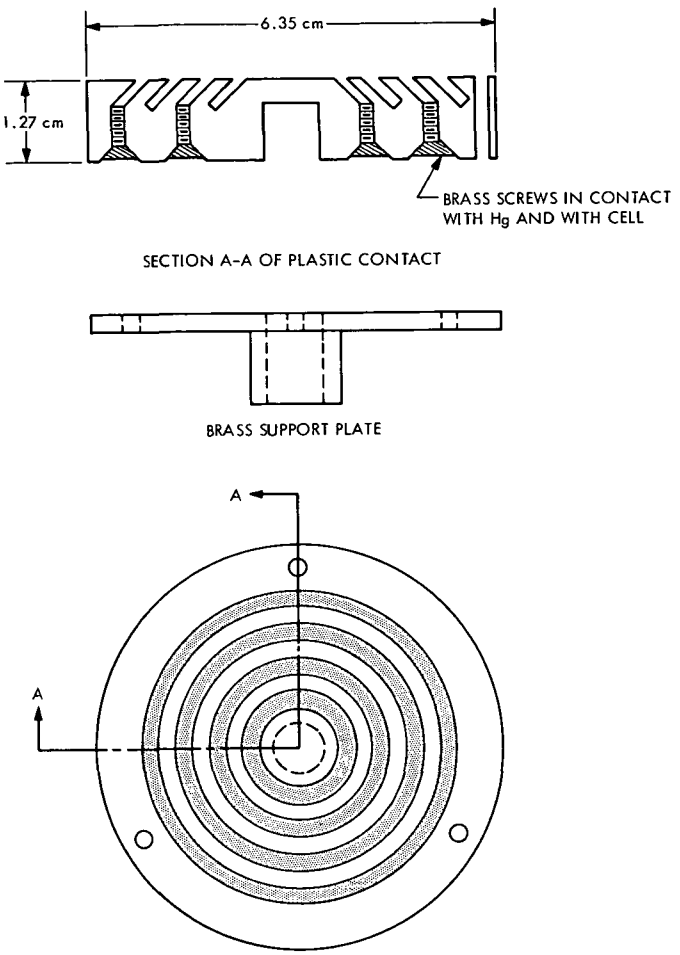


**Fig. A-4. Rotating mercury contact (Divine)**

## V. Experimental Equipment

The experimental equipment (see Fig. A-5) consisted of:

(1) A two-channel strip chart recorder[7] with auxiliary input resistances as follows:

(a) Channel 1, the reference electrode circuit, had 5 MΩ on the 0 to 500-mV range, 10 MΩ on the 0 to 1.0-V range, and 500 kΩ on the 0 to 5.0-V range.

(b) Channel 2, the current circuit, had 100 kΩ for both the 0 to 10-mV and 0 to 1.0-V scales, 500 kΩ for the 0 to 50-mV and 0 to 5.0-V scales, 1.0 MΩ on the 0 to 100-mV scale, and 5 MΩ on the 0 to 500-mV scale.

[7]Servo-riter Recorder, Texas Instruments Inc., Houston, Texas.

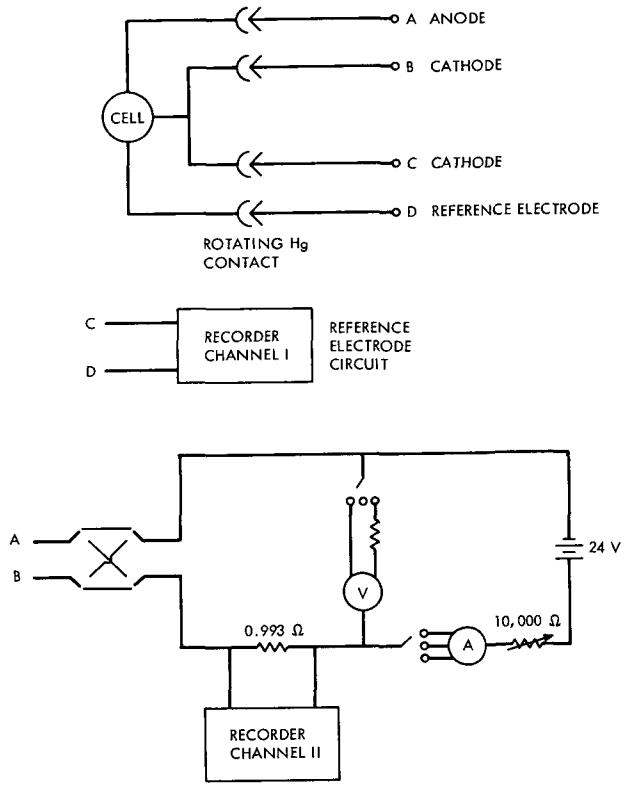


**Fig. A-5. Circuit schematic (Divine)**

(2) A 0.993-Ω ±0.5% resistor constructed of Nichrome wire.

(3) A variable resistor, 0 to 10, 400 Ω.

(4) A 0 to 150-mV meter[8] doubling, with a series resistance inserted, as a 0 to 1.5-V meter.

(5) A 0 to 500 milliammeter.[8]

(6) A 0 to 3.0, 0 to 15.0 ammeter.[9]

(7) A 24-V aircraft battery used as a power source.

(8) A portable precision potentiometer, 0 to 80 mV.[10]

## VI. Centrifuge, Stroboscope, and Voltage Regulator

A commercial model centrifuge[11] was converted by the substitution of a lid with a transparent window for the original solid top. The addition of the window permitted the use of an electrode stroboscope[12] capable of a precision of 1% for the measurement of speeds after calibration.

Both the centrifuge and stroboscope were supplied with power by the voltage regulator.[13] In this manner, the system was free from common variations of voltage.

[8]Model 420, Triplett Electrical Instrument Company, Bluffington, Ohio.

[9]Model 931, Weston Electrical Instrument Company, Newark, New Jersey.

[10]Catalog No. 8662, Leeds and Northrup Company, Philadelphia, Pennsylvania.

[11]Size 2, Model V, International Equipment Company, Boston, Massachusetts.

[12]Strobtac, type 1531-A, General Radio Company, West Concord, Massachusetts.

[13]Model 2000-S, A. C. Voltage Regulator, A. E. Sorenson and Company, Stamford, Connecticut.

# Appendix B

# Equipment Used by Arcand (Ref. 9)

## I. Cell and Electrodes

The cell employed by Arcand had the shape of a cylinder with a diameter of 3.7 cm. The electrodes were separated by a distance of 1.3 cm, and a spacer kept the electrodes rigidly in place after the cell was assembled. The significant dimensions of the system are shown in Fig. B-1.

A mask having a 1-cm-square hole in the center was placed against the anode for most of the tests. The cathode plate was made from Delco-Remy[14] sintered silver plate welded to sheet silver and electrolytically formed according to the company specifications. Provision was made to place a Viskon Nonwoven Battery Separator Fabric at distances of 0, 0.5, and 1.3 cm from the zinc electrode.

In all studies, the anode consisted of a polished zinc electrode surface which was renewed after each test.

## II. Electrolyte and Reference Electrode

The electrolyte employed in this study consisted of a 10 M solution of KOH saturated with ZnO. Contrary to the construction of most silver–zinc batteries, a large volume of free electrolyte existed between the electrodes in this test cell.

The reference electrode consisted of a short piece of 99.99% zinc wire sealed into the cell about 0.7 cm from the anode surface. Preliminary tests indicated that limiting current was realized when the potential difference between the reference and working electrodes was more than 1 V.

[14]Delco-Remy Division, General Motors Corporation, Anderson, Indiana.

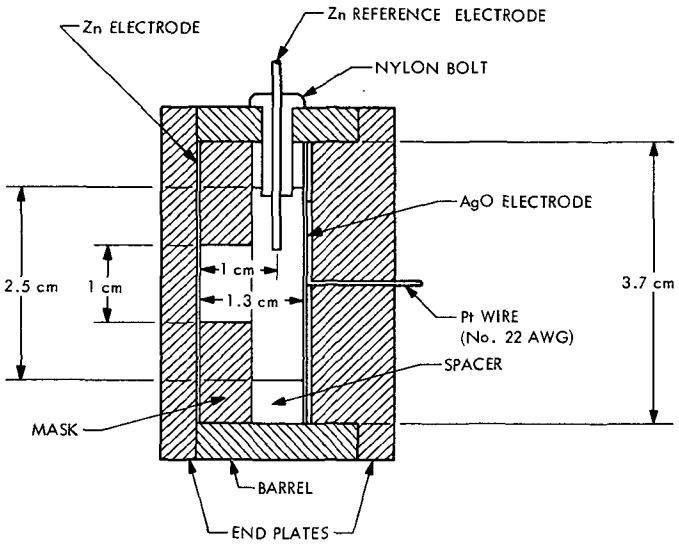


**Fig. B-1. Cell geometry (Arcand)**

## III. Procedure

Before each test, the zinc anode plate was cleaned by polishing with steel wool, rinsing in acetone, repeatedly dipping in dilute HCl, and rinsing with distilled water after each acid treatment. Only one run was made with each cell. After the test, the cell was opened and the zinc plate was either reversed or polished again.

After assembly, current was passed through the cell in such a direction as to cause oxidation of the working electrode. The current was increased stepwise at 1-min intervals until the voltage between the reference and working electrodes exceeded 1 V.

The data from a minimum of 22 runs were averaged to determine one data point.

# Appendix C

## Acceleration Tests on Mariner-Type Batteries

The data in Table C-1 are measurements of zinc electrode thickness in centimeters after the cells containing the electrodes were subjected to four charge–discharge cycles at the acceleration value listed. Each battery tested contained ten cells and each cell contained 13 anodes. In each of the cells, four anodes were spot-measured at the top, center, and bottom of the electrode.

These data were averaged, and a least-squares correlation was employed on the average values to give the information used in making Fig. 50.

Because the cells used in these batteries did not contain excess electrolyte, the term "starved" is used in labeling Fig. 50.

**Table C-1. Effects of charge–discharge cycles on zinc electrode thickness**

| Electrode thickness, cm | | | | | |
|---|---|---|---|---|---|
| Top | Center | Bottom | Top | Center | Bottom |
| 1-G relative acceleration | | | 10-G relative acceleration | | |
| .0938 | .0762 | .0800 | .0848 | .0843 | .0947 |
| .1207 | .1105 | .1067 | .1222 | .1132 | .1168 |
| .1156 | .1207 | .1219 | .1229 | .1234 | .1161 |
| .1092 | .1194 | .1156 | .1204 | .1191 | .1069 |
| .0876 | .0787 | .0801 | .0866 | .1013 | .0856 |
| .1156 | .1097 | .1250 | .1062 | .1179 | .1229 |
| .1072 | .1150 | .1059 | .1196 | .1001 | .1209 |
| .1308 | .1232 | .1006 | .0973 | .1133 | .1203 |
| .1041 | .0805 | .0876 | .0955 | .0912 | .0831 |
| .1130 | .1212 | .1207 | .1100 | .1113 | .1146 |
| .1113 | .1275 | .1207 | .1181 | .1107 | .1237 |
| .1265 | .1120 | .1123 | .1328 | .1120 | .1077 |
| .0965 | .0749 | .0970 | .0828 | .0732 | .1021 |
| .1224 | .1181 | .1074 | .1255 | .1097 | .1374 |
| .1339 | .1087 | .1250 | .1133 | .1232 | .1105 |
| .1222 | .1138 | .1184 | .1252 | .1021 | .1097 |
| .1113 | .0792 | .0978 | .0925 | .0818 | .1003 |
| .1412 | .1199 | .1125 | .1262 | .1242 | .1059 |
| .1252 | .1067 | .1008 | .1201 | .1021 | .1311 |
| .1260 | .1222 | .1013 | .1186 | .1113 | .1229 |
| .0950 | .0803 | .0754 | .0894 | .0820 | .0826 |
| .1197 | .1224 | .1097 | .1194 | .1095 | .1148 |
| .1234 | .1283 | .1229 | .1171 | .1110 | .1077 |
| .1143 | .1143 | .1168 | .1224 | .1069 | .0935 |
| .0851 | .0790 | .0879 | .0777 | .0851 | .0820 |
| .1173 | .1107 | .1036 | .1173 | .1186 | .1013 |
| .1077 | .1280 | .1123 | .1128 | .1107 | .1255 |
| .1212 | .1214 | .1120 | .1242 | .1163 | .1001 |
| .0958 | .0754 | .0836 | .0897 | .0828 | .0823 |
| .1222 | .1087 | .1133 | .1069 | .1260 | .1133 |
| .1135 | .1146 | .1085 | .1082 | .1125 | .1130 |
| .1120 | .1166 | .1148 | .1110 | .1102 | .1123 |
| .0848 | .0782 | .0706 | .0820 | .0815 | .0846 |
| .1196 | .1240 | .1171 | .1209 | .1148 | .1158 |
| .1107 | .1123 | .1189 | .1110 | .1133 | .1234 |
| .1133 | .1209 | .1097 | .1097 | .1171 | .1204 |
| .0818 | .0909 | .0942 | .0935 | .0800 | .0919 |
| .1171 | .0996 | .1168 | .1209 | .1204 | .1135 |
| .1168 | .1138 | .1120 | .1148 | .1224 | .1110 |
| .1209 | .1072 | .1247 | .1168 | .1123 | .1184 |

**Table C-1 (contd)**

| Electrode thickness, cm | | | | | |
|---|---|---|---|---|---|
| Top | Center | Bottom | Top | Center | Bottom |
| 20-*G* relative acceleration | | | 30-*G* relative acceleration | | |
| .0792 | .0828 | .0935 | .0861 | .0828 | .0803 |
| .1229 | .1143 | .1062 | .1105 | .1133 | .1222 |
| .1072 | .1151 | .1359 | .0965 | .1100 | .1309 |
| .1156 | .1189 | .1115 | .1049 | .1118 | .1255 |
| .0869 | .0790 | .1074 | .0968 | .0826 | .1024 |
| .1184 | .1118 | .1006 | .1227 | .1153 | .1059 |
| .1219 | .1168 | .1069 | .1123 | .1156 | .0956 |
| .1275 | .1069 | .1100 | .1184 | .1082 | .1184 |
| .0765 | .0833 | .0953 | .0853 | .0757 | .0970 |
| .1214 | .1148 | .1151 | .1151 | .1128 | .1224 |
| .1285 | .1128 | .1186 | .1298 | .1260 | .1260 |
| .1189 | .1026 | .1026 | .1072 | .1196 | .0904 |
| .0909 | .0762 | .1077 | .0917 | .0732 | .0930 |
| .1184 | .1056 | .1168 | .1173 | .1186 | .1151 |
| .1085 | .1176 | .1059 | .1085 | .1240 | .1313 |
| .1240 | .1245 | .1191 | .1032 | .1146 | .1021 |
| .0820 | .0721 | .0892 | .0965 | .0701 | .0902 |
| .1344 | .0980 | .1295 | .0676 | .1204 | .1044 |
| .1250 | .1082 | .1224 | .1041 | .0978 | .1173 |
| .1026 | .1168 | .1113 | .1095 | .1133 | .1095 |
| .0930 | .0879 | .1067 | .0876 | .0734 | .0945 |
| .1300 | .1128 | .0973 | .1173 | .1222 | .1364 |
| .1186 | .1128 | .1176 | .1125 | .1082 | .1344 |
| .1158 | .1212 | .1115 | .1344 | .1204 | .1052 |
| .0846 | .0721 | .0973 | .0869 | .0767 | .1003 |
| .1196 | .1273 | .1077 | .1229 | .1095 | .1245 |
| .1222 | .1163 | .1234 | .1107 | .1115 | .1184 |
| .1138 | .1138 | .1217 | .1074 | .1143 | .1260 |
| .0869 | .0734 | .0950 | .0813 | .0932 | .0955 |
| .1123 | .1003 | .1072 | .1265 | .0638 | .0935 |
| .1143 | .1298 | .1115 | .1184 | .1290 | .1204 |
| .1199 | .1242 | .1189 | .1097 | .1100 | .1300 |
| .0973 | .1016 | .0879 | .0917 | .0823 | .0828 |
| .1209 | .1082 | .1069 | .1179 | .1224 | .1113 |
| .1080 | .1115 | .1234 | .1052 | .1074 | .1247 |
| .1212 | .1046 | .1133 | .1156 | .1024 | .1186 |
| .0800 | .0772 | .0950 | .0803 | .0820 | .0823 |
| .1387 | .1212 | .1222 | .1133 | .1201 | .1085 |
| .1118 | .1123 | .1176 | .1008 | .1100 | .1486 |
| .1102 | .1209 | .1252 | .1260 | .1201 | .1092 |

**Table C-1 (contd)**

| Electrode thickness, cm | | | | | |
|---|---|---|---|---|---|
| Top | Center | Bottom | Top | Center | Bottom |
| 50-*G* relative acceleration | | | 75-*G* relative acceleration | | |
| .0859 | .0782 | .0973 | .0828 | .0841 | .1102 |
| .0970 | .1334 | .0968 | .0958 | .1245 | .1344 |
| .0996 | .1300 | .1201 | .0889 | .1334 | .1415 |
| .1095 | .1146 | .1326 | .0930 | .1173 | .1113 |
| .0856 | .0919 | .0762 | .0691 | .0815 | .0876 |
| .0956 | .1186 | .1402 | .1036 | .1163 | .1036 |
| .0980 | .1255 | .1097 | .0955 | .1097 | .1196 |
| .0955 | .1059 | .1222 | .1095 | .1224 | .1189 |
| .0719 | .0762 | .1143 | .0780 | .0701 | .1105 |
| .1031 | .1349 | .1240 | .0996 | .1097 | .1260 |
| .0996 | .1209 | .1034 | .0978 | .1397 | .1046 |
| .1072 | .0998 | .1186 | .0823 | .0841 | .1252 |
| .0742 | .0721 | .1029 | .0904 | .0752 | .1135 |
| .1097 | .1115 | .1260 | .1006 | .1148 | .1158 |
| .1029 | .1069 | .1041 | .1234 | .1293 | .1113 |
| .0968 | .1288 | .1072 | .0800 | .1133 | .1186 |
| .0729 | .0869 | .1034 | .0846 | .0714 | .1278 |
| .0953 | .1204 | .1074 | .0853 | .1135 | .1128 |
| .1008 | .1288 | .1204 | .0930 | .1346 | .1041 |
| .0907 | .1163 | .1074 | .0922 | .1290 | .0945 |
| .0851 | .0762 | .1019 | .0815 | .0686 | .0993 |
| .0912 | .1186 | .1262 | .1128 | .1135 | .1252 |
| .1092 | .1212 | .1107 | .0889 | .1161 | .1087 |
| .0950 | .1194 | .1092 | .0843 | .1194 | .1161 |
| .0808 | .0836 | .0942 | .0701 | .0686 | .1024 |
| .1260 | .1036 | .1133 | .0940 | .1222 | .1214 |
| .0958 | .1232 | .1168 | .0815 | .1207 | .1143 |
| .1001 | .1240 | .1186 | .1113 | .1229 | .0950 |
| .0846 | .0876 | .1105 | .0777 | .0693 | .0538 |
| .0998 | .1204 | .0881 | .0983 | .1163 | .1036 |
| .1110 | .1135 | .1120 | .0879 | .1216 | .1240 |
| .1138 | .1069 | .1407 | .0917 | .1217 | .0980 |
| .0810 | .1095 | .0986 | .0818 | .0836 | .1085 |
| .1026 | .1171 | .1186 | .0937 | .1146 | .1265 |
| .0889 | .1100 | .1189 | .0973 | .1128 | .1430 |
| .0945 | .1008 | .1133 | .0958 | .0942 | .1374 |
| .0813 | .0752 | .1234 | .0688 | .0765 | .1092 |
| .1013 | .1237 | .0930 | .0897 | .1026 | .1323 |
| .1054 | .1115 | .1102 | .0889 | .1224 | .1039 |
| .1049 | .1224 | .1201 | .0770 | .1095 | .0965 |


NASA — JPL — Coml., L.A., Calif.